UNIVERSITY OF NAIROBI

ASSESSMENT OF TEMPERATURE AND PRECIPITATION EXTREMES OVER KENYA USING THE COORDINATED REGIONAL DOWNSCALING EXPERIMENT MODEL OUTPUTS

MISIANI HERBERT OMONDI

I56/70062/2013

A Dissertation Submitted in Partial Fulfillment of the Requirements for the Award of the Degree of Master of Science in Meteorology of the University of Nairobi

JULY 2015

DECLARATION

I declare that this thesis is my original work and has not been submitted elsewhere for examination, award of a degree or publication. Where other people's work or my own work has been used, this has properly been acknowledged and referenced in accordance with the University of Nairobi's requirements.

Signature…….. Date……..

Herbert Omondi Misiani
I56/70062/2013
misianihabat@gmail.com
Department of Meteorology,
University of Nairobi

This dissertation is submitted for examination with our approval as University supervisors.

Signature…….. Date……..

Dr. F. Opijah
Department of Meteorology,
University of Nairobi
fopijah@gmail.com

Signature…….. Date……..

Prof. L. A. Ogallo
IGAD Climate Prediction and Applications Centre
logallo@icpac.net

DEDICATION

This work is dedicated to my wife Emily, daughter Kaylee and my parents, Mr. and Mrs. Misiani A. Odhiambo

ACKNOWLEDGEMENT

I am highly grateful to God for giving me the strength to study throughout the entire length of this course at the University of Nairobi.

I also wish to thank my supervisors Prof. L. Ogallo and Dr. F. Opijah for their advice, guidance, support and encouragement during the research period.

I wish also to extend my thanks to colleagues at the ICPAC laboratory as well as my classmates for their valuable inputs and positive criticism that improved the output of this study. Many thanks also go to Hussen Endris for his invaluable advice.

Finally, I would like to thank IGAD Climate Predictions and Applications Centre (ICPAC) for awarding me the scholarship to pursue my Master of Science degree at the University of Nairobi and for providing me with the material support and mentorship throughout my study period. I pray that you may continue nurturing more talented young scientists in the region.

ABSTRACT

Climate related extremes such as floods and droughts have presented significant challenges to nations worldwide and especially developing countries. Kenya is not an exception to the effect of the periodic extremes in temperature and precipitation events which have drastically affected its people as well as the economy. It is necessary to investigate the past, current and future characteristics of these extreme events so as to come up with concrete information that can provide the basis for effective contingency planning.

The main objective of the study was to determine the past, present and future changes in extreme temperature and rainfall over Kenya using the Coordinated Regional Downscaling Experiment (CORDEX) model outputs. Data employed in this study included daily observed rainfall and temperature datasets from IGAD Climate Prediction and Applications Centre (ICPAC), gridded datasets from Climate Research Unit (CRU) and the CORDEX model outputs. The study utilized extreme indices to determine the observed and modeled temperature and rainfall extremes. Methods for assessing the skill of the models included spatial and time series analysis, difference plots and correlation analysis.

Climate extreme indices indicate that maximum and minimum temperatures have decreased in the western parts of the country. The diurnal temperature range has increased in the coastal parts of Kenya; however, there has been a decrease in the urban centers especially in Nairobi and Kisumu. Mean monthly maximum and minimum temperatures have increased in the arid and semi-arid parts of Kenya. Rainfall indices indicate that dry days have decreased while wet days have increased in some parts of the northern arid and semi-arid regions. Total precipitation has increased in most of the arid and semi-arid regions and has decreased in urban centers and western parts of Kenya. Extreme wet days have slightly increased over the central highlands.

Most models suggest an increase in the future number of wet days in the southern arid and semi-arid parts of Kenya during the MAM season. Decrease in wet days is expected in areas that usually receive rainfall during the JJA season. Much of the arid and semi-arid regions are expected to experience increase in wet days in the future during the OND season. Increase in the number of extreme wet days is expected in the western parts of Kenya during the MAM, JJA and OND seasons. Much of the country is expected to warm by at least 20% of the 90th percentile

baseline threshold in all the seasons.

These findings provide the much needed information to stakeholders to put in place adaptation strategies that will help protect the lives and livelihoods of people living in places where significant changes are expected considering the RCP4.5 scenario. Future studies should perform the necessary bias corrections before proceeding with further analysis of projection data from these models.

Contents

LIST OF FIGURES

LIST OF TABLES

LIST OF ACRONYMS

AOGCMs	Atmospheric-Ocean General Circulation Models
BADC	British Atmospheric Data Centre
CanESM2	Second Generation Canadian Earth System Model
CCl/CLIVAR	Climate Variability
CCCma	Canadian Centre for Climate Modeling and Analysis
CDD	Maximum number of consecutive days with RR<1 mm
CDO	Climate Data Operators
CNRM-CM5	Centre National de Recherches Meteorologiques Coupled Model version Five
CNRM-CERFACS	Centre National de Recherches Meteorologiques and Centre Européen de Recherche et de Formation Avancée en Calcul Scientifique
CORDEX	Coordinated Regional Climate Downscaling Experiment
CRU	Climate Research Unit
CWD	Maximum number of consecutive days with RR >=1 mm
DTR	Monthly mean difference between TX and TN
EC-EARTH	Europe-wide Consortium Earth
ENSO	El Niño Southern Oscillation
ERA	ECMWF ReAnalysis
ESMs	Earth System Climate Models
ET	Expert Team
ETCCDI	Expert Team (ET) on Climate Change Detection and Indices

GCM	General Circulation Model
GEV	Generalized Extreme Value
GFDL-ESM	Geophysical Fluid Dynamics Laboratory-Earth System Model
GHA	Greater Horn of Africa
GP	Generalized Pareto
GPCC	Global Precipitation Climatology Centre
GPD	General Pareto Distribution
HadGEM2-ES	Second version of the Hadley Centre Global Environmental Model Earth System configuration
ICHEC	Irish Centre for High-End Computing
ICPAC	IGAD Climate Prediction and Applications Centre
IIASA	International Institute for Applied Systems Analysis
IMAGE	Integrated Model to Assess the Global Environment
IOD	Indian Ocean Dipole
IPCC	Intergovernmental Panel on Climate Change
ITCZ	Inter-tropical Convergence Zone
JJA	June-July-August
MAD	Mean Absolute Deviation
MAE	Mean Absolute Error
MAM	March-April-May
MDGs	Millennium Development Goals

MESSAGE	Model for Energy Supply Strategy alternatives and their General Environmental impacts
MIROC	Model for Interdisciplinary Research on Climate
MJO	Madden-Julian Oscillations
MOHC	Met Office Hadley Centre
MPI-ESM-LR	Max Planck Institute Earth System Model-Low Resolution grid
MPI-M	Max Planck Institute for Meteorology
NAO	North Atlantic Oscillation
NCC	Norwegian Climate Centre
NE	North Easterlies
NOAA	National Oceanographic and Atmospheric Administration
NOAA-GFDL	National Oceanographic and Atmospheric Administration- Geophysical Fluid Dynamics Laboratory
NorESM1-M	Norwegian Climate Center's Earth System Model
OND	October-November-December
PCA	Principal Component Analysis
POT	Peaks over Threshold
PRECIS	Providing REgional Climates for Impact Studies
PRCPTOT	Annual total PRCP in wet days (RR >=1 mm)
PRCP	Precipitation
QBO	Quasi-biennial Oscillations
R99p	Annual total PRCP when RR > 99^{th} percentile

RACMO2	Regional Atmospheric Climate Model
RCMs	Regional Climate Models
RCP	Representative Concentration Pathways
RFEs	Rainfall Estimates
RMSE	Root Mean Square Error
RR	Rainfall
SE	South Easterlies
SEI	Stockholm Environment Institute
SO	Southern Oscillation
SST	Sea Surface Temperatures
TAMSAT	Tropical Applications of Meteorology using SATellite
TMAXmean	Annual mean maximum temperature
TMINmean	Annual mean minimum temperature
TNx	Monthly maximum value of daily minimum temp
TXx	Monthly maximum value of daily maximum temp
TRMM	Tropical Rainfall Measuring Mission
WCRP	World Climate Research Program
WHO	World Health Organization
WMO	World Meteorological Organization
WMO-CCL	World Meteorological Organization – Commission for Climatology

CHAPTER ONE

1.0 INTRODUCTION

1.1 Outline

This chapter provides the background of the study, including the problem statement, objectives, justification, and domain of study as well as the major climate systems that control the space-time patterns of rainfall over the region.

1.2 Background

Climate related extremes such as floods and droughts present significant challenges to nations worldwide and especially developing countries. The extreme related impacts have resulted in major drawbacks to the gains made by developing countries and global partners in their endeavor to meet the millennium development goals (MDGs). A recent IPCC statement indicates that the severity and frequency of the extremes are increasing over parts of the world with future projections showing increased extremes embedded in the future climate changes at global, regional, and local scales (IPCC, 2007; 2013). The changes in future climate extremes will force disaster managers to come up with new strategies for managing them since coping and response mechanisms and economic planning for disasters based on past vulnerabilities may no longer be useful (Sperling and Szekely, 2005).

It is expected that future climate extremes will result in much greater impacts to societies and ecosystems which are not well prepared and this will be made worse by other compounding factors such as changing patterns of vulnerabilities including changes in land-use patterns, poverty and rising populations. It has been suggested that systems and countries with current low level risk preparedness will be the ones with high future projections of vulnerability levels (World Bank, 2012).

Disasters, epidemics and conflicts are usually propagated and worsened by extreme climate events and their linkage is not new to the Greater Horn of Africa region. For example, the Darfur war was propagated and worsened by the 1984 drought that resulted in food insecurity and malnutrition (Welzer, 2012). The diarrheal outbreak in Sudan in 1980 (WHO, 2015) and the Rift Valley fever outbreak in Kenya and Somalia in December 1997 (FAO, 1998) were as a result of

extreme rains.

Periodic floods and droughts in Kenya have substantially affected the economy with the cost sometimes running into billions of dollars thereby reducing long-term growth. An example was the 1998-2000 droughts which lead to the loss of crops and livestock, resulted in forest fires, caused substantial damage to fisheries, reduced hydropower generation that resulted in reduced industrial production, power rationing and overall reduction in water supply. In the extreme case of heavy precipitation, at least one million people in Kenya were affected by the 1997/98 floods and this had costs to the economy ranging between 0.8 to 1.2 billion US dollars with a range of effects to public health, infrastructure and loss in crops (SEI, 2009). It is therefore clear that Kenya, like most African countries, is not well adapted to deal with the effects posed by climate risks.

This study attempts to provide a glimpse into the potential space-time characteristics of the past and future climate extremes in Kenya. Such climate change scenarios will provide critical climate information that will support science-informed policies for building a resilient society and economy and further strengthen national sustainable development efforts.

1.3 Problem Statement

The severity and frequency of extremes in rainfall and temperature have been observed to have increased over several parts of the world. These extremes are the main cause of most climate-related socio-economic challenges. It is necessary to investigate the possible evolution of these extremes into the future in order for disaster managers to come up with concrete contingency measures.

Some regional studies by Omondi *et al.,* (2014), Shongwe *et al.,* (2011) among others have provided regional climate extreme projections at coarse scales. Such studies were also not focused on climate extremes that have far reaching implications on the states of our future environment, society and the economy. In addition, it is expected that future extremes will generate new threats which some regions may not have experience in dealing with. Comprehensive information of past, present and future extremes is necessary for disaster risk reduction (DRR) managers.

This study attempts to examine the past and present patterns of rainfall and temperature extremes over Kenya, and present projections of future climate extremes which will provide climate change scenarios required for building a resilient society and economy in support of national disaster risk reduction, climate change adaptation and strengthening national sustainable development efforts.

1.4 Overall Objectives

The main objective of the study was to assess the past, present and future changes in extreme temperature and rainfall over Kenya using the Coordinated Regional Downscaling Experiment (CORDEX) model outputs. The specific objectives are to:

i. Determine space-time patterns of past and present temperature and rainfall extremes over Kenya

ii. Assess the skill of CORDEX models and the ensemble in simulating the observed past and present temperature and rainfall over Kenya

iii. Determine the seasonal patterns of temperature and rainfall extremes over Kenya from CORDEX climate projections

1.5 Justification of Study

Climate extremes such as droughts and floods are already threatening the socio-economic survival of many developing countries such as Kenya. Future changes in climate extremes would therefore be very devastating to Kenya and many developing countries if no concrete action is taken to cope with the future changes.

Climate models for projections of future climate are constantly undergoing improvements. New insights into the various atmospheric processes have constantly been integrated into these models which have substantially increased model performance. In addition, increased computing power has enabled model developers to increase model resolution. Therefore, relatively small scale processes can now be simulated and downscaled with improved skill. It is necessary to frequently update the available information on extreme climate events with the availability of projection datasets so as to provide highly skilled information for early warning systems.

1.6 Domain of the Study

The study area, Kenya with a total area of approximately 586, 646 km^2, is found in Eastern Africa region and lies between longitudes 34°E to 42°E and latitudes 5.5°N to 5°S. It is bordered by five countries namely, Sudan, Ethiopia, Uganda, Tanzania and Somalia. Furthermore, Kenya is bordered to the East by the Indian Ocean (Figure 1).

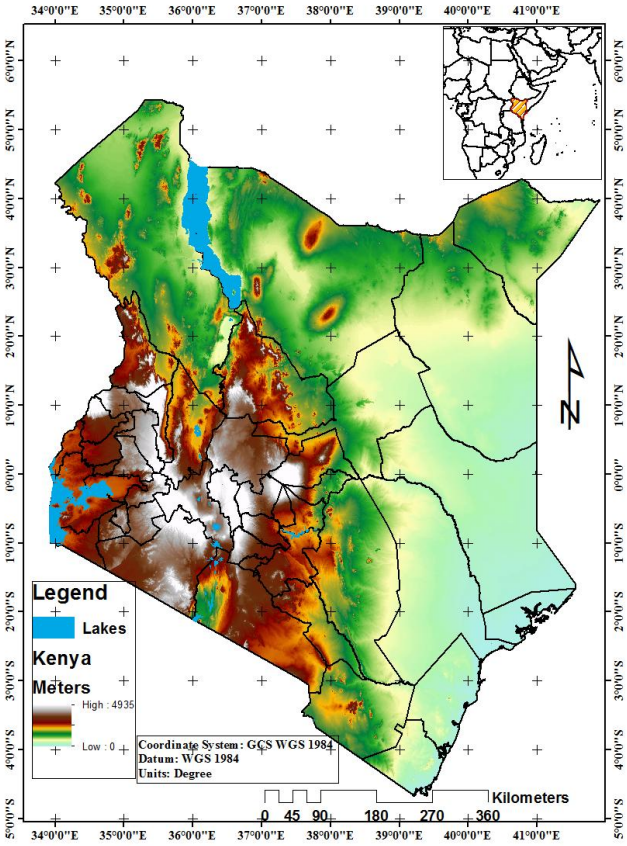

Figure 1: Map of the study area showing some of the physical features. The lakes are in blue and elevations rise from the coast westwards (Digital Elevation Map courtesy of DIVA-GIS).

1.7 Physical Features of the Study Area

Kenya is dotted with complex topographies that include the Yatta plateau and Mt. Kenya which peaks at 5199 m. Other features found in the study area include Mt. Elgon (4321 m), Aberdare Ranges (3999 m) and the Mau escarpment (3000 m) respectively. There also exist large water bodies that include Lake Turkana and Lake Victoria as well as the Indian Ocean. The Great Rift

Valley is also another important physical feature found in the study area.

1.8 Rainfall Climatology of the Study Area

The distribution of the physical features over the country brings about complex circulation and rainfall patterns. Over the coastal lowlands (near the Indian Ocean) and western Kenya, substantial rainfall is received during three major rainfall seasons March – May (MAM), June – August (JJA) and October – December (OND). Most parts of the country however receive rainfall during two rainfall seasons: MAM "long rains" and OND "short rains" season.

1.9 Systems Influencing Rainfall Distribution over Kenya

Rainfall distribution in Kenya is influenced by several systems. These systems range from local scale to global scale as well as local physical features. They interact in complex ways to bring about the observed distribution of rainfall in Kenya. These systems include mesoscale systems (for example, land, lake and sea breezes), synoptic scale systems like the tropical cyclones, subtropical quasi-permanent anticyclones (Mascarene, St. Hellena, Arabian, and Azores), global teleconnections with global climatic anomalies like El Nino Southern Oscillation (ENSO), dipole modes like the Indian Ocean Dipole (IOD), Quasi-biennial Oscillations (QBO), Madden-Julian Oscillations (MJO), Jet streams, Monsoons and easterly waves. The subsequent sections offer brief descriptions of how these systems affect the Kenyan climate.

1.9.1 Inter Tropical Convergence Zone (ITCZ)

The ITCZ is a low pressure region that encircles the tropical regions of the globe often discernible as a band of clouds and has much influence on rainfall patterns. Folland, *et al.*, (1991) describes it as a quasi-continuous belt of unsettled weather around the tropics, sandwiched between fine weather to the North and South of the subtropical highs. ITCZ is the main synoptic scale system that controls the intensity and migration of seasonal rainfall over Kenya. Over the East Africa region, the ITCZ has two components; the normal east-west orientation called the zonal arm and the north-south oriented component referred to as meridional arm (Ininda, 1995; Okoola, 1999).

1.9.2 Tropical Monsoons

Monsoons are prevailing winds which shift direction by 120° between January and July blowing with a mean wind speed exceeding 3 m s^{-1} Ramage (1971). The monsoon winds blow in response to the differential heating between continents and oceans. Monsoons coincide with the months of the year when the ITCZ is further from East Africa and thus are associated with relatively little rainfall (Okoola, 1999). Monsoon winds have a strong zonal component and bring warm moist air into the East Africa region from the Indian Ocean (Sadler *et al.,* 1987). The two monsoons that affect eastern and southern Africa are the Northeast monsoons during December-February and Southeast monsoon in June-August (Trewartha, 1981).

1.9.3 El Niño Southern Oscillation

El Niño Southern Oscillation (ENSO) is one of the largest global tele-connections that is caused by recurring redistributions of heat and atmospheric momentum in the Equatorial Pacific Ocean and brings about climate variability on inter-annual time scales (Godinez-Dominguez *et al*., 2000). The occurrence of the ENSO phenomenon perturbs the Walker circulation (Walker, 1932) thereby setting off shifts in rainfall patterns in the tropics, disrupting circulations in the atmosphere, and thereby affecting climate across the globe.

The period of ENSO is irregular, normally ranging from two to seven years with large areal extent and global impacts. Since ENSO is due to coupled ocean-atmosphere interaction, El Niño/La Niña and SO both rely on and modulate each other. El Niño and La Niña are the warm and the cold phases of ENSO usually associated with floods and droughts across the Equatorial East Africa region, respectively.

1.9.4 Indian Ocean Dipole

The Indian Ocean Dipole (IOD) is a coupled ocean-atmosphere phenomenon in the equatorial Indian Ocean normally measured by an index which is the difference between sea surface temperature anomalies in the western (50°E to 70°E and 10°S to 10°N) and eastern (90°E to 110°E and 10°S to 0°S) equatorial Indian Ocean (Saji *et al.,* 1999). It is characterized by positive and negative phases. Positive IOD phase corresponds to warmer than normal water in the eastern Indian Ocean and cooler than normal water in the tropical western Indian Ocean. A negative

phase is the opposite of the positive phase (Saji et al., 1999).

The IOD SST anomalies, especially positive IOD phase, have marked influence on the moisture supply to the adjacent land masses (Reason, 2001). Associated with these changes is the westward shift of the normal convection situated over the warm pool of the eastern Indian Ocean which results in rainfall over East African region.

1.9.5 Madden-Julian Oscillation

The Madden-Julian Oscillation (MJO), which is a coupled ocean-atmosphere system, influences tropical weather from small-scale tropical convection through to planetary-scale circulations (Madden and Julian, 1994). The atmospheric component, characterized as an oscillation, has a spatial scale of 12,000-20,000 km (wavelength) and propagates eastwards at speeds of 5 ms^{-1} (a period of roughly 30-60 days) (Hendon and Liebmann, 1990). Although the atmospheric signature is less evident in the mid-tropospheric winds, it is more evident in lower and upper-troposhperic winds, sea level pressure and in fields representative of deep convection (such as relative humidity or outgoing long-wave radiation) (Madden and Julian, 1971; 1972; 1994). The period for the oceanic component is more or less longer than that of the atmospheric component with a period of 60-75 days and the signature is evident in the sea surface temperatures (SSTs), mixed layer depth, surface latent heat flux and surface wind stress fields.

The MJO is strongest during December to February season and during neutral ENSO (Hendon and Liebmann, 1990). It is suppressed during either strong El Niño or La Niña events. Its impacts on the tropical atmosphere range from variation in local rainfall and increased frequency of tropical cyclones to modulation of active and break phases of the Asian-Australian and African monsoons (Hendon and Liebmann, 1990).

Weak zonal ocean surface stress anomalies results from the influence of the MJO on zonal wind anomalies linked to the excitation of oceanic Kelvin waves that modulates the thermocline in the equatorial Pacific Ocean (Kessler *et al.*, 1995). Thus the interannual variation of the ENSO may be affected by the phase of the MJO (Fink and Speth, 1997). This is because Kelvin waves have been known to be the triggering mechanism for ENSO (Lau and Chan, 1985). MJO impacts Equatorial East Africa rainfall during DJF season through the alteration of wet and dry periods.

1.9.6 Quasi-Biennial Oscillation

Quasi-biennial oscillation (QBO) is an oscillation that is discernible in the zonal winds in the lower equatorial stratosphere with winds oscillating roughly with a period of two years from westerly to easterly and back in turn changing the vertical wind shear of the troposphere and the associated stability. QBO impacts a wide range of atmospheric phenomena in both the troposphere and stratosphere. It affects atmospheric variations associated with ENSO thereby affecting the monsoons (Hatsushika and Yamazaki, 2001). It also affects tropical cyclone numbers in North Indian Ocean during the easterly phase (negative zonal wind anomalies) (Chan, 1995). An association between East Africa rainfall and QBO was found by Indeje *et al.*, (2000) to be strongest during the boreal summer season (June-August) and weakest in boreal winter (December-February). The strongest correlations were found over western parts of East Africa.

1.9.7 Tropical cyclones

Tropical cyclones are most prevalent over tropical warm waters and are characterized by low pressure, heavy rainfall and strong winds. The South West Indian Ocean is a prime area of formation of tropical cyclones that affect weather over the East African region. They form during northern spring and late fall and move northward into the Arabian Sea. They rarely make landfall over Somalia but when they do, they usually affect weather over North eastern parts of Kenya. Moisture laden south easterlies are normally diverted to the low pressure area of a tropical cyclone should it pass over Madagascar. This denies the region moisture thereby causing dry spells over East African region (Asnani, 1993).

1.9.8 Subtropical Anticyclones

The subtropical anticyclones are characterized by anticyclonic circulation and are as a result of the descending arm of the Hadley cell. They are the major drivers of trade winds and their strengths dictate the position of the ITCZ. Their intensity depends on the season; they are stronger during winter than in summer season of each hemisphere.

During the October – November (OND) season, the Arabian High pressure cell is usually strong compared to the Mascarene cell making the north easterlies (NE) to be stronger than the south

easterlies (SE). The NE are usually moisture deficient from their long trajectory over continental areas. This together with the fact that the southward movement of the ITCZ is faster than the northward movement results in the short period of rainfall during the OND season. On the contrary, during the March – May (MAM) season, the Mascarene cell is much stronger driving strong SE towards the East African region. This together with the slow movement of the ITCZ northwards results in long rainfall period during this season. Intensification of the St. Helena cell normally drives the moist westerlies from Congo basin to the East African region. The meeting point of the westerlies and the easterlies defines the meridional arm of the ITCZ.

1.9.9 Mesoscale Systems

Lakes, mountains, and the Kenyan highlands are some of the forcing features that influence the mesoscale weather. The intense insolation, circulation patterns over Lake Victoria and their interaction with large scale systems results in frequent thunderstorms and enhanced rainfall activities in the afternoon over the western sector than the eastern sector (Okeyo, 1987). Moisture from the Congo Basin and the lake basin may be blocked from reaching the eastern parts of the country through the action of high physical features like highlands and mountains or the blocking of easterlies from the Indian Ocean. Action of orographic lifting may lead to wetter conditions on either side of the highland (Oettli and Camberlin, 2005).

The western parts of the Indian Ocean act as a source of moisture for the coastal areas and are also a forcing feature for mesoscale systems like the sea breeze (Kijazi and Reason, 2009). This is why the coastal region, near the Indian Ocean, receives rainfall almost throughout the entire year.

CHAPTER TWO

2.0 LITERATURE REVIEW

This chapter reviews the available literature on climate extremes regionally and globally. Increase or decrease in extremes may result when the mean of a distribution changes (Figure 2a), or when the variance changes (Figure 2b), or when both the mean and variance change (Figure 2c). The modifications of temperature may result in the changes in intensity and frequency of these events.

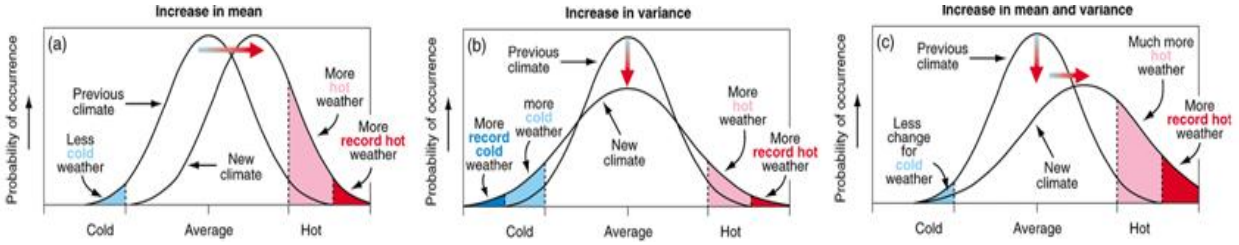

Figure 2: Normal distribution curve showing various changes in extreme events. The figure shows changes in extreme temperature events as a result of (a) changes in mean, (b) changes in variance and (c) changes in mean and variance (Source: IPCC, 2013).

Most studies have utilized the WMO recognized climate indices for ease of comparison while others have utilized statistical methods that rely on extreme value distributions to model the rare extremes and their return levels.

2.1 Climate Extreme Indices

Climate extreme indices are recommended by the World Meteorological Organization (WMO) as a benchmark for comparing climate extremes across the globe. They were originally developed by the Climate Variability (CCl/CLIVAR) Working Group on Climate Change Detection and later improved by Experts Team (ET) to aid in the uniformity when analyzing extreme climate events across the globe (Karl *et al.*, 1999; Peterson *et al.*, 2001).

There are two approaches in generating the extreme indices; the first method is through the use of percentile based thresholds while the second method is through the use of fixed thresholds. These approaches are suitable for assessing moderate extremes which usually occur a few times every year. Other high-impact, once-in-a-decade, extreme events may be better assessed through

other methods that model the occurrence of these events at the tail end of the distribution, e.g., Generalized Extreme Value (GEV) and Generalized Pareto (GP) distributions (e.g., Coles, 2001).

Climate extreme indices have been widely used to study extremes in different parts of the world (e.g., Keggenhoff *et al.,* 2014; Ly *et al.,* 2013; Wang *et al.,* 2012; Vincent *et al.,* 2011; and Kruger 2006). In general, warming trends have been observed by a number of authors where in some regions trends of extremes in minimum temperature were found to be consistent with long-term trends, whilst trends in extremes of maximum temperatures have been found to be part of multi-decadal climate variability (Klein *et al.,* 2006). In some regions, however, an asymmetry in changes in seasonal and diurnal extreme temperature events was found in comparison to recent increases in temperature means (Choi *et al,* 2009). It is also worth noting that trends in rainfall are not as spatially coherent as the trends in temperature (Ly *et al.,* 2013; Alexander *et al.,* 2006; Kostopoulou and Jones 2005). An example is the case of Mongolia where although the number of days with precipitation showed a slight increase, there was no significant increase in annual total precipitation (Nandintsetseg *et al.,* 2007).

It has been concluded that the increase in extreme precipitation and variability and climate uncertainty is greater in the recent past through the use of the climate extreme indices (Costa and Soares, 2009). Some studies such as Aguilar *et al.,* (2009) showed results which are contrary to the global averaged values, specifically over Guinea where they found a decrease in total and heavy precipitation in contrast to the increasing global averaged.

In the Eastern Africa region, climate extreme indices have been used by authors to analyze the extremes associated with temperature and rainfall. For example, King'uyu *et al.,* (2000) studied extremes in minimum and maximum temperature over the Eastern Africa region during 1955 to 1990 period. They found that trends were significantly correlated with the patterns of convective activities especially ENSO, cloudiness and above or below normal rainfall. The study on extremes in temperature and precipitation over the Greater Horn of Africa (GHA) region was done by Omondi *et al.,* (2014) involving observed data running over the period 1971 to 2006 and projection by PRECIS model. They used a total of 19 indices for temperature and precipitation where they also found lack of spatial coherence in precipitation indices.

2.2 Extreme Value Distributions

Extreme distributions have been used to analyze extreme events over several places. These distributions include, the Generalized Extreme Value (GEV) and Generalized Pareto (GP) distributions (e.g., Coles, 2001). There are several authors who have used these methods to analyze extreme climate events, for example, Shongwe *et al.,* (2011) who used the method of peaks over threshold (POT) and General Pareto distribution (GPD) to analyze the precipitation extremes and their return levels over East Africa. Return levels are used in many studies due to their simplicity (e.g., Kharin and Zwiers 2000; Kharin *et al.*, 2007). Katz (1999) described an extreme value theory for precipitation where he showed that the effective return period for a particular location is most sensitive to the scale parameter of the intensity distribution. Studies have also shown that changes in extremes in precipitation, in most cases, parallels changes in the mean precipitation (Shongwe *et al.*, 2009).

2.3 Association of Climate Extremes with Circulation Patterns

Large scale climatic patterns such as ENSO usually influence climate extremes in several places. For example, You *et al.,* (2011) associated changes in daily climate extremes to large scale atmospheric circulation where they found that temperature extremes had high correlations with the annual mean temperature. Systems like the southern oscillation (SO) influence the estimation of global surface temperature anomalies (Halpert and Ropelewski., 1992) and have been observed to influence even remote parts around the globe (George *et al.,* 1989). Variations in low latitude circulation, such as high pressure cells, have also been associated with climate extremes (Hastenrath, 1976). Extreme rainfall indices were also investigated by (Haylock and Goodess, 2004) to have a link with sea level pressure observations.

Extreme weather events normally occur as result of anomalous climatic and oceanic circulation systems. The association of the climate and ocean with daily rainfall extremes was investigated by Williams *et al.,* (2007) over South Africa. With proxy daily data from satellite, their objectives included describing the main patterns of variability over South Africa as well as selecting the dates of occurrence of extreme rainfall within these patterns and finally showing the effect of resolution in identifying the location and intensity of SST anomalies associated with these extremes. Using the method of principal component analysis (PCA), their results showed

that for spatial patterns accounting for the highest amount of variability, higher spatial resolution extraction of extremes showed coherent indication regarding intensity and location of anomalous SST regions.

Griffiths *et al.,* (2005) investigated how mean temperature has changed as an indicator for extreme temperature change in the Asian Pacific region. Mean temperature and frequency of extreme temperature correlations were strongest in the Tropical Pacific region while they were weaker in continental locations which they attributed partly to urbanization. Their results supported the hypothesis that changes in mean temperature may be used to predict changes in extreme temperature.

Kenyon and Heggerl (2008) investigated the influence of modes of climate variability, ENSO, NAO and Pacific interdecadal variability, on global temperature extremes. They used indices for monthly temperature extremes from worldwide landmasses and utilized a number of exceedances over defined thresholds. They also examined the extremes that showed statistically significant difference between the negative and positive phases of the circulation regime.

2.4 General and Regional Circulation Models and Projections of Climate Extremes

Global climate models have now become very significant tools in climate studies especially in the study of climate variability and change (Endris *et al.,* 2013). Their projections are mainly based on future concentrations of the green house gases. The Earth System Models (ESMs) have improved climate simulations through the addition of various bio-geochemical feedbacks that play important roles in understanding past and future responses of the earth system to external forcings (IPCC, 2013). At the moment AOGCMs are able to simulate global atmospheric patterns at spatial scales of the order 100 km to 250 km (Shongwe *et al.,* 2009). They are however not capable of simulating climatic patterns at regional and local scales necessary for national climate change assessments (Wang *et al.,* 2004). Downscaling of the AOGCMs outputs to regional scales is therefore necessary to capture the climate variability at local scales using either dynamical or statistical means. World Climate Research Program (WCRP) has been coordinating the dynamical downscaling of Global climate outputs at regional scales under a project called Coordinated Regional Climate Downscaling Experiment (CORDEX) and availing the data freely for regional scale climate change assessments.

It is often necessary to assess the performance of any model before applying it to various climate change assessments. Several methods including model bias, correlation analysis, root mean square error (RMSE) and even mean absolute deviation (MAD) have been used. Further, it is prudent to assess how models simulate large-scale climate signals, like the ENSO, as well as the annual cycle and inter-annual variability. Studies that have assessed the performance of CORDEX models have found that most CORDEX RCMs perform reasonably well over most parts of Africa. For example over Eastern Africa (e.g., Endris *et al.,* 2013) which is also in agreement with Gbobaniyi *et al.,* (2014) who did a similar experiment with CORDEX over West Africa. Similar studies and results were also obtained over Southern Africa (e.g., Kalognomou *et al.,* 2013).

Mason and Joubert (1997) utilized a general circulation model (GCM) to investigate changes in extreme rainfall over Africa (in the southern hemisphere) as a result of doubling of carbon dioxide. Spatially coherent results of simulated increases in rainfall intensity were found. Increases in the intensity of the lowest frequency floods were also found to be particularly severe. Simulations over most of the subcontinent exhibited increases in both the frequency and intensity of extreme rainfall. Similar results were found in the Australian region however the model had sensitivity to sharp changes in topography over southern Africa.

With the potential severe nature of climate extremes on society, it is important to investigate future projections to inform current adaptation strategies. It is for this reason that Roth *et al.*, (2014) projected the precipitation extremes over North-Western Germany and Netherlands using RACMO2 regional climate model driven by two different general circulation models. In their projections, they found significant increase in extreme summer precipitation for both simulations which was due to the increase of the variability of the excesses over the threshold. They also found that the trend of magnitude in extreme summer precipitation is dependent on the driving GCM. Further still, an increase in extreme precipitation corresponding with an increase in mean precipitation was found for both simulations and this trend was attributed to threshold increase.

Marengo *et al.,* (2009) investigated the future changes in temperature and precipitation extremes using PRECIS regional climate model over South America under the IPCC A2 and B2 scenarios. Their results showed that, for the present climate, the model simulates well the spatial distribution of extremes in temperature and rainfall when compared with the observed datasets.

Significant and often different changes in rainfall and temperature extremes were projected in all the future climate scenarios in all parts of the region. Future occurrences of warm nights were projected to be more frequent over the entire tropical South America while cold night events were projected to decrease.

CHAPTER THREE

3.0 DATA AND METHODOLOGY

This chapter describes the datasets, data quality control measures and the methodologies which were employed to achieve the objectives of the study.

3.1 Data

The datasets which were used in this study included daily observed station data, Climate Research Unit (CRU) gridded observed datasets and the newly downscaled climate scenario datasets from CORDEX Africa.

3.1.1 Observed Data

The daily observed rainfall data for twelve stations (Table 1) in the twelve homogeneous zones (Figure 3) across Kenya from January to December for a period of 30 years were used in this study to analyze the extremes in temperature and rainfall over Kenya and to assess the skill of the CRU datasets. The datasets were obtained from IGAD Climate Prediction and Applications Centre (ICPAC). The datasets included rainfall and both maximum and minimum temperature. Similar datasets have been used by Omondi, *et al.,* (2014).

Table 1: Rainfall Stations Used in the Study and their Coordinates for (a) MAM and (b) OND Seasons

(a)

Station ID	Station	Lat (°)	Lon (°)	Elevation (m)	Zone
Lod	Lodwar	3.7	35.37	506	1
Moy	Moyale	3.32	39.02	1097	2
Waj	Wajir	1.45	40.04	244	3
Gar	Garissa	-0.29	39.38	147	4
Lam	Lamu	-2.16	40.54	30	5
Mom	Mombasa	-4.02	39.37	55	6
Voi	Voi	-3.24	38.34	597	7
Dag	Dagoretti	-1.18	36.45	1798	8
Nan	Nanyuki	0.03	37.02	1905	9
Nar	Narok	-1.08	35.5	1890	10
Mar	Marsabit	2.18	37.54	1345	11
Kis	Kisumu	-0.06	34.45	1146	12

(b)

Station ID	Station	Lat (°)	Lon (°)	Elevation (m)	Zone
Lod	Lodwar	3.7	35.37	506	1
Moy	Moyale	3.32	39.02	1097	2
Man	Mandera	3.56	41.52	230	3
Waj	Wajir	1.45	40.04	244	4
Kak	Kakamega	0.17	34.47	2133	5
Nak	Nakuru	-0.16	36.06	1901	6
Dag	Dagoretti	-1.18	36.45	1798	7
Gar	Garissa	-0.29	39.38	147	8
Voi	Voi	-3.24	38.34	597	9
Mom	Mombasa	-4.02	39.37	55	10
Lam	Lamu	-2.16	40.54	30	11
Kis	Kisumu	-0.06	34.45	1146	12

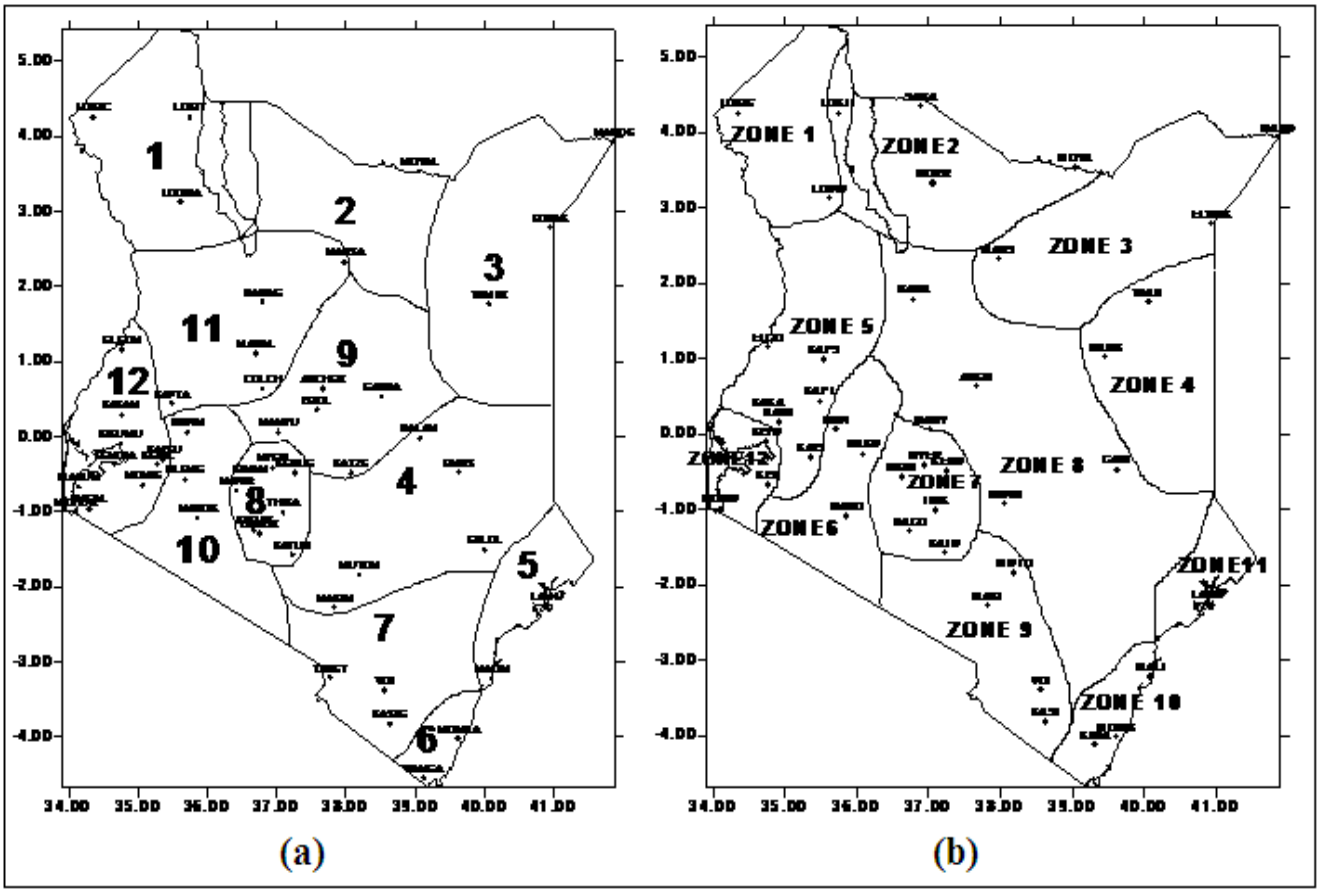

Figure 3: Homogeneous rainfall zones over Kenya for (a) MAM and (b) OND seasons. The stations within each homogeneous zone can be used to represent the entire zone. Source: Rainfall Atlas (Authors: Muhindi, Ndichu and Oloo, Kenya Meteorological Dept)

3.1.2 Climate Research Unit (CRU) Datasets

This study utilized monthly datasets, including precipitation and maximum and minimum temperature, from the Climatic Research Unit Time Series version 3.22 (CRU TSv3.22) to validate the model outputs. The CRU TSv3.22 datasets was gridded at 0.5°x0.5° resolution over land areas from 1901 to 2013 and include monthly datasets of precipitation, maximum and minimum temperatures, cloud cover, diurnal temperature range, vapor pressure, potential evapo-transpiration, frost day frequency and wet day frequency (Harris, *et al.*, 2014). The dataset is based on the analysis of several homogenized observed parameters from over 4000 weather stations.

3.1.3 Coordinated Downscaling Experiment (CORDEX) Africa Datasets

CORDEX is a project that coordinates the dynamical downscaling of Global Climate Model (GCM) datasets to regional scales using specified domains over the entire globe. The African domain covers 45.76°S to 42.24°N and 24.64°W to 60.28°E with a resolution of 0.44 degrees and employing ten Regional Climate Models (RCMs). In total, eight RCMs forced by lateral and surface boundary conditions from ERA-INTERIM reanalysis have downscaled data over the African domain focusing on both RCP4.5 and RCP8.5 scenarios. An additional RCP2.6 scenario was made for EC-EARTH GCM running in transient mode for the period 1951-2100. Datasets for HadGEM2-ES RCP4.5 end in November 2099 while those for RCP8.5 end in December 2099. HadGEM2-ES has the 360 day calendar, with all months having 30 days. Monthly dataset from CORDEX were used to assess the model performance and additional daily datasets were used to assess future climate extremes.

3.1.4 Estimation of Missing Data and Quality Control

The main objective of data quality control is to ensure the data consistency within a collection of datasets. There are significant inconsistencies present in rainfall datasets due to rainfall measurements associated with human and instruments errors (Bosire, 2012). Quality control of data is therefore an integral part of all research and takes place at various stages, for example, during data collection and data entry or digitization. Basic quality control procedures such as gross error checking for the verification of values within acceptable range limits and flagging of suspicious records was done by checking whether maximum temperature was lower than minimum temperature and whether observed rainfall had negative values.

Climate analyses usually require complete datasets with no missing records in between the time series. It is therefore necessary to fill in the missing data before undertaking the analysis of the dataset provided the percentage of missing data is less than 10% for a particular station. In this study, the missing data were coded as -99.9 for ease of calculation since the iteration process for the indices involved counting values which fall above a certain predefined threshold.

3.1.5 Homogeneity Test

Homogeneity requires that variations in climate time series be due to variations in climatic factors only (Agular *et al.,* 2003). Variations caused by non-climatic factors may hide the true signal and thus bias the conclusions of studies. Furthermore, precipitation measurements are particularly susceptible to irregularities that may affect the analysis of extreme precipitation events (Costa and Soares, 2009). It is for this reason that basic homogeneity testing should be performed before using long time datasets.

Methods for the assessment of the homogeneity of observed data have been proposed by several authors. These methods include double-mass curve analysis (Kohler, 1949) Buishand range test (Buishand, 1982), standard normal homogeneity test (Alexanderson, 1986) and Multiple linear regression (Vincent, 1990). Peterson, *et al.*, (1998) have given detailed discussion on these and more methods in their review paper.

In this study homogeneity test was done using the single mass curve. This test involves plotting cumulative values of climatological records against time where a homogeneous record is indicated by a straight line. Heterogeneity is indicated by the existence of a shift in the cumulative line due to a shift in the mean.

3.2 Methodology

This section describes the methods which were used to achieve the objectives of the study which include determination of the space-time patterns of past and present temperature and rainfall extremes over Kenya, determination of the skill of CORDEX models and determination of future climate patterns of temperature and rainfall extremes over Kenya.

3.2.1 Determination of the space-time patterns of past and present temperature and rainfall extremes

The methods adopted in this study to examine space-time patterns of past and present temperature extremes included spatial plots of climate indices at specific locations and trend analysis of the climate indices.

Table 2 shows a list of 10 core indices from ETCCDI which were used in this study to analyze

trends in extremes in temperature and precipitation. The formulas for calculating each of the indices are given in Table 3. It is worth to note that indices based on percentile thresholds normally capture, uniformly, the extremes in different climatic zones as is the case for Kenya. The spatial maps of the temperature and rainfall trends over Kenya were produced to show the spatial distribution in the trends of these indices.

Table 2 : List of ETCCDI Core Climate Indices Used in this Study (Source: Zhang and Yang, 2004)

ID	Indicator name	Definitions	UNITS
TMAXmean	Mean Tmax	Annual mean maximum temperature	°C
TMINmean	Mean Tmin	Annual mean minimum temperature	°C
TXx	Max Tmax	Monthly maximum value of daily maximum temp	°C
TNx	Max Tmin	Monthly maximum value of daily minimum temp	°C
DTR	Diurnal temperature range	Monthly mean difference between TX and TN	°C
CDD	Consecutive dry days	Maximum number of consecutive days with RR<1 mm	Days
CWD	Consecutive wet days	Maximum number of consecutive days with RR >=1 mm	Days
R99p	Extremely wet days	Annual total PRCP when RR > 99th percentile	mm
PRCPTOT	Annual total wet-day precipitation	Annual total PRCP in wet days (RR >=1 mm)	mm

Table 3: List of the Climate Indices used in this Study and their corresponding formulas (Source: Zhang and Yang, 2004)

ID	Expression
TXx	Let TX_x be the daily maximum temperatures in month *k*, period *j*. The maximum daily maximum temperature of each month is then: $TX_{xkj}=\max(TX_{xkj})$
TNx	Let TN_x be the daily minimum temperatures in month *k*, period *j*. The maximum daily minimum temperature of each month is then: $TN_{xkj}=\max(TN_{xkj})$
DTR	Let TX_{ij} and TN_{ij} be the daily maximum and minimum temperature respectively on day *i* in period *j*. If *i* represents the number of days in *j*, then: $DTR=\sum_{i=1}^{N}\frac{(Tx_{ij}-Tn_{ij})}{N}$
CDD	Let RR_{ij} be the daily precipitation amount on day *i* in period *j*. Count the largest number of consecutive days where: $RR_{ij} < 1mm$
CWD	Let RR_{ij} be the daily precipitation amount on day *i* in period *j*. Count the largest number of consecutive days where: $RR_{ij} \geq 1mm$
R95p	Let RR_{wj} be the daily precipitation amount on a wet day *w (RR ≥ 1.0mm)* in period *i* and let $RR_{wn}95$ be the 95th percentile of precipitation on wet days in the 1961-1990 period. If *W* represents the number of wet days in the period, then: $R95P_j=\sum_{w=1}^{W}RR_{wj}, \quad where\ RR_{wj}>RR_{wn}95$
R99p	Let RR_{wj} be the daily precipitation amount on a wet day *w (RR ≥ 1.0mm)* in period *i* and let $RR_{wn}99$ be the 99th percentile of precipitation on wet days in the 1961-1990 period. If *W* represents the number of wet days in the period, then: $R99P_j=\sum_{w=1}^{W}RR_{wj}, \quad where\ RR_{wj}>RR_{wn}99P$
PRCPTOT	Let RR_{ij} be the daily precipitation amount on day *i* in period *j*. If *i* represents the number of days in *j*, then $PRCPTOT_j=\sum_{i=1}^{I}RR_{ij}$

3.2.1.1 Estimating Magnitude of Trend

The magnitude of the slope was determined through Sen's slope estimator (Sen, 1968) method. This method has been used to determine the magnitude of slopes by several authors (e.g., Partal and Kahya, 2006). It assumes a linear trend in the time series. This method, first, involves calculation of slopes (Z_i) of all data pairs by Equation (1),

$$Z_i=\frac{x_i-x_k}{i-k} \quad for\ i=1,2,\ldots,N \qquad \ldots\ldots\ldots\ldots\ldots\ldots\ldots\ldots\ldots\ldots\ldots\ldots\ldots\ldots\ldots\ldots(1)$$

In Equation (1), N is the number of data points; x_i and x_k are observed data values at time i and k ($i > k$), respectively. The median of these N values of Z_i is the Sen's estimator of slope, β. It is calculated using Equation (2);

$$\beta = \begin{cases} Z_{\frac{N+1}{2}} & N\ is\ odd \\ \frac{1}{2}\left(Z_{\frac{N}{2}} + Z_{\frac{N+2}{2}}\right) & N\ is\ even \end{cases} \quad \text{.....(2)}$$

A positive value of β indicates an upward (increasing) trend and a negative value indicates a downward (decreasing) trend in the time series. The significance was determined by Equation (3),

$$C_\alpha = Z_{1-\alpha/2}\sqrt{Var(Z_i)} \quad \text{.....(3)}$$

In Equation (3) C_α is the confidence interval, $Z_{1-\alpha/2}$ is obtained from the standard normal distribution table and $Var(Z_i)$ is the variance of the slopes. In this study the confidence interval was computed at α = 0.05 significance level.

3.2.2 Assessment of Model Skill in Simulating Observed Temperature and Precipitation Extremes over Kenya

In this section, methods for assessing the model skill in simulating the observed changes are briefly described. These include spatial plots, model bias, simple correlation analysis and time series plots during MAM, JJA and OND seasons. The models together with the ensembles were then used to analyze future extremes in temperature and rainfall over Kenya.

3.2.2.1 Spatial plots of Rainfall and Temperature

Spatial plots of rainfall and temperature can be used to assess how the models simulate the spatial variability of rainfall and temperature across the study area. Firstly, spatial plots of seasonal climatology, for example MAM, JJA and OND, were plotted to determine how the models simulate the large scale systems, such as ITCZ and seasonal migration of the overhead sun, that affect rainfall over the study area. Secondly, spatial plots were generated during years when strong (with a ±1.5 to ±1.9 SST anomaly), moderate (with a ±1.0 to ±1.4 SST anomaly) and weak (with a ±0.5 to ±0.9 SST anomaly) El Niño as well as La Niña episodes was

experienced. This was done so as to analyze how the models simulate rainfall resulting from ENSO signals over the study area.

3.2.2.2 Difference Plots

The difference between each of the CORDEX models and the observed was calculated and used to assess the average deviations of model simulations from the observed. The difference value of a model is the expected value of the model minus the observed. The difference values (Diff) were calculated and plotted spatially over the study area for the three seasons, MAM, JJA and OND over the 1971 to 2000 climatology period. It is given by Equation (4);

$$Diff = Y - X \dots\dots\dots\dots\dots\dots\dots\dots\dots\dots\dots\dots\dots\dots\dots\dots\dots\dots\dots\dots\dots\dots\dots\dots\dots\dots\dots\dots\dots\dots (4)$$

In Equation 4, Y and X are the average seasonal model simulations and observed data respectively and the sample considered was thirty years (*N=30*). A positive value indicates that the model on average over-estimates the observed while the reverse is true.

3.2.2.3 Correlation Analysis

The simple correlation coefficient can be used to measure the level of association between two variables. In this study, it was used to assess the level of association between the observed values and the model outputs. A simple correlation coefficient of 1.0 and -1.0 denotes a perfect positive (direct) and negative (inverse) linear relationship in the observed and predicted values, respectively, while a correlation coefficient equal to 0.0 represents no association between the two variables. Biases may still occur with a perfect correlation coefficient because the coefficient is normalized by the overall mean of each variable whereas low values of the coefficient may result due to non-linear relationships (Bosire, 2012). The simple correlation coefficient may be given by Equation (5);

$$r = \frac{\frac{1}{N}\sum_{t=1}^{N}(X_t - \bar{X})(Y_t - \bar{Y})}{\sqrt{\frac{1}{N}\{\sum_{t=1}^{N}(X_t - \bar{X})^2\}\{\sum_{t=1}^{N}(Y_t - \bar{Y})^2\}}} \dots\dots\dots\dots\dots\dots\dots\dots\dots\dots\dots\dots\dots\dots\dots (5)$$

In Equation (5), X_t and $Y_t$are observed and model outputs at time t, and $\bar{X}$ and $\bar{Y}$ arithmetic means of $X_t$and $Y_t$at time t respectively. N is the record length.

Estimation of the statistical significance of *r* was done through the use of student t-test given by

the Equation (6);

$$t_{N-2} = r\sqrt{\frac{N-2}{1-r^2}} \dots \dots (6)$$

In equation (6), t_{N-2} is the student t-distribution value with $N - 2$ degrees of freedom and N is the total number of observations.

3.2.2.4 Time Series Plots

Time series plots are usually done to assess the temporal evolutions of variables. In this study, the annual cycle of rainfall and temperature were plotted for the observed and the individual models during the three seasons (MAM, JJA, and OND) to assess how they capture the variability. Further, time series of year to year variability were also done for the same seasons during the climatology base period of 1971 to 2000.

3.2.3 Analysis of Future Extremes in Rainfall and Temperature from CORDEX Model Outputs over Kenya

Future climate projections from CORDEX from all the models were analyzed for extreme events over Kenya. Table 4 shows a total of eight model datasets which are available from the CORDEX Africa project with different calendar days. All the eight models were used to generate an ensemble. Extreme climate indices which have been implemented in Climate Data Operators (CDO) (Schulzweida, *et al.*, 2006) were used to analyze the extreme climate events in the model projections for RCP4.5 scenario during the period 2021-2050. The description of the representative concentration pathways scenarios are shown in Table 5.

Table 4: List of the General Climate Models Downscaled in the CORDEX Africa Project. The standard calendar has 365.25 days in a year.

	Institute Name	**GCM Name**	**Calendar**
1	CCCma (Canada)	CanESM2	365 days
2	CNRM-CERFACS (France)	CNRM-CM5	standard
3	MOHC (UK)	HadGEM2-ES	360 days
4	NCC (Norway)	NorESM1-M	365 days
5	ICHEC (Europe)	EC-EARTH	standard
6	MIROC (Japan)	MIROC5	365 days
7	NOAA-GFDL (USA)	GFDL-ESM2M	365 days
8	MPI-M (Germany)	MPI-ESM-LR	standard

Table 5: Description of Different RCP Scenarios for the Fifth Assessment Report (AR5) (Source: Chaturvedi, *et al.*, 2012)

RCP	Description
RCP2.6	Radiative forcing level first reaches a value of around 3.1 W/m^2 returning to 2.6 W/m^2 by 2100. Under this scenario greenhouse gas emissions and emissions of air pollutants are reduced substantially over time.
RCP4.5	Stabilization scenario where total radiative forcing is stabilized before 2100 by employing a range of technologies and strategies for reducing greenhouse gas emissions.
RCP6.0	Stabilization scenario where total radiative forcing is stabilized after 2100 without overshoot by employing a range of technologies and strategies for reducing greenhouse gas emissions.
RCP8.5	Characterized by increasing greenhouse gas emissions over time representative of scenarios in the literature leading to high greenhouse gas concentration levels.

3.2.3.1 Climate Indices

Since the model projections are in grid format, three climate indices: frequency of wet days and extremely wet days and frequency of days warmer than the 90th percentile were calculated at each grid point using Climate Data Operators (CDO) tool for both temperature and precipitation. Spatial maps of the resulting extreme indices were then plotted using Ferret software (Hankin *et al.*, 2007) to show the future spatial variability of climate extremes in Kenya.

The frequency of wet days (FWD) for the reference period (1961-1990) and the future (2021-2050) were calculated together with their differences as percentages and spatially plotted to assess the percentage increase or decrease in the frequency of wet days. A wet day is defined as any day where precipitation is greater than one millimeter (Hankin *et al.*, 2007). The count of a wet day for the whole dataset is given by Expression (7),

$$Q_i = \begin{cases} 1, y_i \geq 1mm \\ 0, y_i < 1mm \end{cases} \quad \text{......(7)}$$

In Expression (7) Q_i is a given day and y_i is the precipitation simulated by the models in a given day i. Frequency of Wet Day (FWD) is given by summing Expression (8);

$$FWD = \sum_{i=1}^{n} Q_i \quad \ldots\ldots\ldots\ldots\ldots\ldots\ldots\ldots\ldots\ldots\ldots\ldots\ldots\ldots\ldots\ldots\ldots\ldots\ldots\ldots\ldots\ldots\ldots\ldots\ldots\ldots\ldots\ldots\ldots\ldots\ldots\ldots\ldots\ldots.. (8)$$

The frequency of extreme rainfall days (R99P) was also calculated for the future (2021-2050) as the number of days which had rainfall greater than the 99th percentile of the baseline (1961-1990) threshold. Similar methodology to Expressions (7) and (8) was used with a threshold of 99th percentile of the baseline period.

The frequency of days with temperature warmer than the 90th percentile (TX90P) calculated for minimum and maximum temperature in the baseline period (1961-1990) and the future (2021-2050). The threshold was used to assess the number of days in the future period (2021-2050), during MAM, JJA and OND seasons, which had temperature above the 90th percentile of the baseline (1961-1990) threshold. Similar methodology to Expressions (7) and (8) were used with a threshold of 90th percentile of the baseline period.

CHAPTER FOUR

4.0 RESULTS AND DISCUSSIONS

4.1 Outline

This chapter presents the discussion and results obtained from the various methods used to achieve the specific objectives of the study. The results include observed spatial and temporal patterns of extremes, skill of CORDEX models in simulating observed temperature and rainfall, and the analyzed extremes in temperature and rainfall from CORDEX models. Before presenting the results, a brief highlight on the data quality is presented.

4.2 Homogeneity Test

The cumulative plots of annual rainfall for two selected stations are shown in Figure 4. The figures show no major shifts from the general trend during the period 1960 to 2012 suggesting that the rainfall from these stations were homogeneous and fit for use in the analysis.

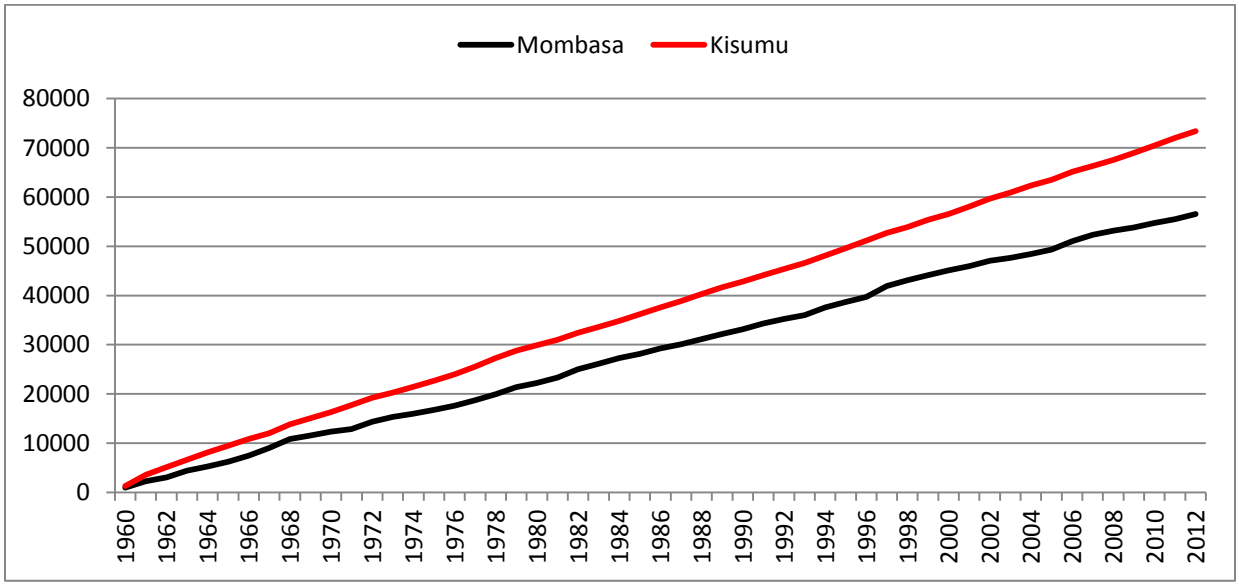

Figure 4: Cumulative plots of annual rainfall (in mm) showing homogeneity of the rainfall data from two stations in Kenya. Red line represents Kisumu, the black line represents Mombasa.

4.3 Spatial and Temporal Distribution of the Observed Climate Extreme Indices

This section presents the results of the spatial and temporal distribution of the observed climate indices.

4.3.1 Trends in Temperature indices

The trends of temperature indices for fourteen stations in the study area are shown in Table 6. The red values indicate significant trends at 5% significant level. Trends were not calculated for those stations that had 25% missing data records and these were indicated with Not Available (NA). The indices with highest and lowest number of stations which had significant trends were monthly maximum value of daily maximum temperature and annual mean minimum temperature respectively. Positive trends in all the temperature indices are more pronounced compared to the negative trends suggesting an overall warming in most parts of the country. The time series, trend and the statistical scores of temperature indices are presented in Figure 5.

Table 6: Trends in the Temperature Indices (1970-2008) at Various Stations in Kenya. Values Significant at 5% Level are Indicated in Red. NA Represents Stations with 25% Missing Data.

Zones	Stations	TMAXmean	TMINmean	TXX	TNX	DTR
1	Lodwar	**0.027**	**0.017**	**0.032**	0.016	0.008
2	Moyale	NA	NA	NA	NA	NA
3	Mandera	0.016	**0.029**	**0.033**	-0.018	-0.009
4	Wajir	NA	NA	NA	NA	NA
5	Kakamega	NA	NA	NA	NA	NA
6	Nakuru	NA	NA	NA	NA	NA
7	Dagoretti	**0.013**	**0.044**	**0.026**	**0.059**	**-0.033**
8	Garissa	-0.01	0.025	0.07	0.015	**-0.038**
9	Voi	0.01	0.031	0	0.007	-0.021
10	Mombasa	**0.012**	-0.013	0.027	0	**0.029**
11	Lamu	**0.039**	**-0.037**	0.067	**-0.041**	**0.077**
12	Kisumu	-0.007	0.007	-0.047	-0.038	-0.012
13	Nanyuki	NA	NA	NA	NA	NA
14	Marsabit	0.018	**0.017**	0.051	**0.038**	0.006

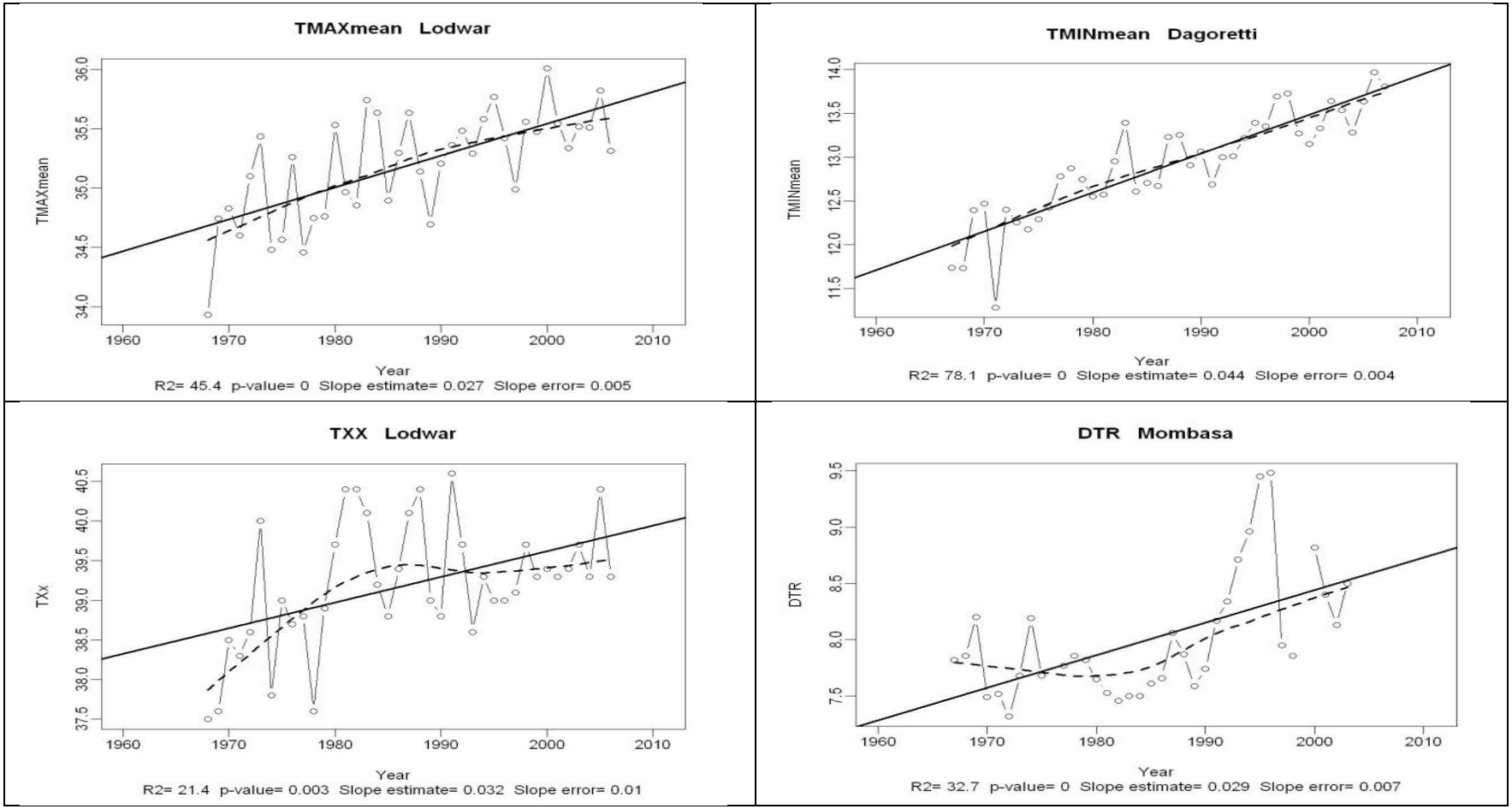

Figure 5: Time series of temperature indices (1970-2008) for selected stations. Annual mean maximum temperature (top-left), annual mean minimum temperature (top-right), monthly maximum value of daily maximum temp (bottom-left) and diurnal temperature range for selected stations in Kenya. The solid line indicates the trend line; the dotted line indicates the moving average line.

4.3.2 Spatial Distribution of Trends in Temperature Indices

The spatial distribution of trends in temperature extremes between 1970 and 2008 are presented in Figures 6 and 7. The spatial distribution indicates a general warming trend in temperature since 1970 to 2008 over most parts of the country. Negative trends were observed in the western, coast and eastern parts of the country. The coastal parts of the country had the lowest negative trends of annual mean minimum temperature and maximum temperature. In Figure 7, trends in annual mean minimum temperature exhibited positive trends all over Kenya except along the coastal strip. Trends in annual mean maximum temperature exhibited positive trends in Kenya except in the western parts of the country as shown in Figure 7. Positive trends of temperature in places like Nairobi may be attributed to urbanization effect.

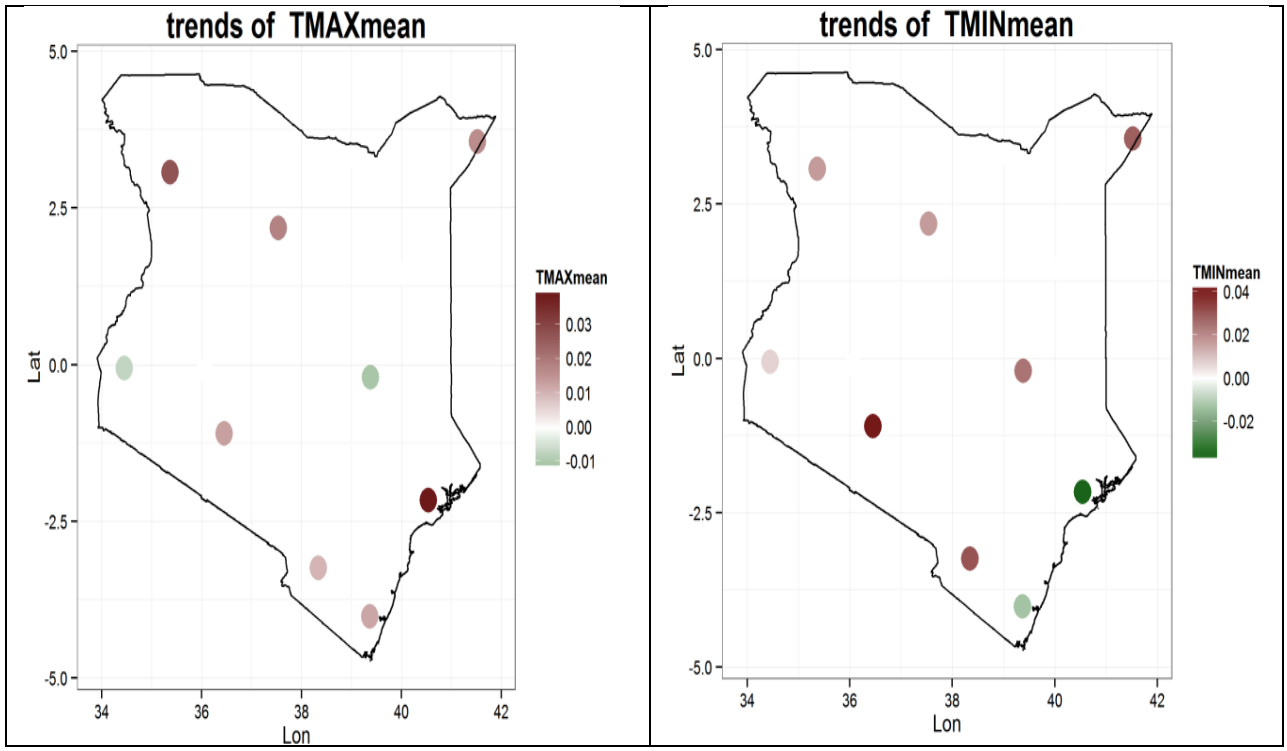

Figure 6: Spatial distribution of trends (1970-2008) in temperature indices over Kenya. The annual mean maximum temperature (left), annual mean minimum temperature (right) are shown Decreasing trends are represented by darker shades of green while increasing trends are represented by darker shades of red. White color represents no trend.

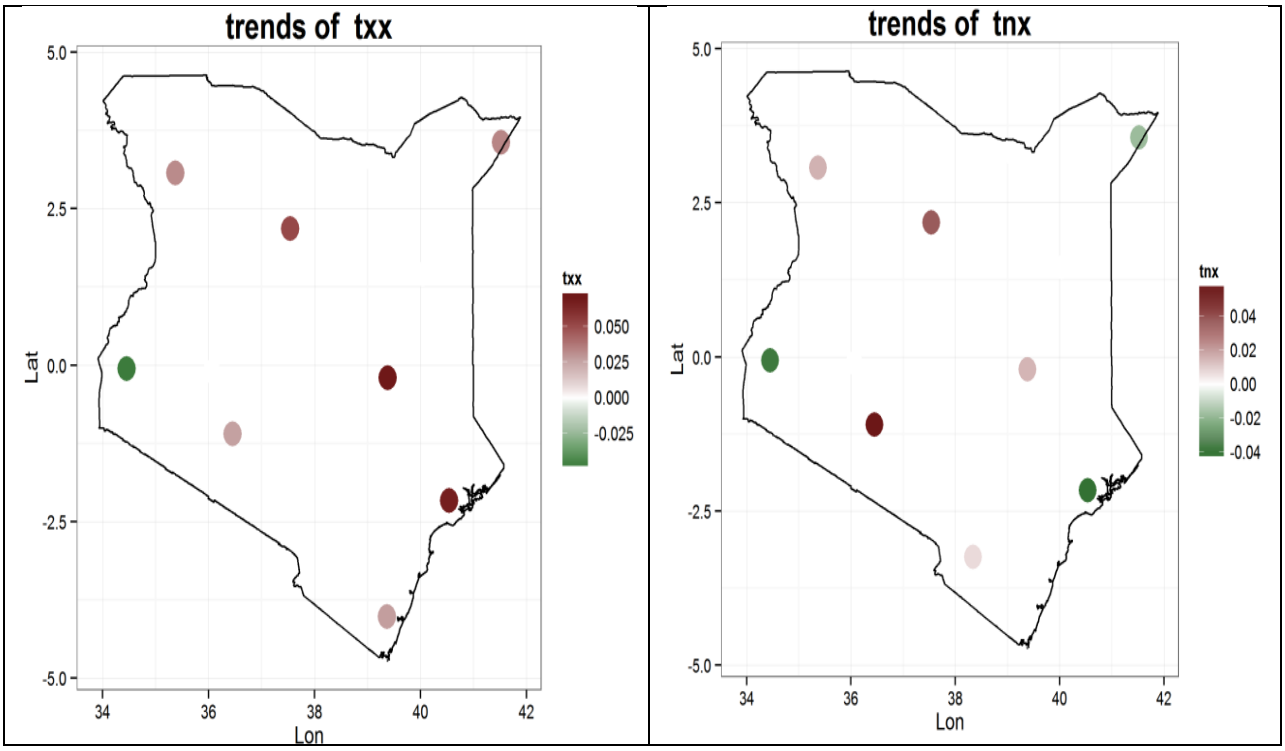

Figure 7: Spatial distribution of trends (1970-2008) in temperature indices over Kenya. The monthly maximum value of daily maximum temp (left) and monthly maximum value of daily minimum temp (right) are shown. Decreasing trends are represented by darker shades of red. White color represents no trend.

4.3.3 Trends in Rainfall indices

The trends of rainfall indices for fourteen stations in the study area are presented in Table 7. The index that had the highest number of stations with significant trends was annual total wet-day precipitation index. Mixed results were observed in the precipitation indices unlike the temperature indices suggesting lack of spatial coherence in precipitation indices similar to other studies (e.g., Omondi *et al.,* 2014). From the table, total annual precipitation has been declining over several stations in Kenya since 1961-2012. Significant increase in total annual precipitation was only observed in Wajir and Marsabit. Conclusive deductions were not able to be drawn from the other precipitation indices due to the low number of stations with significant trends. However, there is an indication that consecutive dry days are increasing over several stations in Kenya.

Figure 8 shows some of the temporal patterns of precipitation indices since 1961-2012 with trend lines and moving average lines superimposed. Statistical scores of the trends have also been

presented. Stations with significant precipitation trends were those that had low p-values, typically less than 0.05.

Table 7: Trends in the Precipitation Indices (1961-2012) at Various Stations over Kenya. Values Significant at 5% Level are Indicated in Red. NA Represents Stations with 25% Missing Data.

Zones	Stations	CDD	CWD	R99p	PRCPTOT
1	Lodwar	-0.491	-0.007	0.535	**-0.958**
2	Moyale	**0.446**	-0.013	-0.736	**-5.091**
3	Mandera	0.318	-0.018	-0.145	-0.352
4	Wajir	**-1.301**	**0.063**	1.062	**4.947**
5	Kakamega	0.033	-0.064	-8.095	-8.521
6	Nakuru	-0.067	-0.022	**1.273**	1.26
7	Dagoretti	0.126	0.005	**-2.79**	**-8.264**
8	Garissa	0.302	-0.013	-0.753	-1.17
9	Voi	-0.014	-0.028	0.041	-2.281
10	Mombasa	0.083	0.021	-0.153	-2.439
11	Lamu	0.042	-0.018	-0.552	-0.263
12	Kisumu	0.172	-0.04	0.324	0.23
13	Nanyuki	-0.012	0.053	0.297	-0.027
14	Marsabit	**-2.335**	**0.125**	-1.015	**6.961**

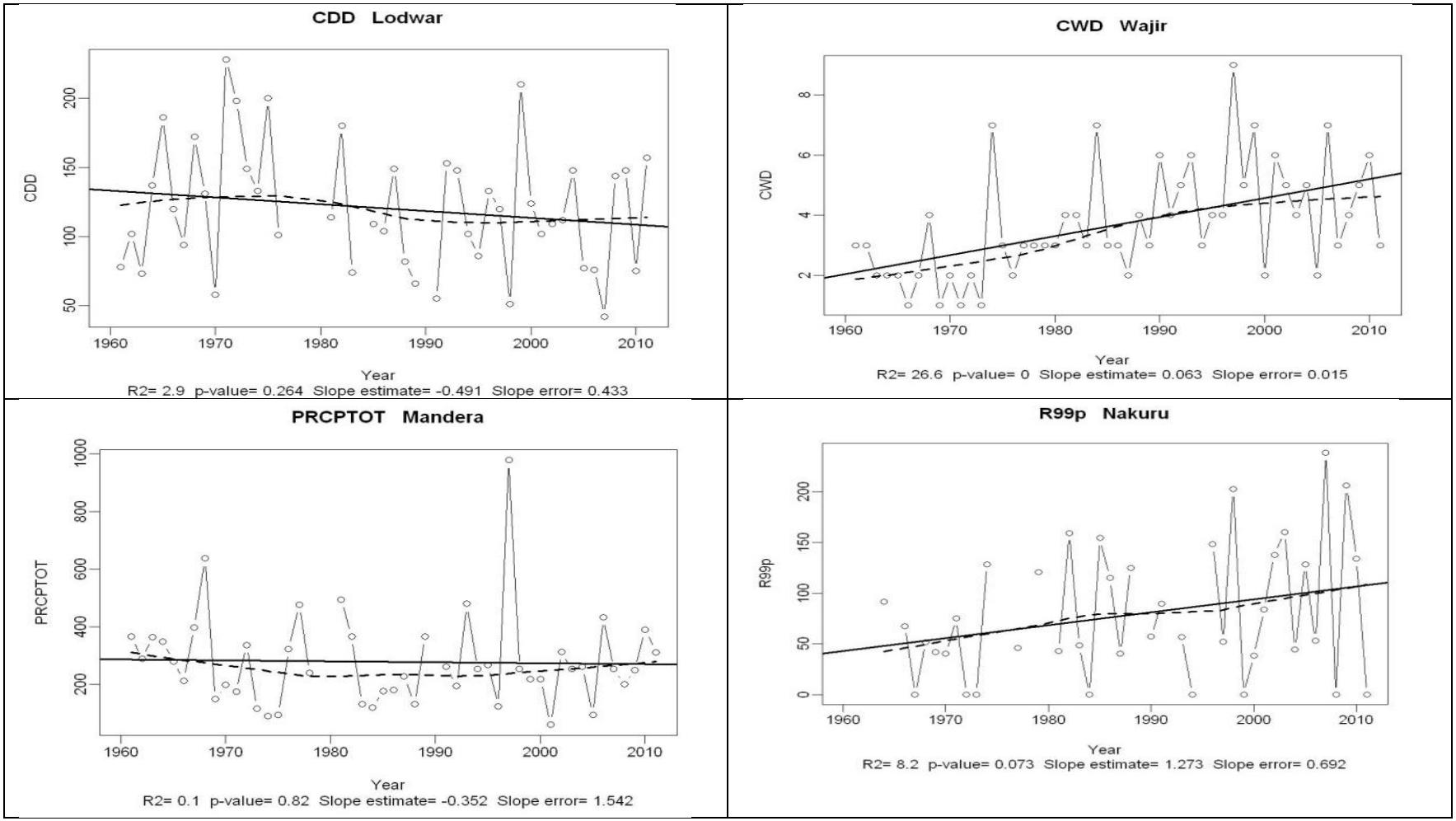

Figure 8: Time series of precipitation indices consecutive dry days (top-left), Consecutive wet days (top-right), annual total wet-day precipitation (bottom-left) and extremely wet days (bottom-right) for selected stations in Kenya. The solid line indicates the trend line; the dotted line is the moving average line.

4.3.4 Spatial Distribution of Trends in Precipitation Indices

The spatial distributions of rainfall extreme indices over Kenya between 1961 and 2012 are presented in Figures 9 and 10. The results of the spatial plots of trends in rainfall indices indicated that consecutive wet days are increasing over several places in Kenya; negative trends were mainly observed in the western parts of Kenya. Total precipitation has increased over northern parts of Kenya, in areas such as Marsabit and Wajir during the period 1961-2012. Decreasing trends of precipitation were observed in Nairobi and western parts of Kenya. The number of consecutive dry days was observed to have decreased over the northern parts of Kenya in areas like Wajir, Marsabit and Lodwar; other parts of the country had low positive or negative trend values. There were no well defined patterns of trends in rainfall indices and this can be attributed to the high spatial variability of rainfall in Kenya.

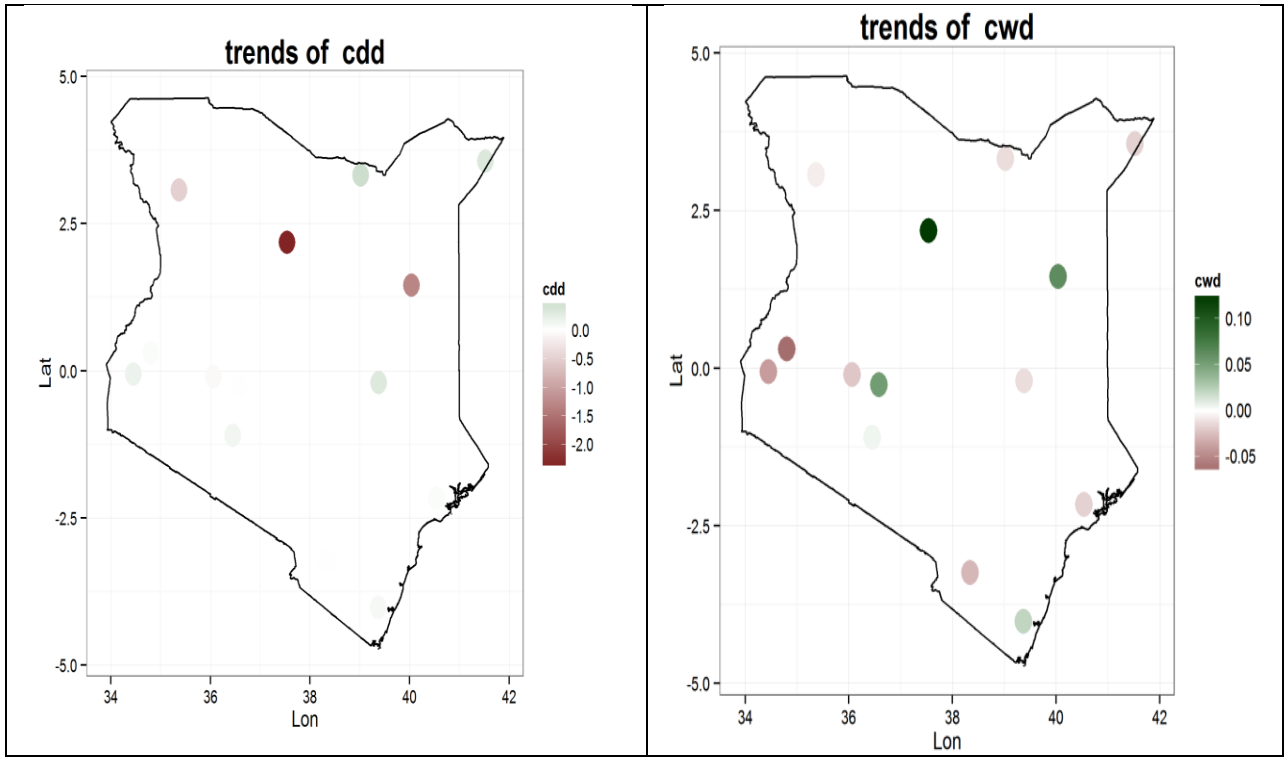

Figure 9: Spatial distribution of trends in precipitation indices over the period 1961-2012. The consecutive dry days (left), consecutive wet days (right) for selected stations in Kenya are shown. Decreasing trends are represented by darker shades of red while increasing trends are represented by darker shades of green. White color represents no trend.

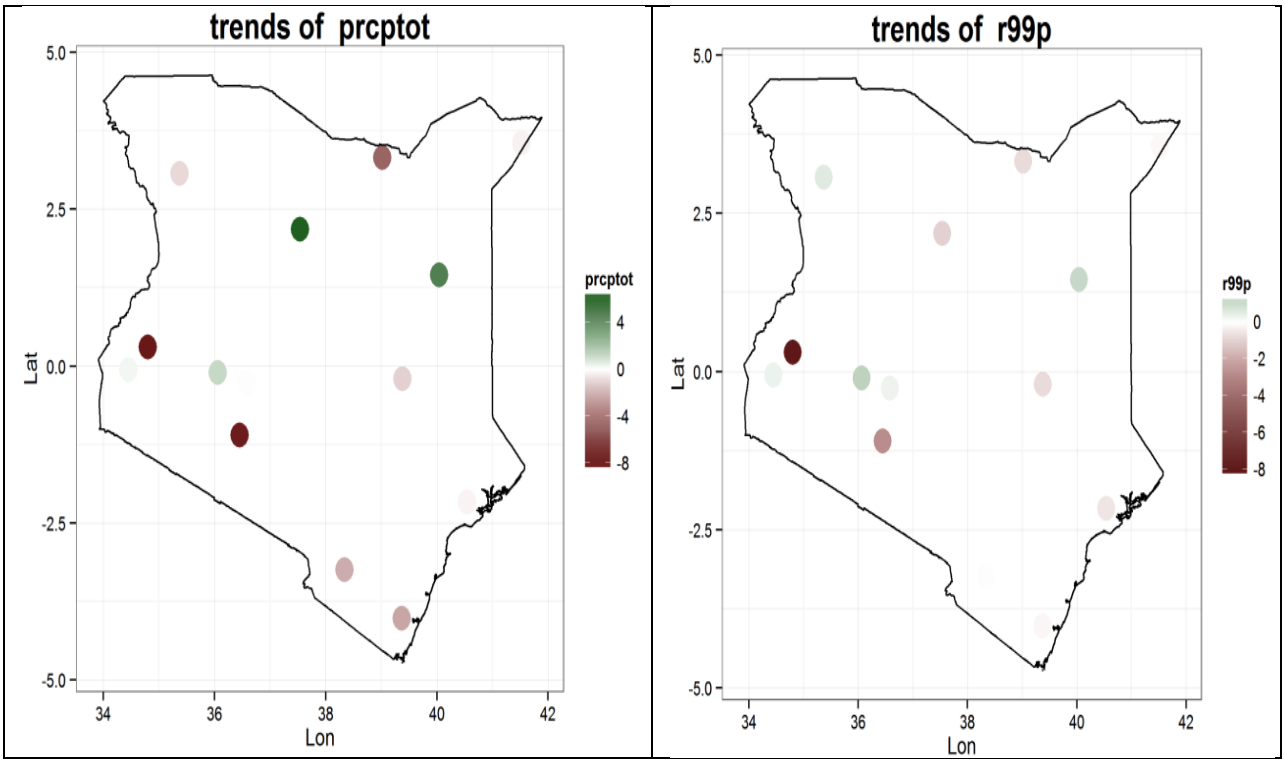

Figure 10: Spatial distribution of trends in precipitation indices over the period 1961-2012. The annual total wet-day precipitation (left) and extremely wet days (right) for selected stations in Kenya. Decreasing trends are represented by darker shades of red while increasing trends are represented by darker shades of green. White color represents no trend.

4.4 Assessment of Model Skill in Simulating the Observed Rainfall and Temperature

4.4.1 Climatology

The observed gridded data and model outputs were plotted to compare how the models simulate the spatial variability of the observed rainfall. The results and discussion of the spatial plots of MAM, JJA and OND seasons for rainfall, as well as for the maximum and minimum temperature, for climatology, ENSO, difference plots and correlation, are presented in the subsequent sections.

4.4.1.1 Rainfall Climatology

The spatial plots of the rainfall climatology of MAM, JJA and OND seasons for the observed (CRU), the eight models and the ensemble (average of all the eight models) is shown in Figures 11, 12 and 13, respectively. In Figure 11, the observed (CRU) shows that rainfall is concentrated

in the western, central and coastal parts of Kenya. This is due to the meso-scale systems and the apparent position of the ITCZ which is usually around the equator in Kenya during MAM. All the eight models and the ensemble are able to simulate the observed rainfall peaks over Mt. Kenya and Mt. Kilimanjaro regions. ICHEC, MIROC, CNRM and MPI models over-estimated rainfall over Mt. Elgon region. All models under-estimated rainfall in the Lake Victoria basin. Under-estimation of rainfall was also evident in several parts of northern Kenya from most models. The similarity in the patterns of rainfall from the models may be due to the lateral and surface boundary conditions from ERA-INTERIM reanalysis. The different schemes employed in the individual models may be the reason why the models are not able to capture the local circulation systems especially in the western parts of the country.

In Figure 12, the observed rainfall distribution is concentrated in the western and coastal parts of the country during the JJA season. This is because the apparent position of the ITCZ has shifted to higher latitudes in the Northern hemisphere hence increased convective activities are located in these latitudes. Most models are able to simulate the observed distribution with the exception of MIROC, CNRM and CCCma. The models, including the ensemble, are still not able to capture the spatial distribution of rainfall in the Lake Victoria basin. This indicates that the models are still not able to replicate the systems around Lake Victoria during the JJA season. The skill is however improved during JJA as compared to MAM since the models are able to simulate the spatial distribution of rainfall during this season. This finding confirms the results by Endris *et al.*, (2013).

The distribution of the observed OND rainfall climatology differs slightly from that of MAM rainfall climatology except for the intensity as shown in Figure 13. This is because the ITCZ is located in the vicinity of the equator in Kenya during OND season. All the models are not able to simulate the observed spatial distribution with high degree of skill especially over mountainous regions. This shows that models are not able to replicate local circulation systems around the mountainous regions.

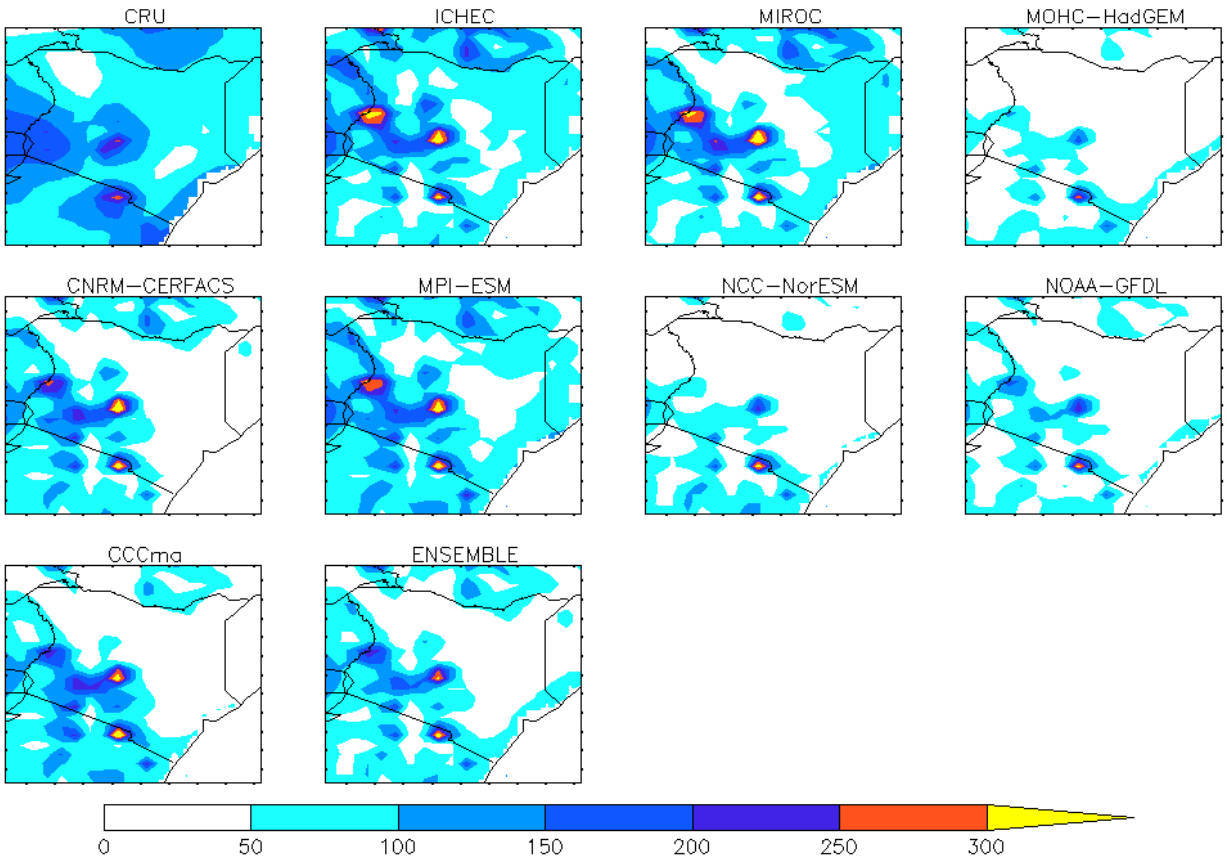

Figure 11: Climatology (1971-2000) of rainfall (in mm) in the observed (CRU), individual CORDEX models and the ensemble over Kenya during the MAM season. High (low) rainfall intensity areas are shown in yellow (white).

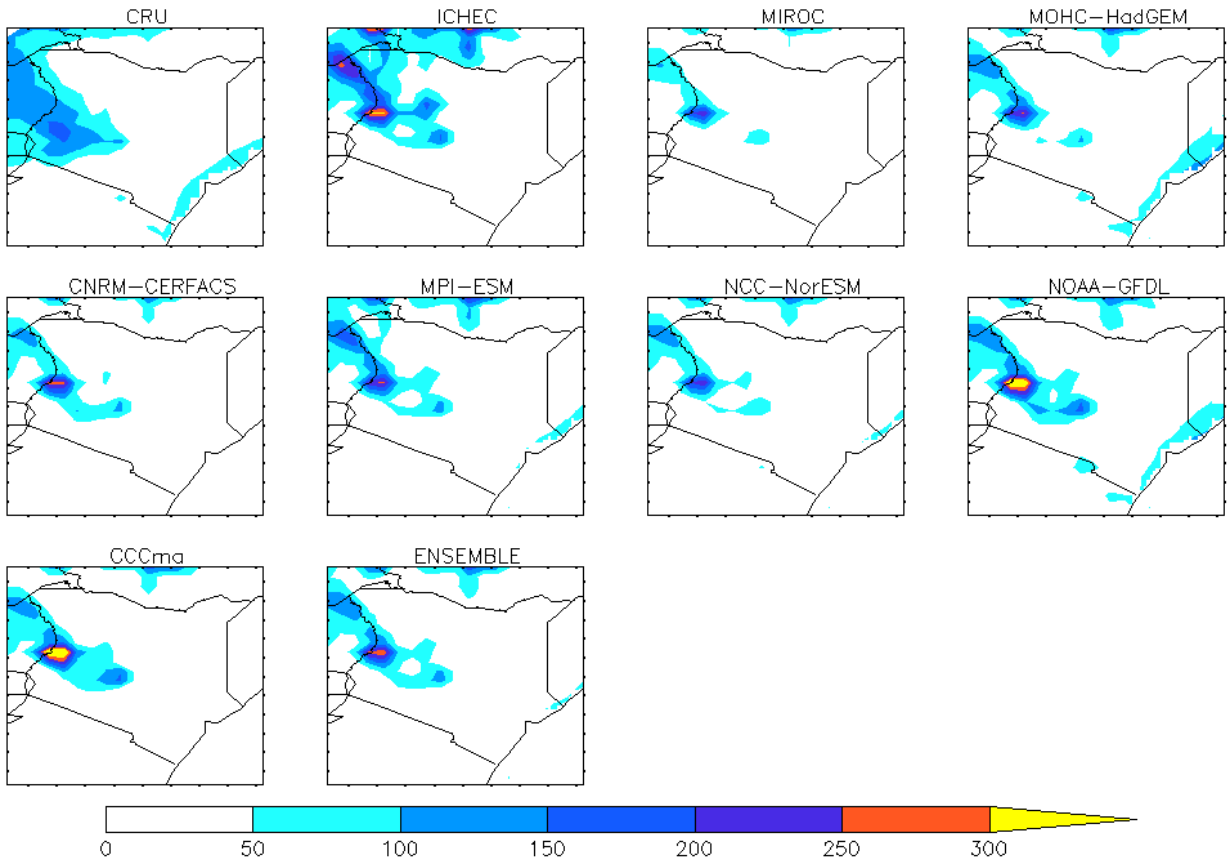

Figure 12: Climatology (1971-2000) of rainfall (in mm) in the observed (CRU), individual CORDEX models and the ensemble over Kenya during the JJA season. High (low) rainfall intensity areas are shown in yellow (white).

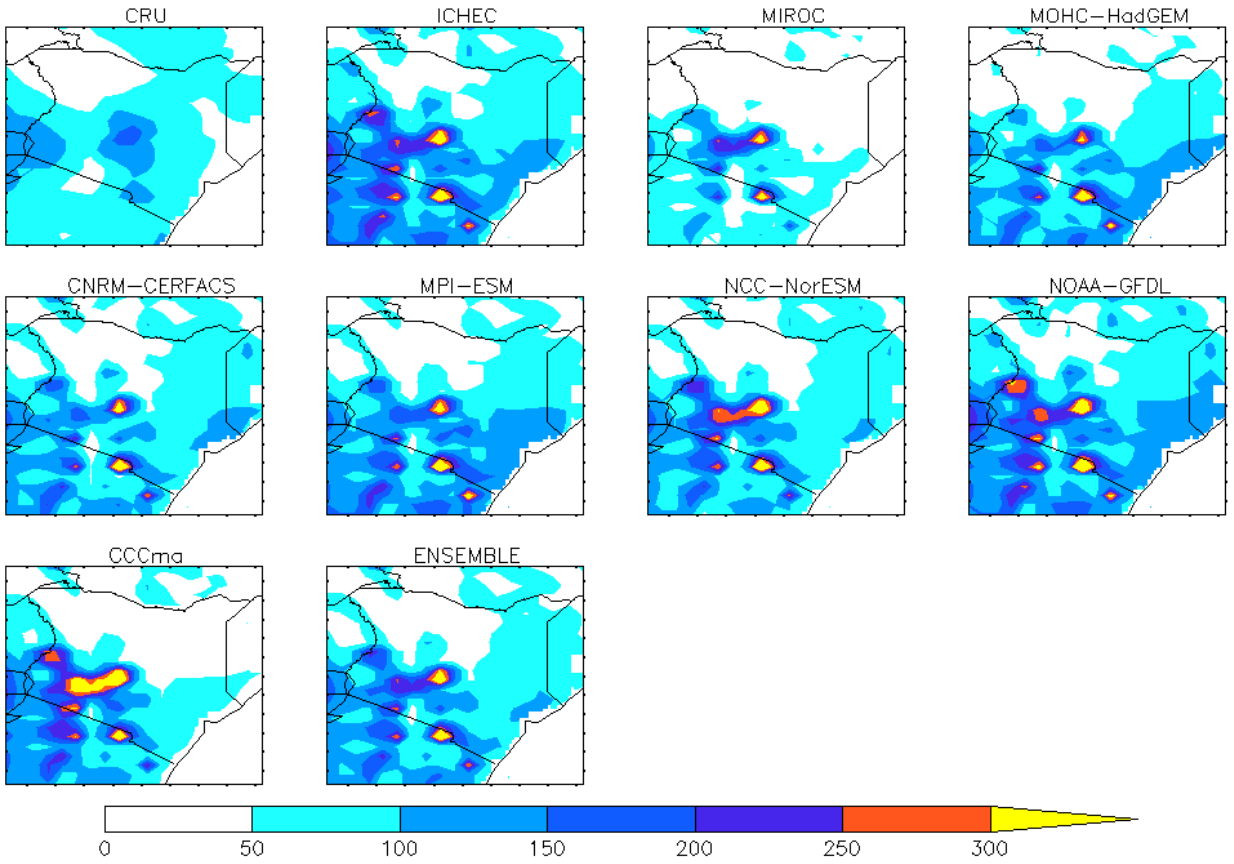

Figure 13: Climatology (1971-2000) of rainfall (in mm) in the observed (CRU), individual CORDEX models and the ensemble over Kenya during the OND season. High (low) rainfall intensity areas are shown in yellow (white).

4.4.1.2 Maximum Temperature Climatology

The spatial distribution of the climatology of the observed maximum temperature for MAM, JJA and OND seasons are shown in Figures 14, 15 and 16, respectively. In Figure 14, all the models are able to simulate the observed spatial distribution of temperature during MAM with some degree of skill. High values of maximum temperatures are mainly concentrated in the northwestern parts, in areas like Lodwar, coastal lowlands and over the northeastern parts of Kenya, for example around Garissa and Wajir. Low maximum temperatures are observed in central parts of Kenya.

The spatial pattern of maximum temperature climatology during JJA is slightly different from that of MAM as shown in Figure 15. Areas of high (temperature ≥ 33°C) maximum temperatures had reduced compared to MAM season whereas low (temperature ≤ 24°C) maximum

temperature areas had increased. This is in relation to the location of the over-head sun which is in the northern hemisphere during the JJA season.

During OND season, the spatial distribution is similar to that during MAM season as shown in Figure 16. The two seasons, MAM and OND, are the seasons where the highest temperatures are usually recorded. The spatial distributions of maximum temperature are attributed to the apparent seasonal movement of the sun.

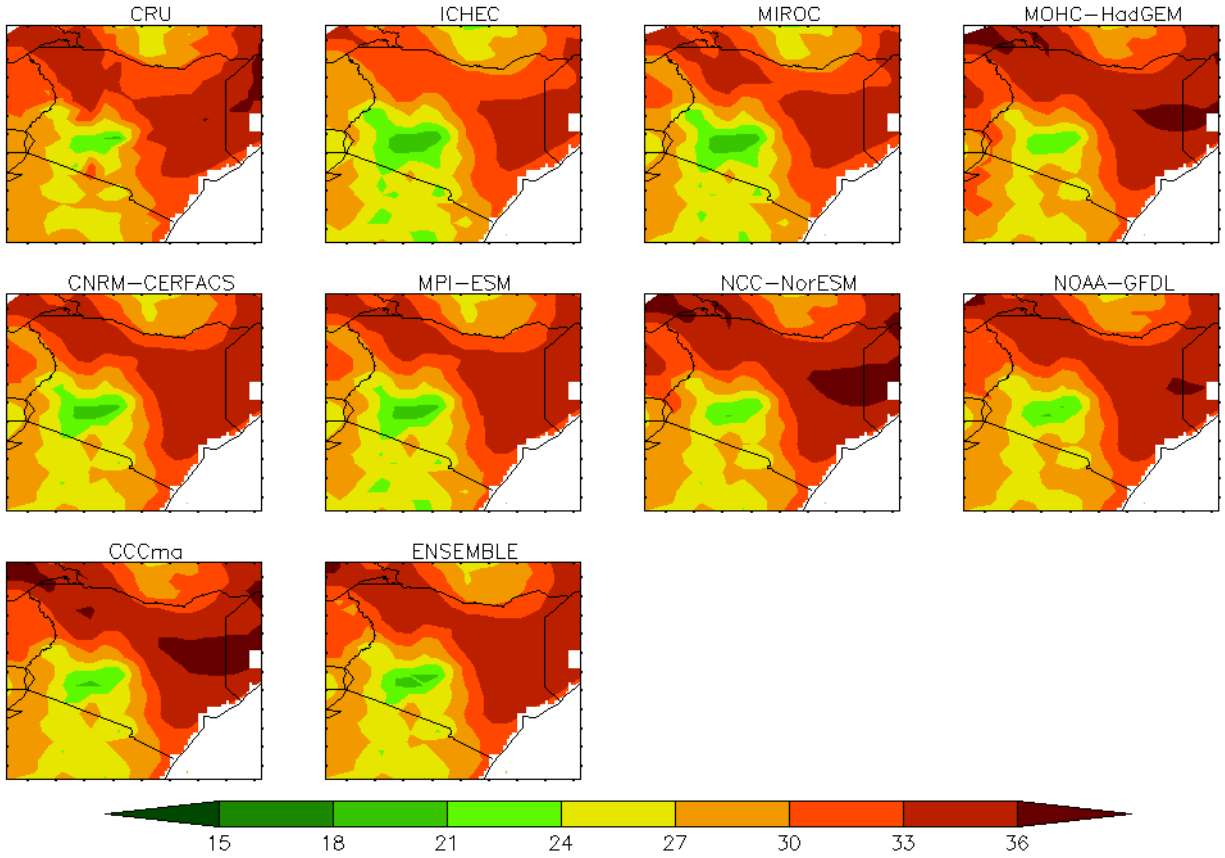

Figure 14: Climatology (1971-2000) of maximum temperature (in °C) in the observed (CRU), individual CORDEX models and the ensemble over Kenya during the MAM season. High (low) temperature areas are shown in dark (green) red.

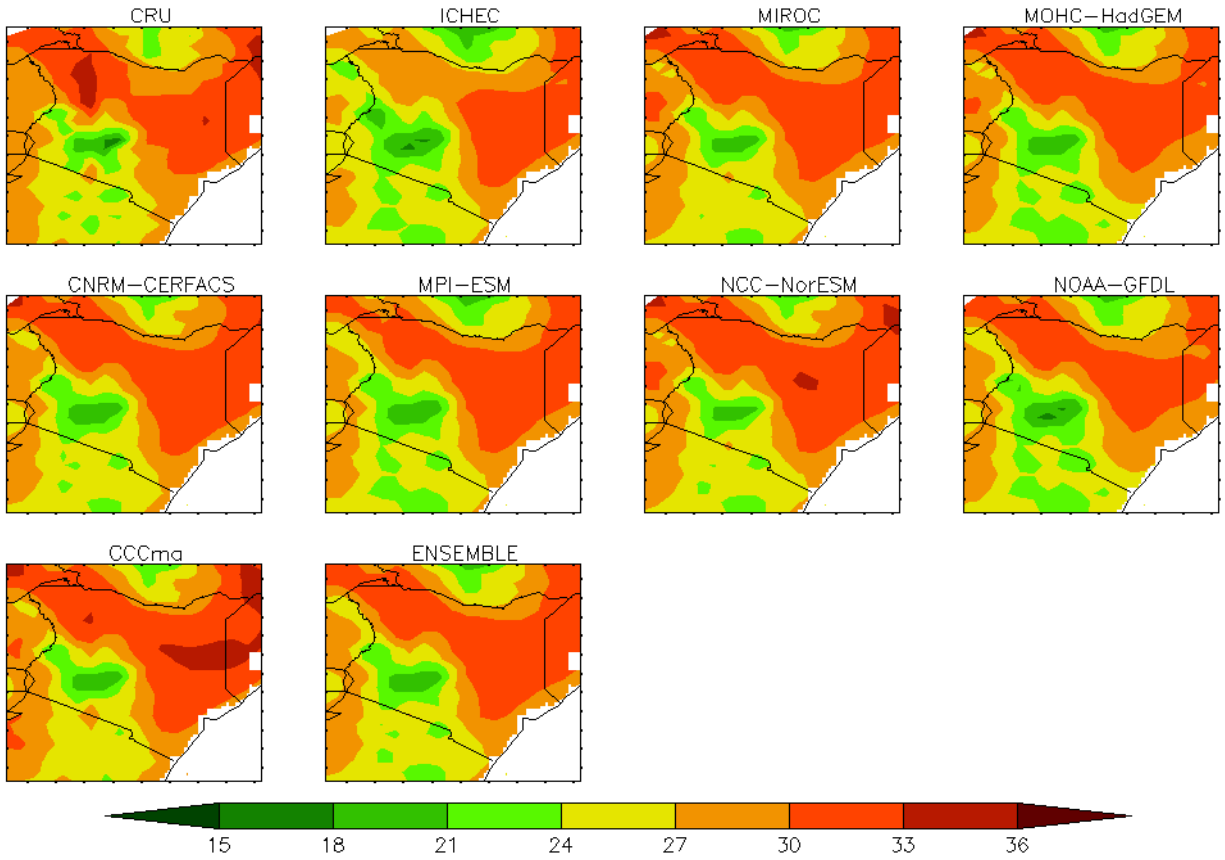

Figure 15: Climatology (1971-2000) of maximum temperature (in °C) in the observed (CRU), individual CORDEX models and the ensemble over Kenya during the JJA season. High (low) temperature areas are shown in dark (green) red.

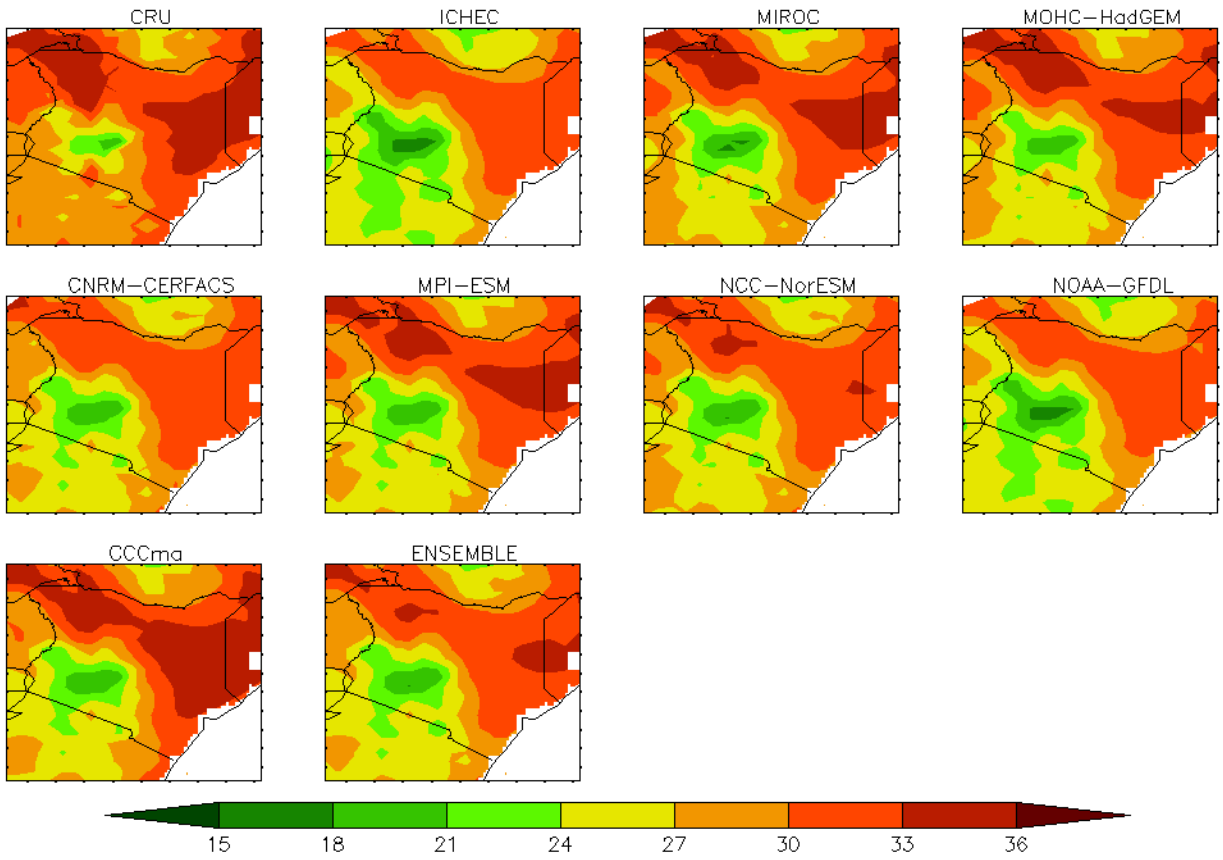

Figure 16: Climatology (1971-2000) of maximum temperature (in °C) in the observed (CRU), individual CORDEX models and the ensemble over Kenya during the OND season. High (low) temperature areas are shown in dark (green) red.

4.4.1.3 Minimum Temperature Climatology

The spatial distribution of the climatology of the observed minimum temperature for MAM, JJA and OND seasons are shown in Figures 17, 18 and 19, respectively. The models and the ensemble are able to simulate areas of low and high minimum temperature in the study region with high degree of skill during all the seasons. In Figure 17, the models which showed slightly different patterns from the observed (CRU) were ICHEC, CNRM and CCCma.

In Figure 18, low values of minimum temperature areas had increased while high values of minimum temperature areas had decreased over Kenya. The patterns are in response to the apparent seasonal shift of the sun.

In Figure 19, the only models which were able to simulate the observed distribution of temperature during the OND season were, MIROC, HadGEM, MPI, NCC and the ensemble.

These patterns are also in response to the effect of the sun.

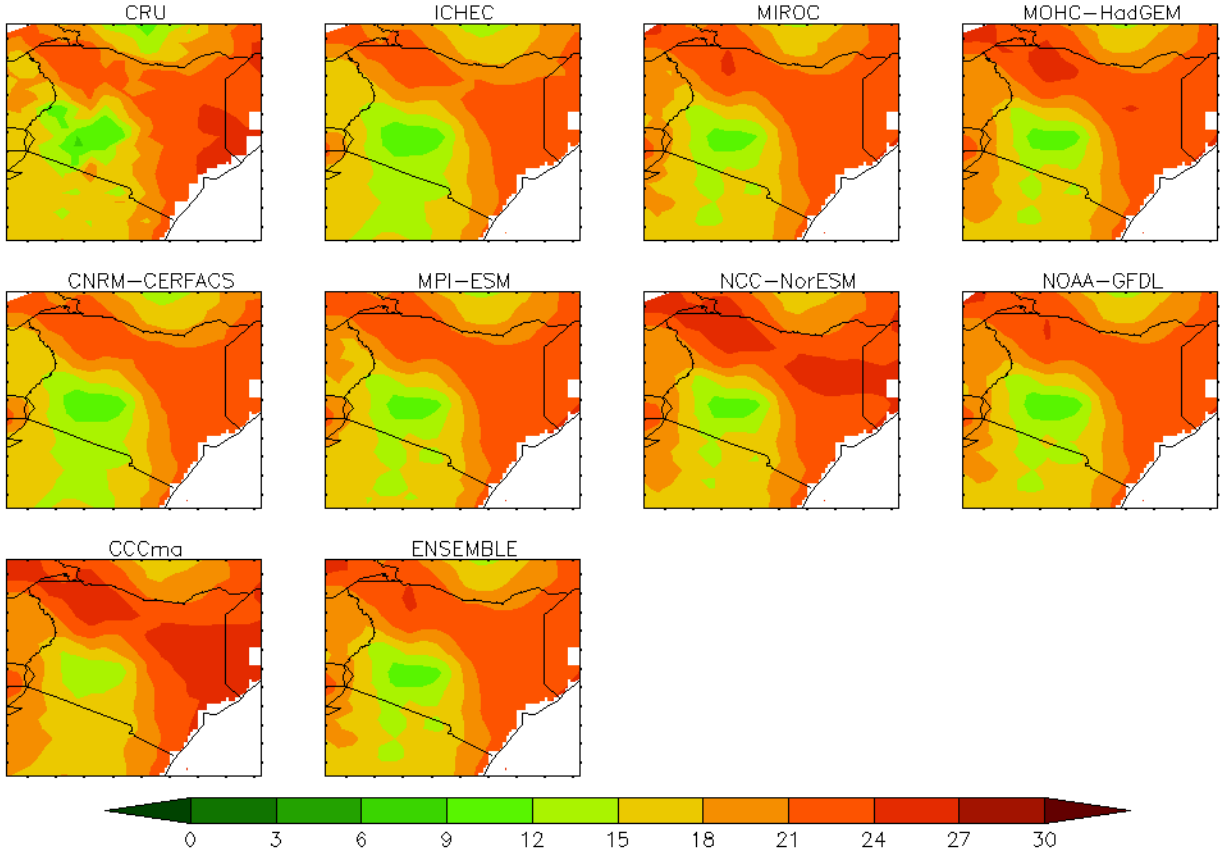

Figure 17: Climatology (1971-2000) of minimum temperature (in °C) in the observed (CRU), individual CORDEX models and the ensemble over Kenya during the MAM season. High (low) temperature areas are shown in dark (green) red.

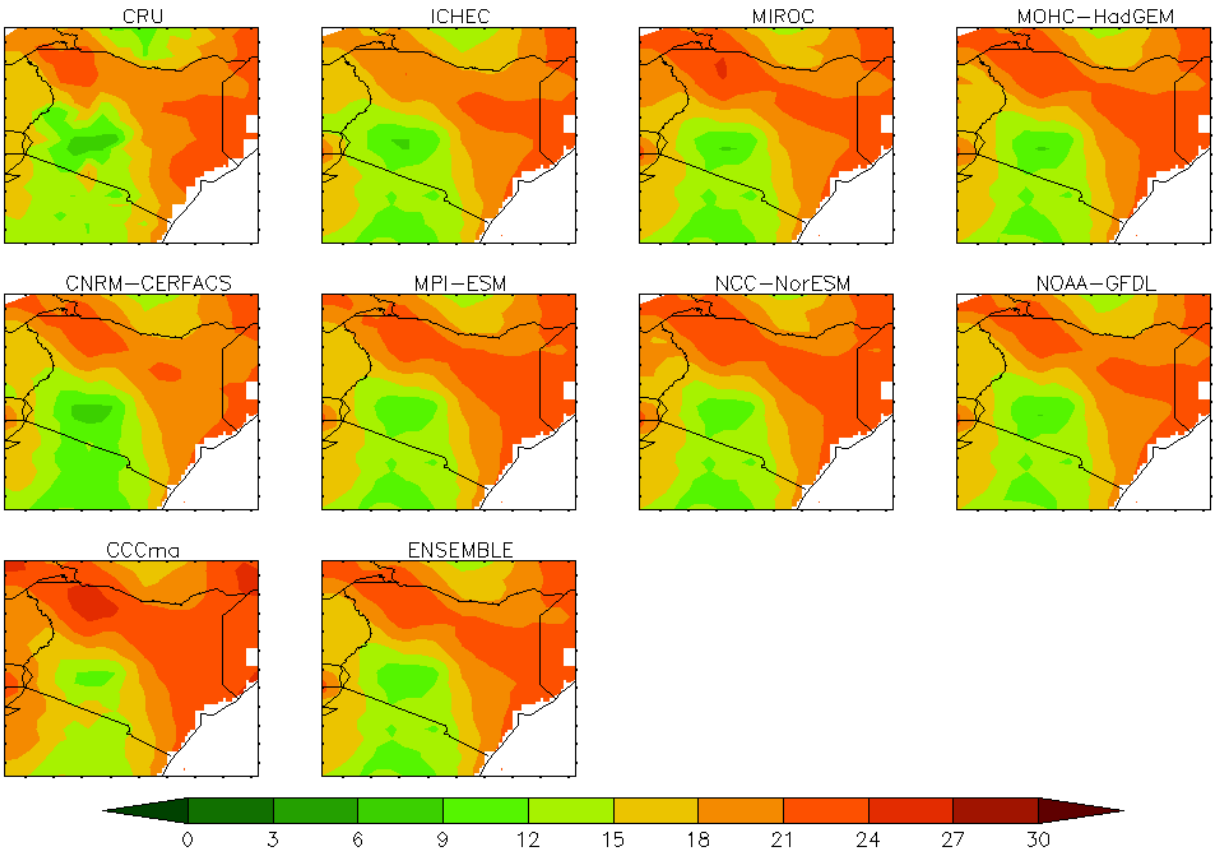

Figure 18: Climatology (1971-2000) of minimum temperature (in °C) in the observed (CRU), individual CORDEX models and the ensemble over Kenya during the JJA season. High (low) temperature areas are shown in dark (green) red.

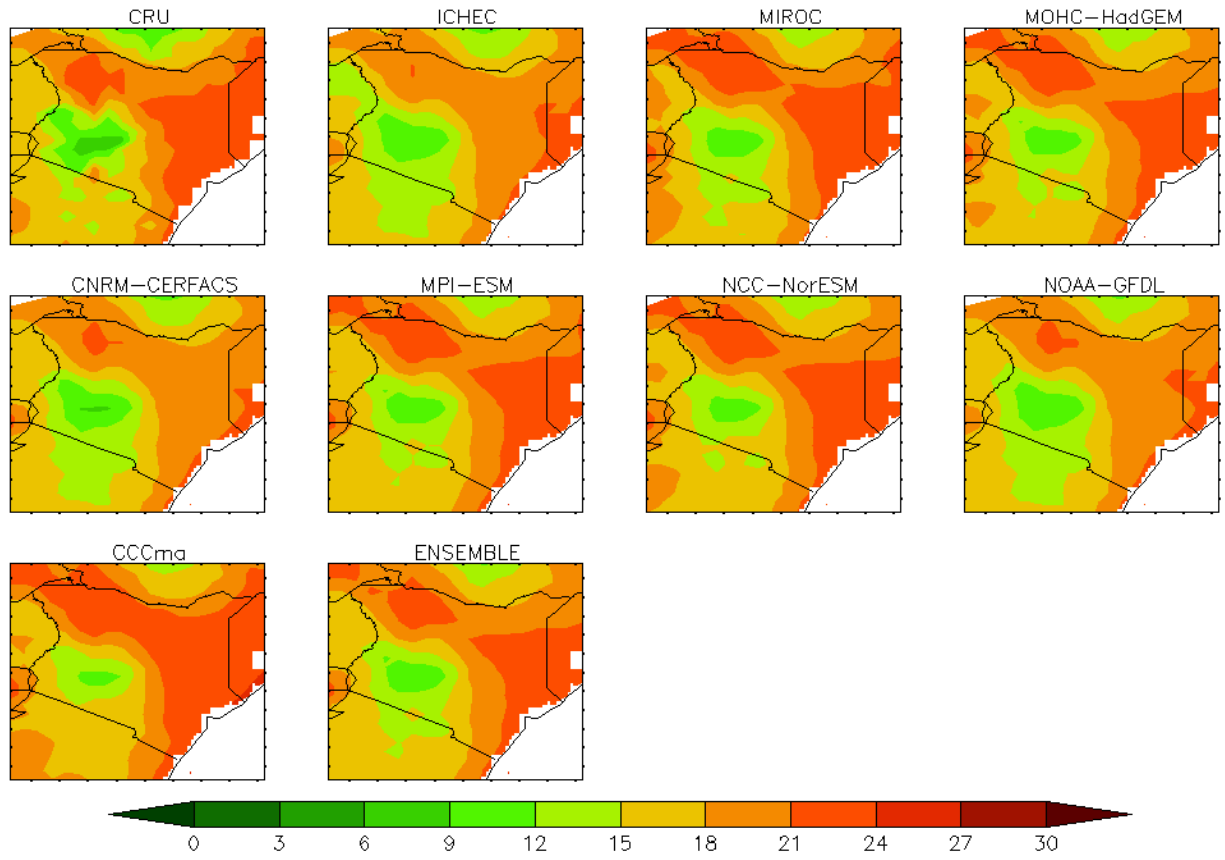

Figure 19: Climatology (1971-2000) of minimum temperature (in °C) in the observed (CRU), individual CORDEX models and the ensemble over Kenya during the OND season. High (low) temperature areas are shown in dark (green) red.

4.4.2 Assessment of Model Skill in Simulating Tele-connection Signals

Rainfall in Kenya is highly variable in space and is dependent on different forcings of varying spatial scales. One forcing, related to global sea surface temperatures (SSTs), that has been found to affect rainfall in the East African region and Kenya in particular is the El Niño/La Niña phenomenon (Ogallo, 1988; Indeje *et al.*, 2000). In this section, spatial plots of rainfall during El Niño and La Niña episodes were done to assess how the models simulate the tele-connection signals within the study region during the OND season. El Niño is usually associated with above normal rainfall while La Niña is usually associated with below normal rainfall in the study region.

In Figure 20, the observed spatial distribution of rainfall during weak El Niño shows rainfall concentrated in the Lake Victoria basin and central parts spreading southwards towards the coast

of Kenya. None of models including the ensemble was able to simulate the observed rainfall distribution. The models over-estimated rainfall in Kenya during weak El Niño and this was more pronounced over highland areas further confirming that the models were not able to replicate the systems in these areas.

In Figure 21, the models were still not able to simulate the effect on rainfall over Kenya. Several models, especially the CCCma, over-estimated rainfall. Other models such as MIROC, under-estimated rainfall over several parts of Kenya especially the northern parts.

Similar results were observed during the strong El Niño whereby the models were not able to locate the high rainfall intensity areas as shown in Figure 22. Most models under-estimated rainfall especially in the northern parts of Kenya. These results show that CORDEX models are not able to replicate the effect of ENSO signals on the Kenyan rainfall.

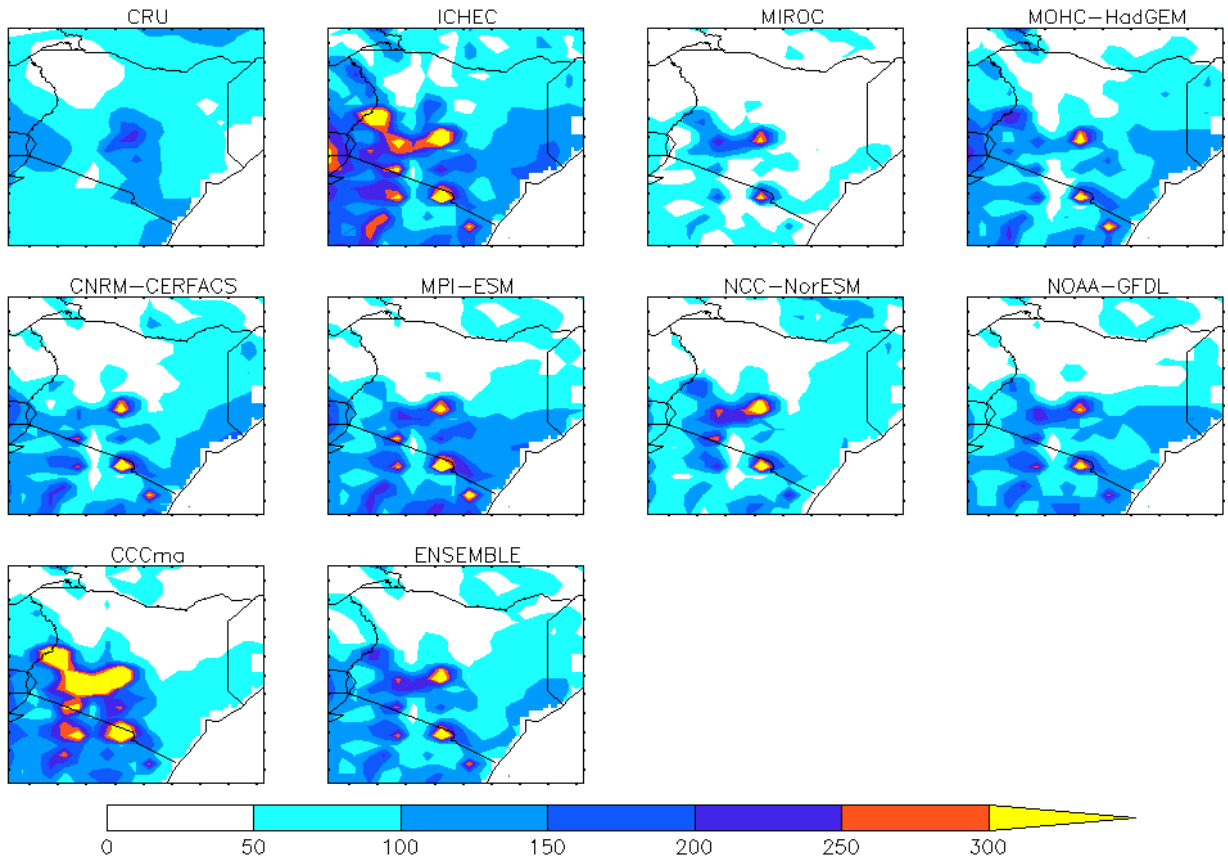

Figure 20: Spatial distribution of rainfall (in mm) during a weak El Niño (2004) as simulated by the observed (CRU), the CORDEX models and the ensemble over Kenya during the OND season. High rainfall intensity areas are shown in yellow.

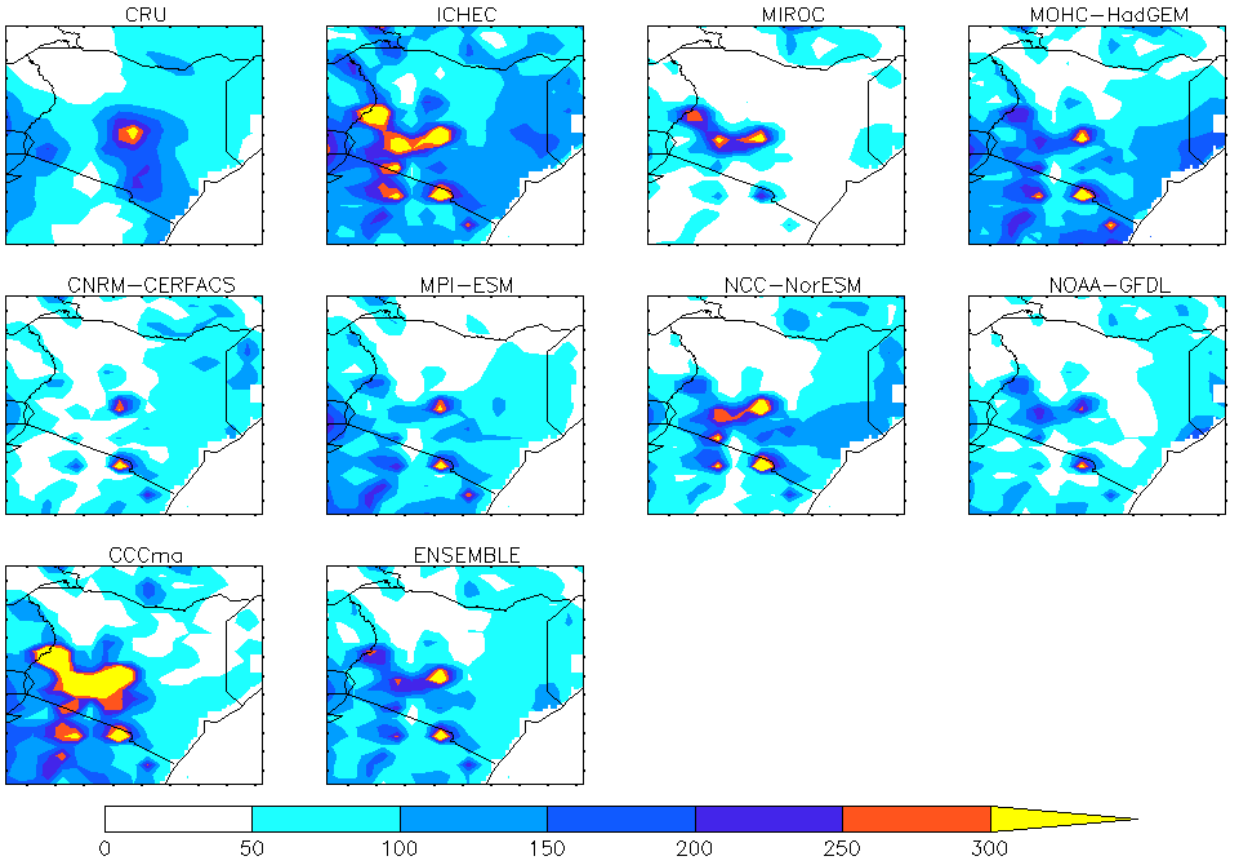

Figure 21: Spatial distribution of rainfall (in mm) during moderate El Niño (1994) as simulated by the observed (CRU), the CORDEX models and the ensemble over Kenya during the OND season. High rainfall intensity areas are shown in yellow.

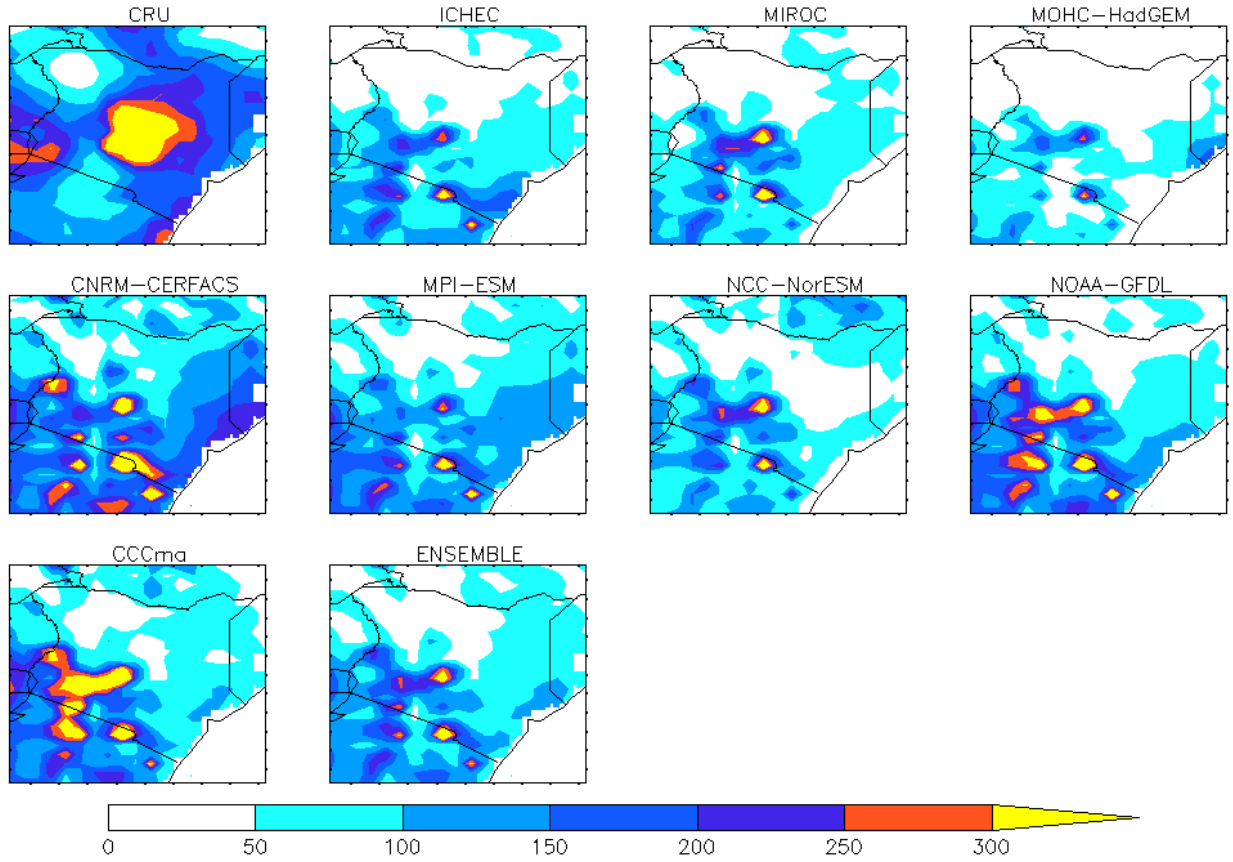

Figure 22: Spatial distribution of rainfall (in mm) during strong El Niño (1997) as simulated by the observed (CRU), the CORDEX models and the ensemble over Kenya during the OND season. High rainfall intensity areas are shown in yellow.

Figures 23 to 25 show the spatial distribution of rainfall during weak (2000), moderate (1970) and strong (1988) La Niña in Kenya. The models and the ensemble had poor skill in simulating the observed distribution of rainfall during the three years which were considered. During the weak La Niña of 2002, the models over-estimated rainfall in most parts of the country especially the southern parts as shown in Figure 23. Over-estimation was evident during the moderate and strong La Niña episodes as shown in Figures 24 and 25 respectively. The models were not able to simulate ENSO signals in Kenya and this may be due to the forcing data from ERA-INTERIM reanalysis not being able to capture the effect of ENSO signals in Kenya.

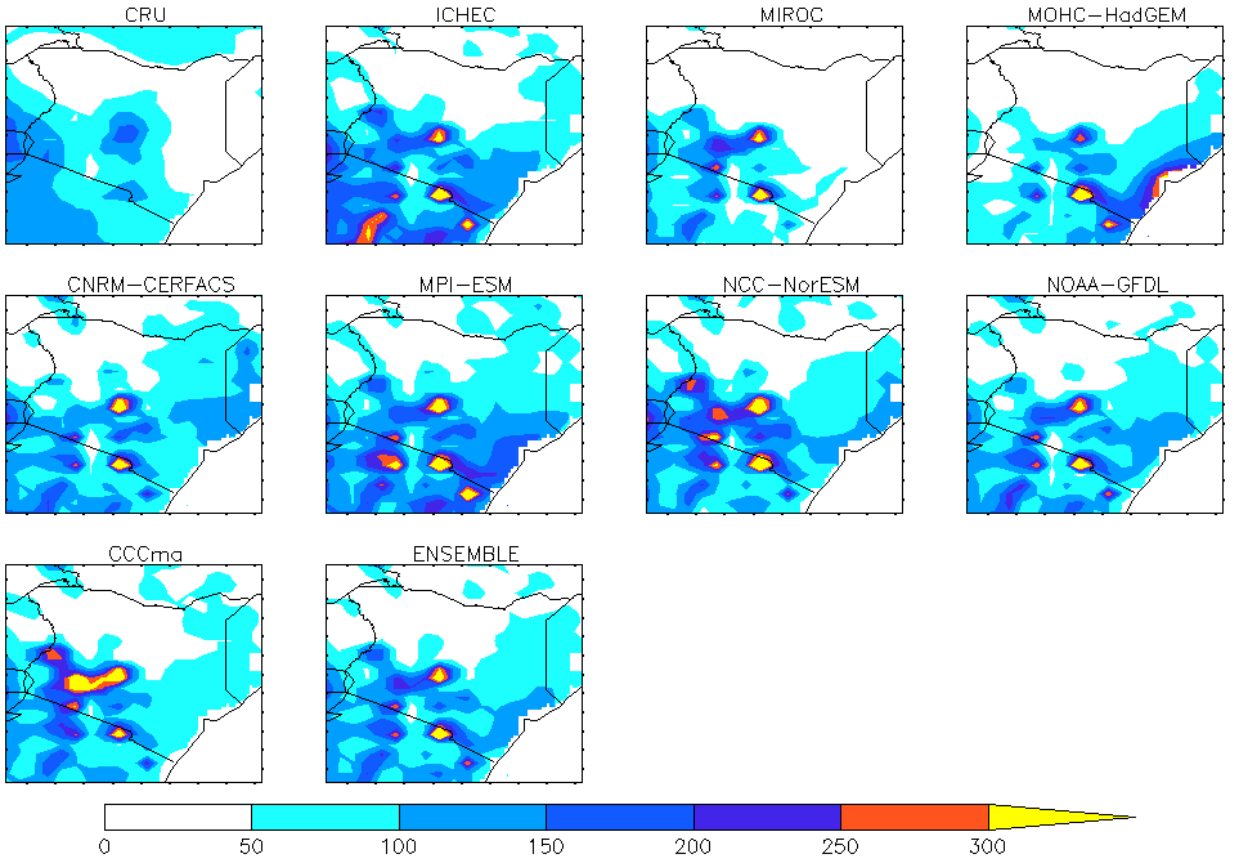

Figure 23: Spatial distribution of rainfall (in mm) during weak La Niña (2000) as simulated by the observed (CRU), the CORDEX models and the ensemble over Kenya during the OND season. High rainfall intensity areas are shown in yellow.

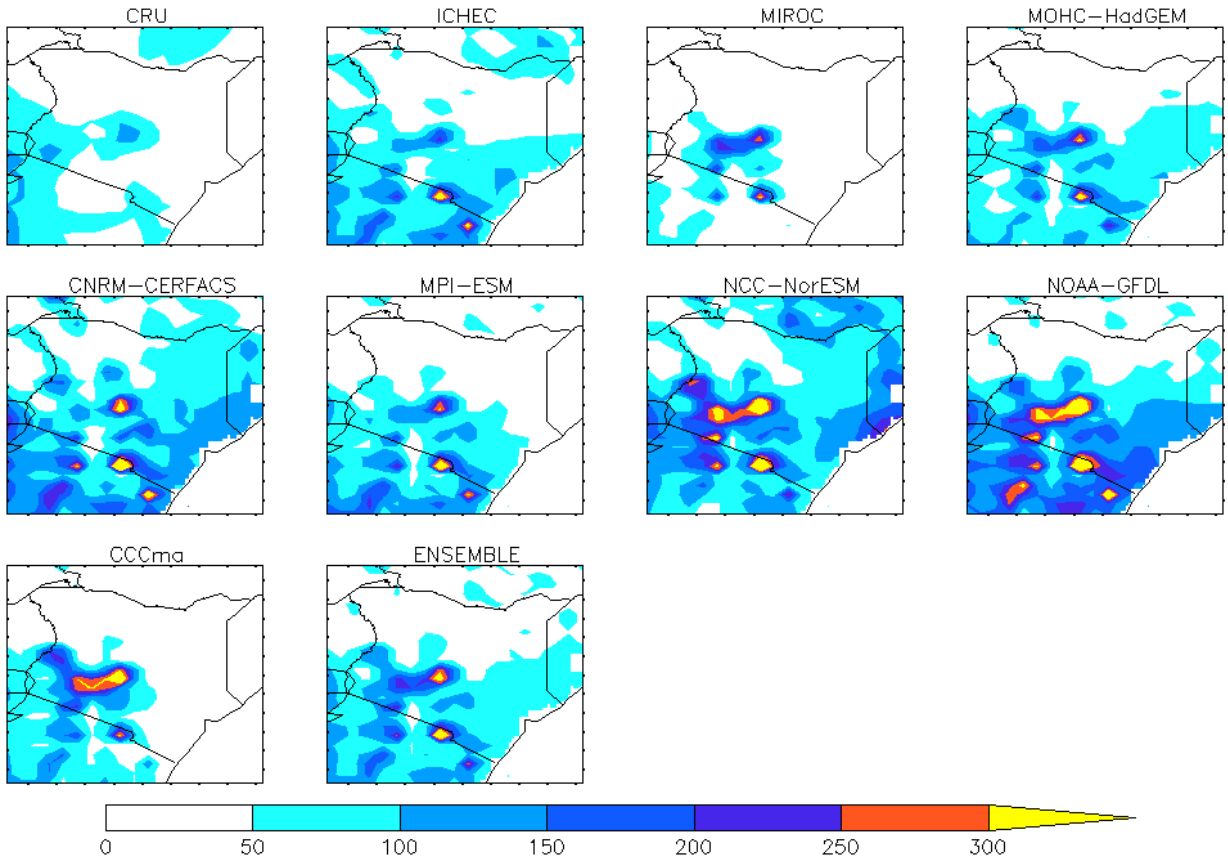

Figure 24: Spatial distribution of rainfall (in mm) during moderate La Niña (1970) as simulated by the observed (CRU), the CORDEX models and the ensemble over Kenya during the OND season. High rainfall intensity areas are shown in yellow.

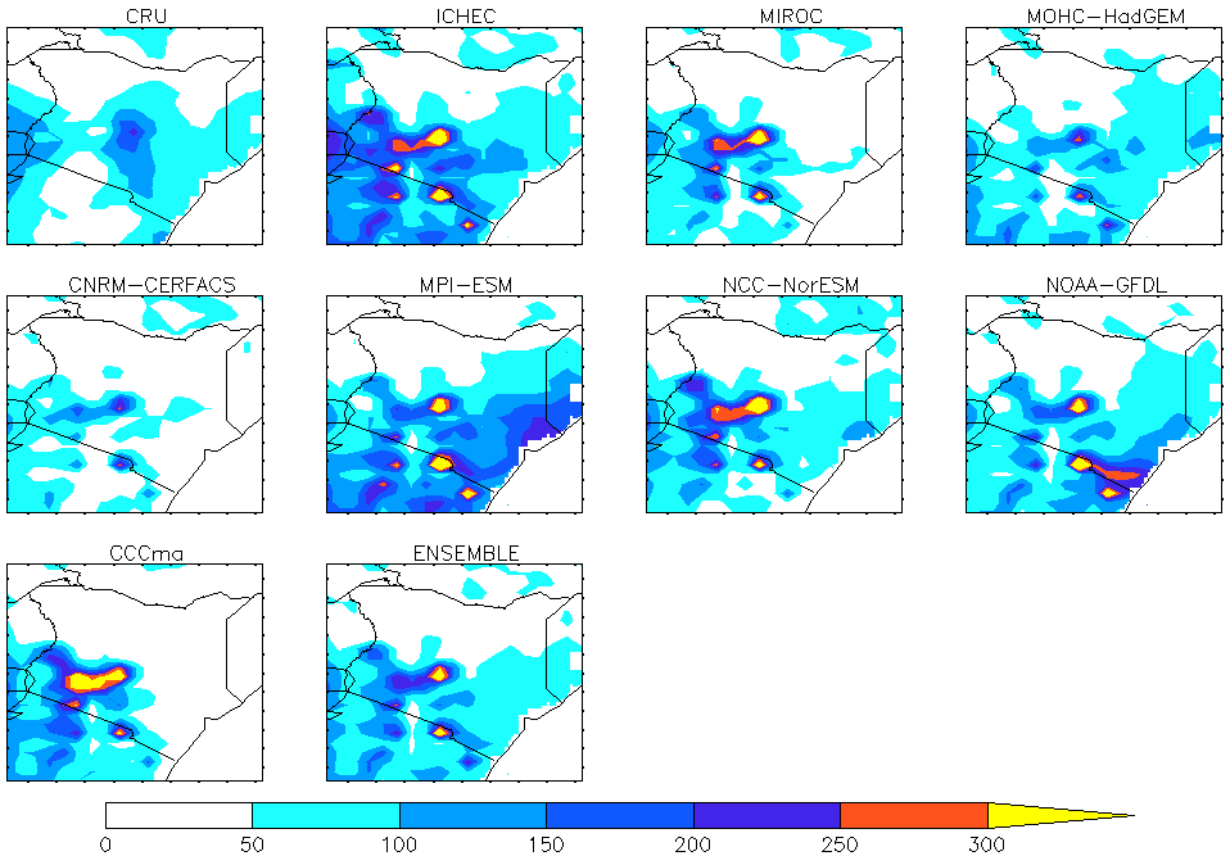

Figure 25: Spatial distribution of rainfall (in mm) during strong La Niña (1988) as simulated by the observed (CRU), the CORDEX models and the ensemble over Kenya during the OND season. High rainfall intensity areas are shown in yellow.

4.4.3 Model Difference Plots

Difference plots have been presented to show the average deviation of the models output datasets from the reference (CRU) datasets. Figures 26, 27 and 28 represent the difference plots during MAM, JJA and OND seasons respectively.

The difference plot of rainfall during MAM indicated that all the models, especially CCCma, NCC, MOHC and NOAA models, under-estimated rainfall over most parts of Kenya as shown in Figure 26. Over-estimation of rainfall by all models was observed over the western parts and highland areas of the country.

During the JJA season, under-estimation of rainfall was mainly observed in the western, Lake Victoria basin and coastal parts of Kenya as shown in Figure 27. It should be noted that these are the main areas which normally receive rainfall during this season. Over-estimation of rainfall

was observed in few places in Kenya except for the ICHEC model which indicated several places in the northern parts of the country.

High positive values were observed during OND season indicating that the models are over-estimating rainfall over western and coastal parts of Kenya as shown in Figure 28. These results were attributed to the models not being able to replicate local circulation systems in Kenya.

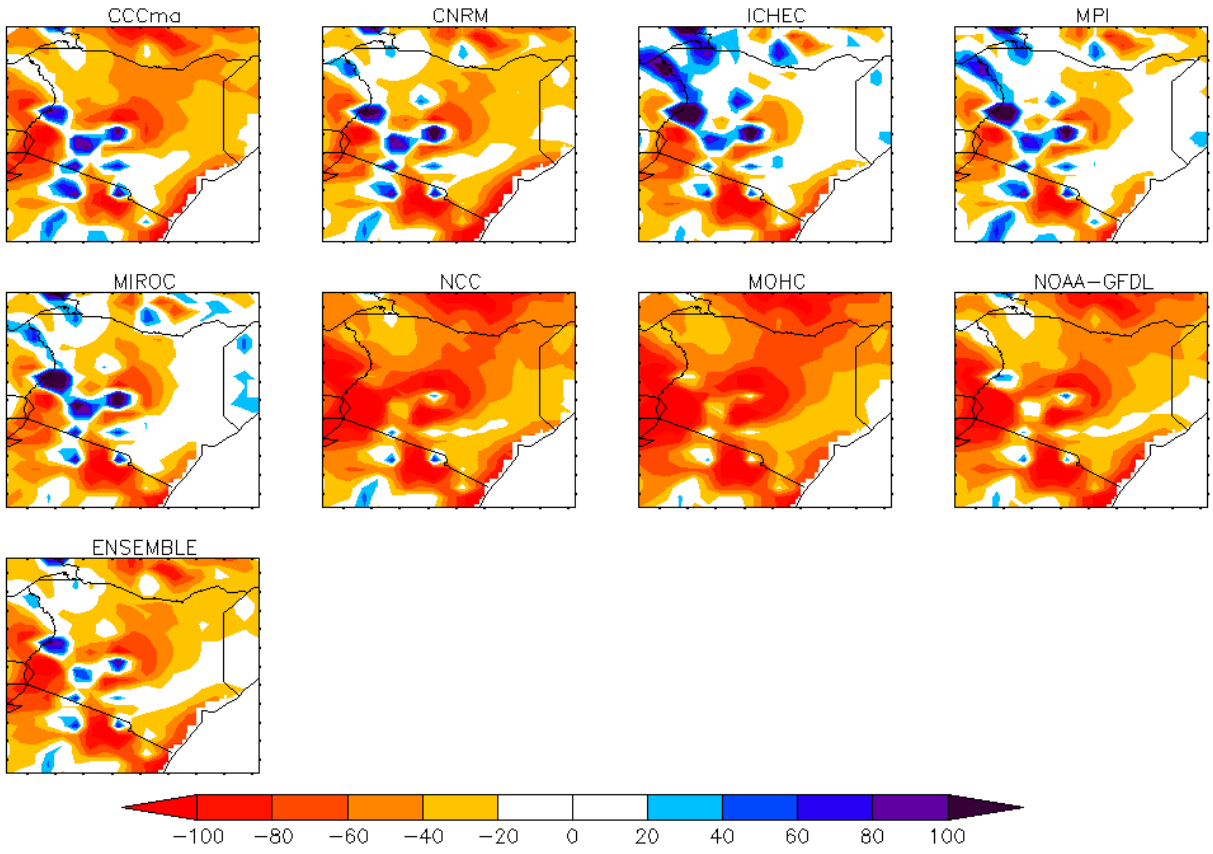

Figure 26: Deviation of average (1970-2000) rainfall (in mm) from the observed (CRU) for the CORDEX models and the ensemble during MAM season over Kenya. Shades of red indicate underestimation while shades of blue indicate overestimation.

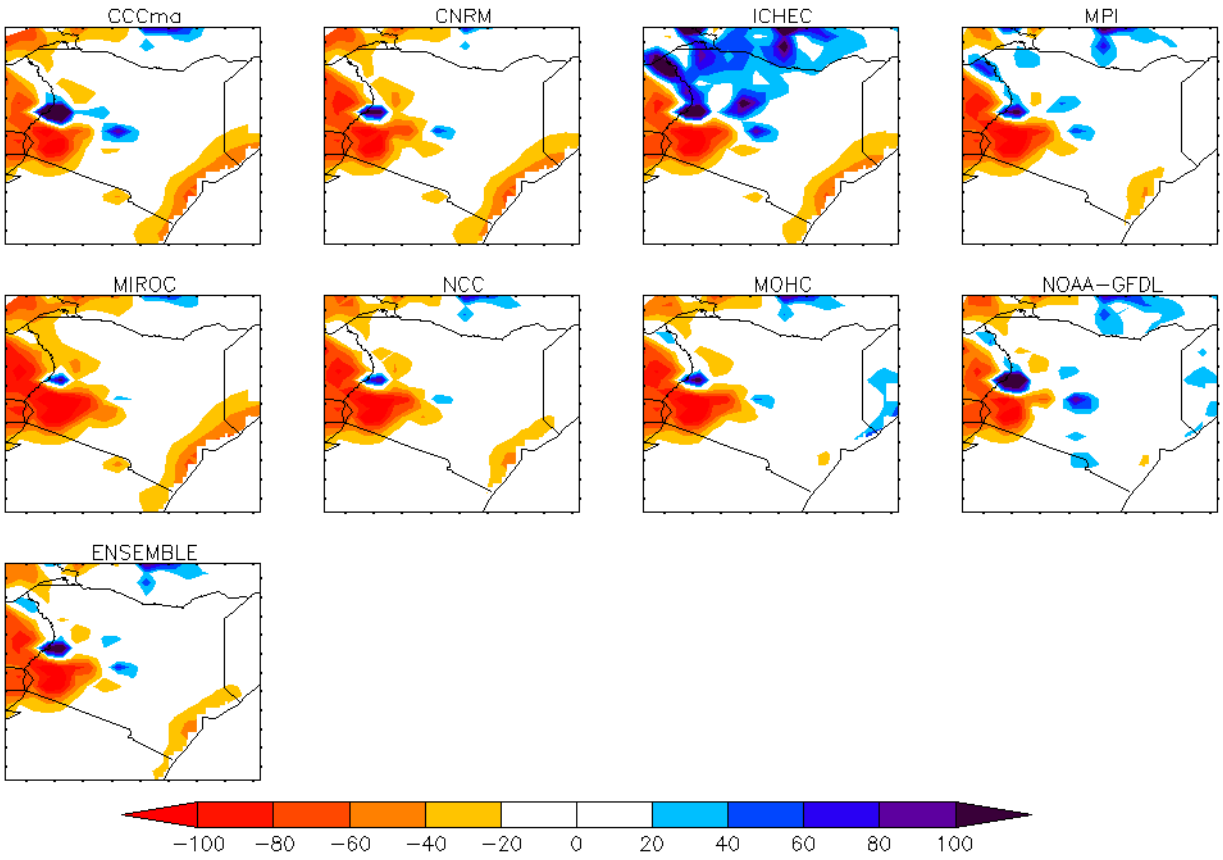

Figure 27: Deviation of average (1970-2000) rainfall (in mm) from the observed (CRU) for the CORDEX models and ensemble during JJA season over Kenya. Shades of red indicate underestimation while shades of blue indicate overestimation.

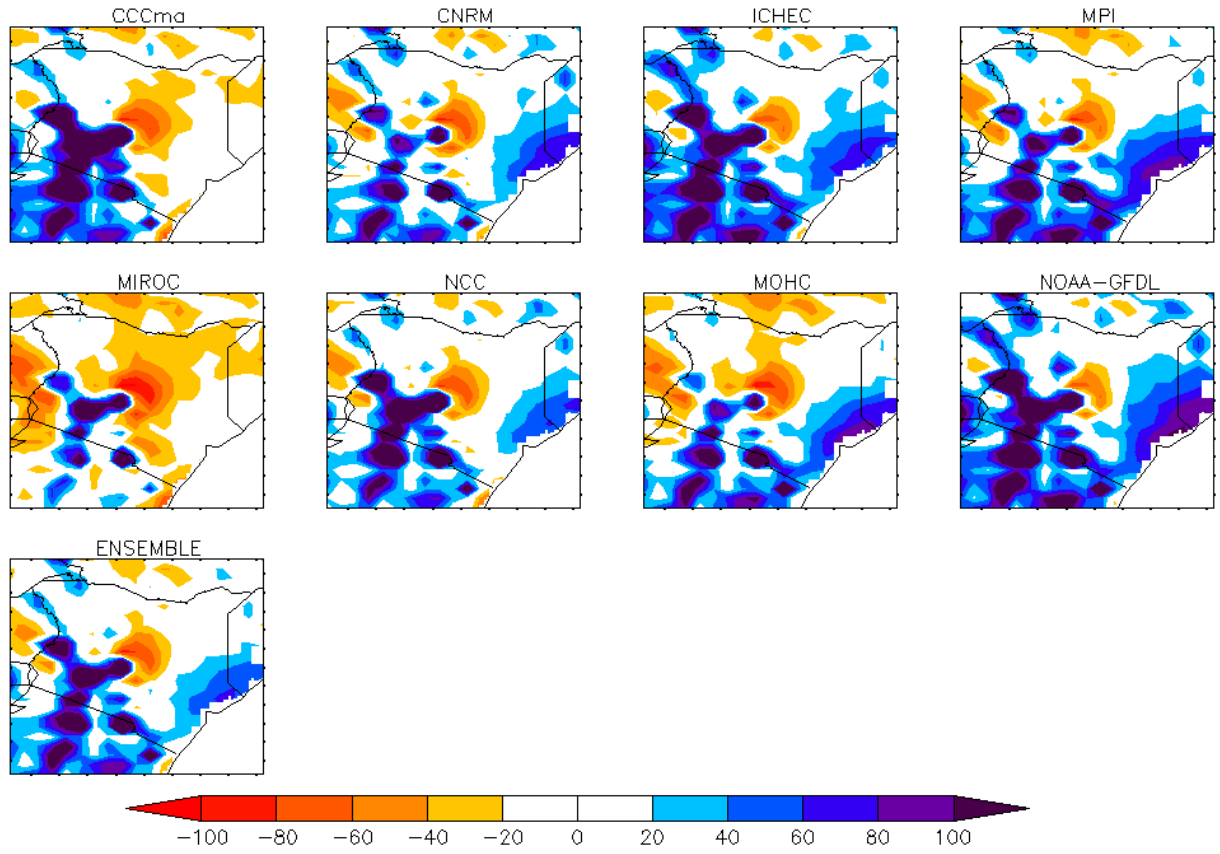

Figure 28: Deviation of average (1970-2000) rainfall (in mm) from the observed (CRU) for the CORDEX models and ensemble during OND season over Kenya. Shades of red indicate underestimation while shades of blue indicate overestimation.

The proceeding results, Figures 29, 30 and 31, represent the average temperature difference between the observed (CRU) and the individual CORDEX models. Temperature differences were generally low compared to rainfall differences. Most models showed positive values in maximum temperature over northern parts of Kenya during MAM season as shown in Figure 29. Under-estimation was mainly observed in the western and central parts of Kenya due to the effect of the highlands and this was more pronounced in the ICHEC and MIROC models.

During JJA season, under-estimation was pronounced in the ICHEC model over north western parts of Kenya as shown in Figure 30. Over-estimation was observed over few places especially in the northern parts of the country. The ensemble had the least difference values.

In Figure 31, negative values in maximum temperature during OND season were simulated by all the models over several parts of Kenya especially in the western parts. The ensemble had the

lowest difference values in all the three seasons compared to the individual models except during OND where the ensemble had similar spatial distribution as NCC, CNRM, MOHC and MIROC. These results can be attributed to the models being able to simulate temperature with high skill compared to rainfall.

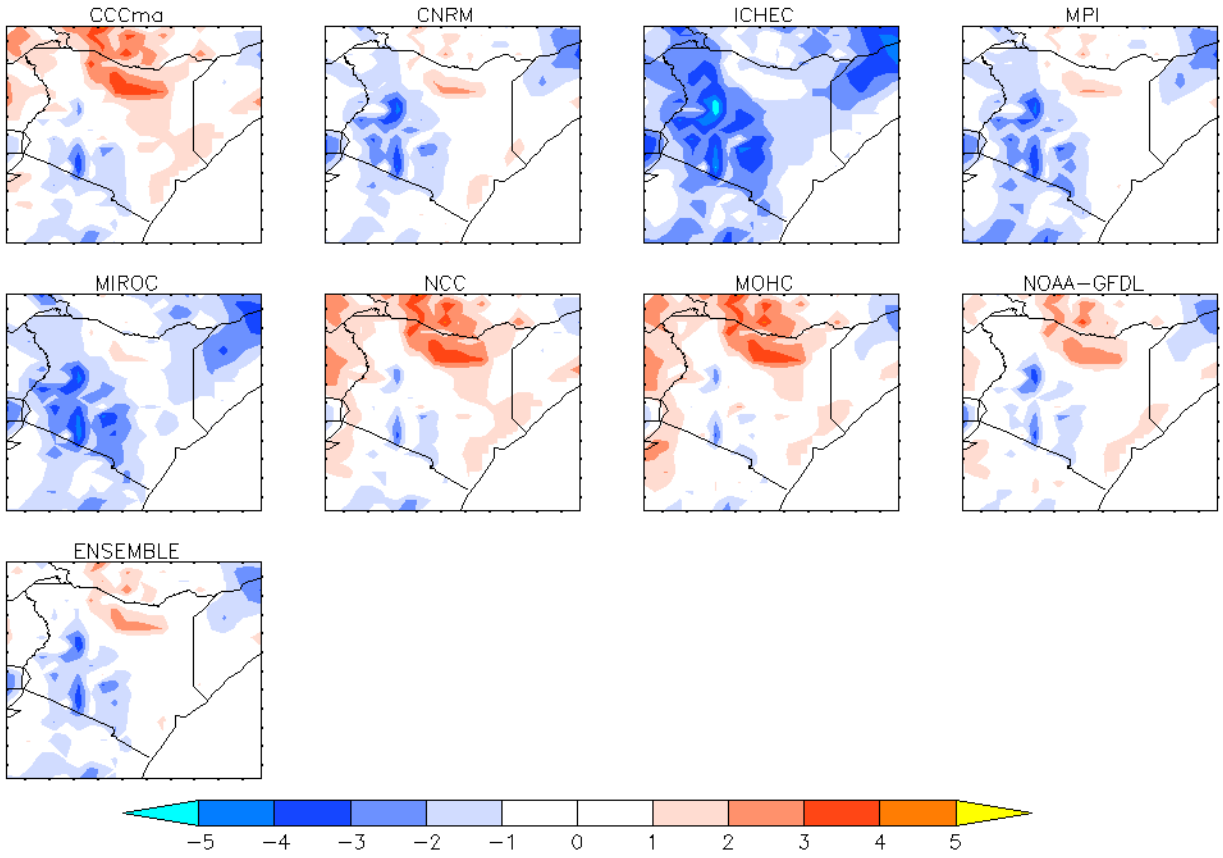

Figure 29: Deviation of average (1970-2000) maximum temperature (in °C) from the observed (CRU) for the CORDEX models and ensemble during MAM season Kenya. Blue shades indicate underestimation while red shades indicate underestimation.

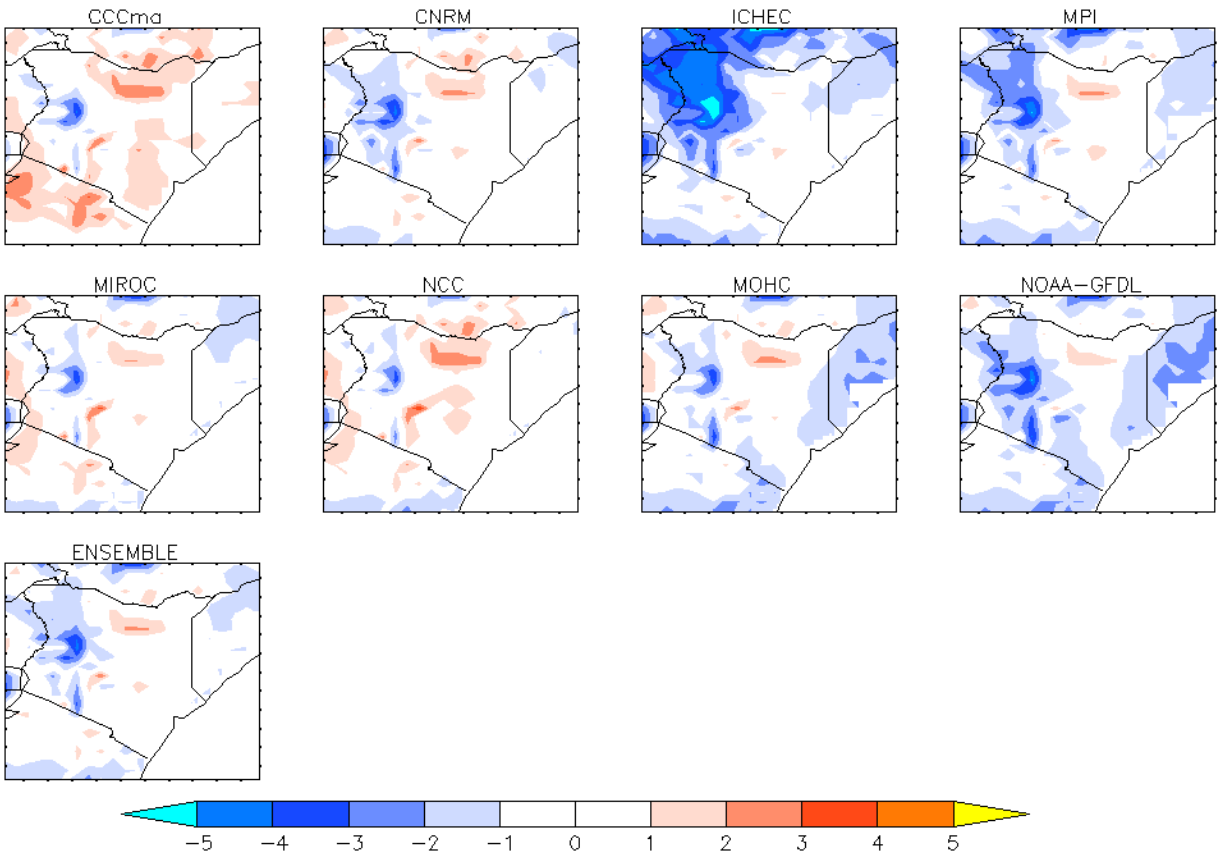

Figure 30: Deviation of average (1970-2000) maximum temperature (in °C) from the observed (CRU) for the CORDEX models and ensemble during JJA season over Kenya. Blue shades indicate underestimation while red shades indicate underestimation.

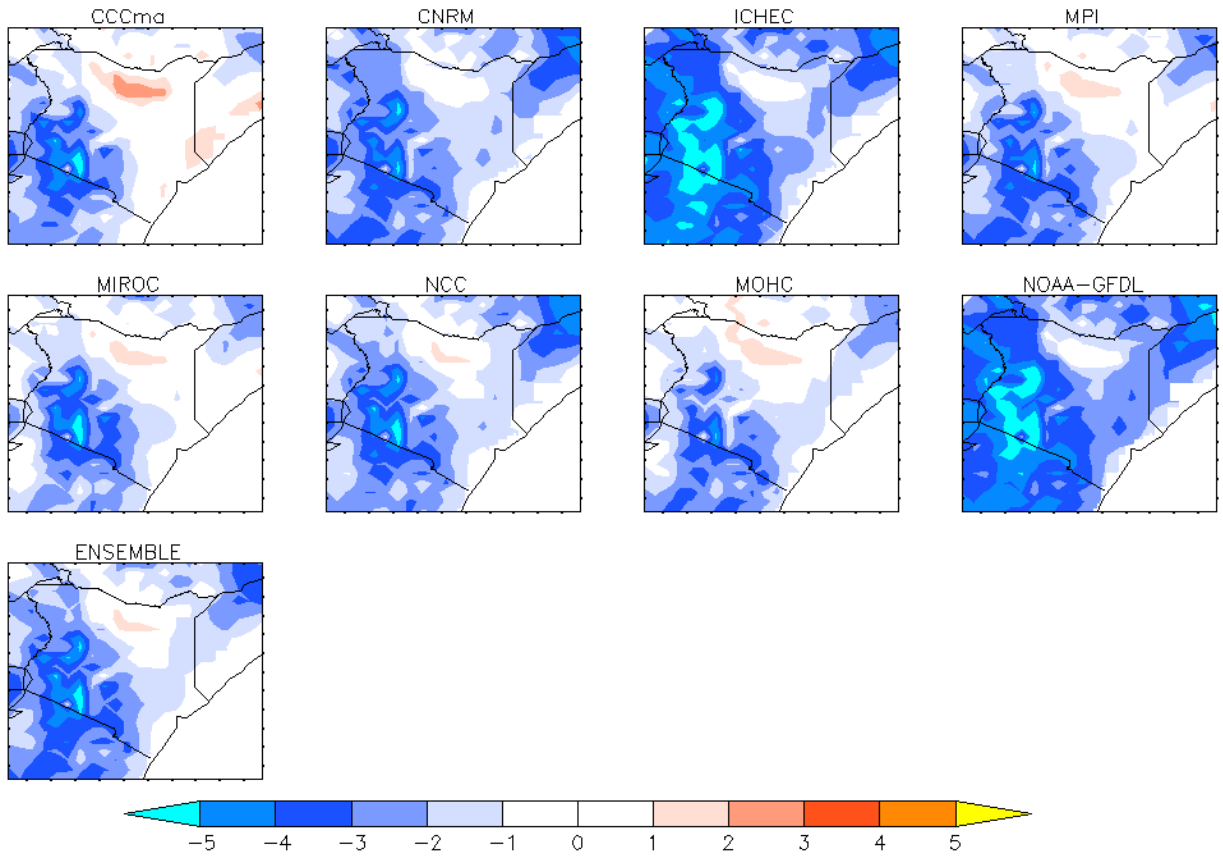

Figure 31: Deviation of average (1970-2000) maximum temperature (in °C) from the observed (CRU) for the CORDEX models and ensemble during OND season over Kenya. Blue shades indicate underestimation while red shades indicate underestimation.

The proceeding results, Figures 32, 33 and 34, represent the average minimum temperature difference between the observed (CRU) and the individual CORDEX models. Minimum temperature simulations by the CORDEX RCMs showed positive difference values over north western parts of the country during MAM season as shown in Figures 32, an indication that the models are over-estimating minimum temperature. Negative difference values were observed over the southern and eastern parts of Kenya. The ensemble showed similar spatial distribution to MIROC, MPI, and NOAA-GFDL models during MAM season.

In Figure 33, over-estimation was observed in the western and northern parts of Kenya and was more pronounced in the CCCma model. Under-estimation was observed over a few places but mainly from the CNRM and ICHEC models. This showed that, on average, most models tend to simulate warmer temperatures during MAM and JJA. The ensemble showed similar spatial distribution to MIROC, NCC, MOHC and MPI during JJA season.

In Figure 34, similar results to the ensemble were simulated by MIROC, MOHC and MPI. In all the seasons the ensemble had low difference values from the observed suggesting improved simulations compared to individual models. These results suggest that minimum temperature simulations agree with the observation over several parts of Kenya during all the seasons.

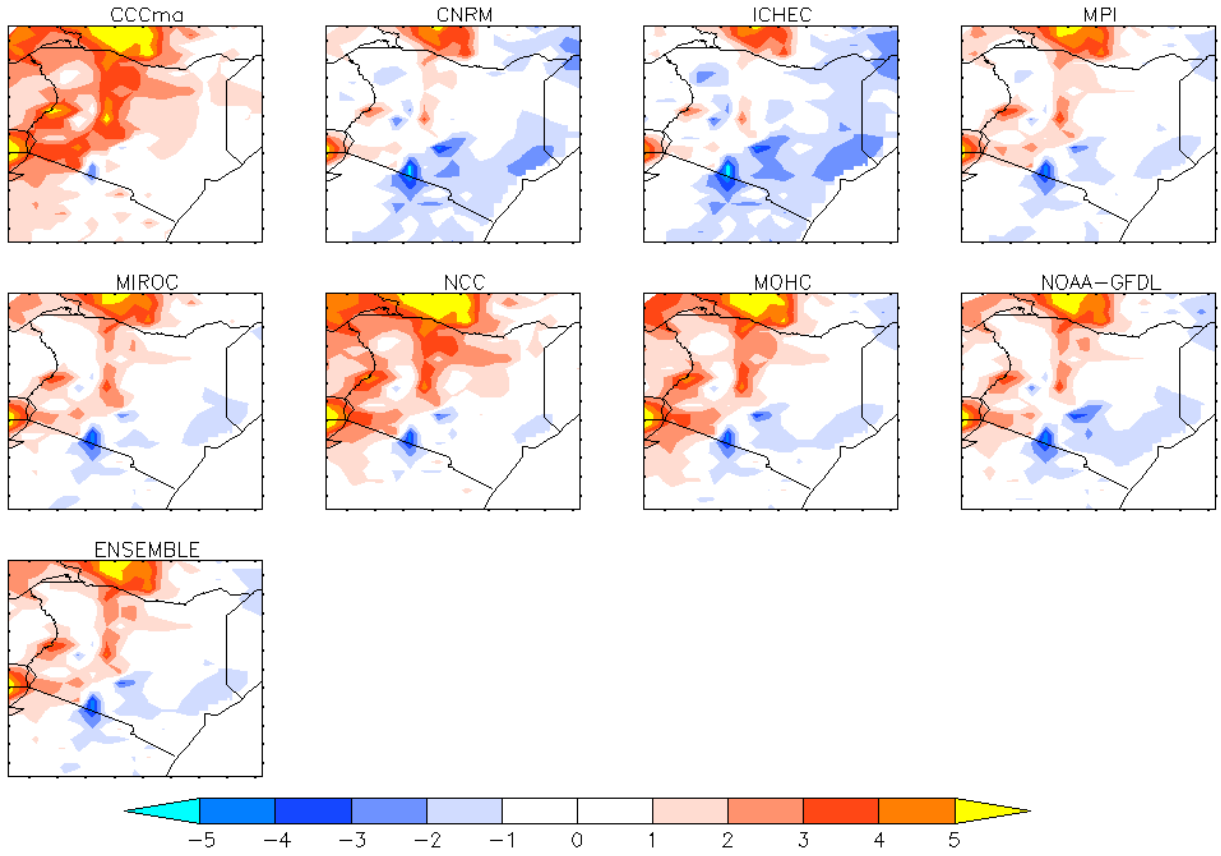

Figure 32: Deviation of average (1970-2000) minimum temperature (in °C) from the observed (CRU) for the CORDEX models and ensemble during MAM season over Kenya. Blue shades indicate underestimation while red shades indicate underestimation.

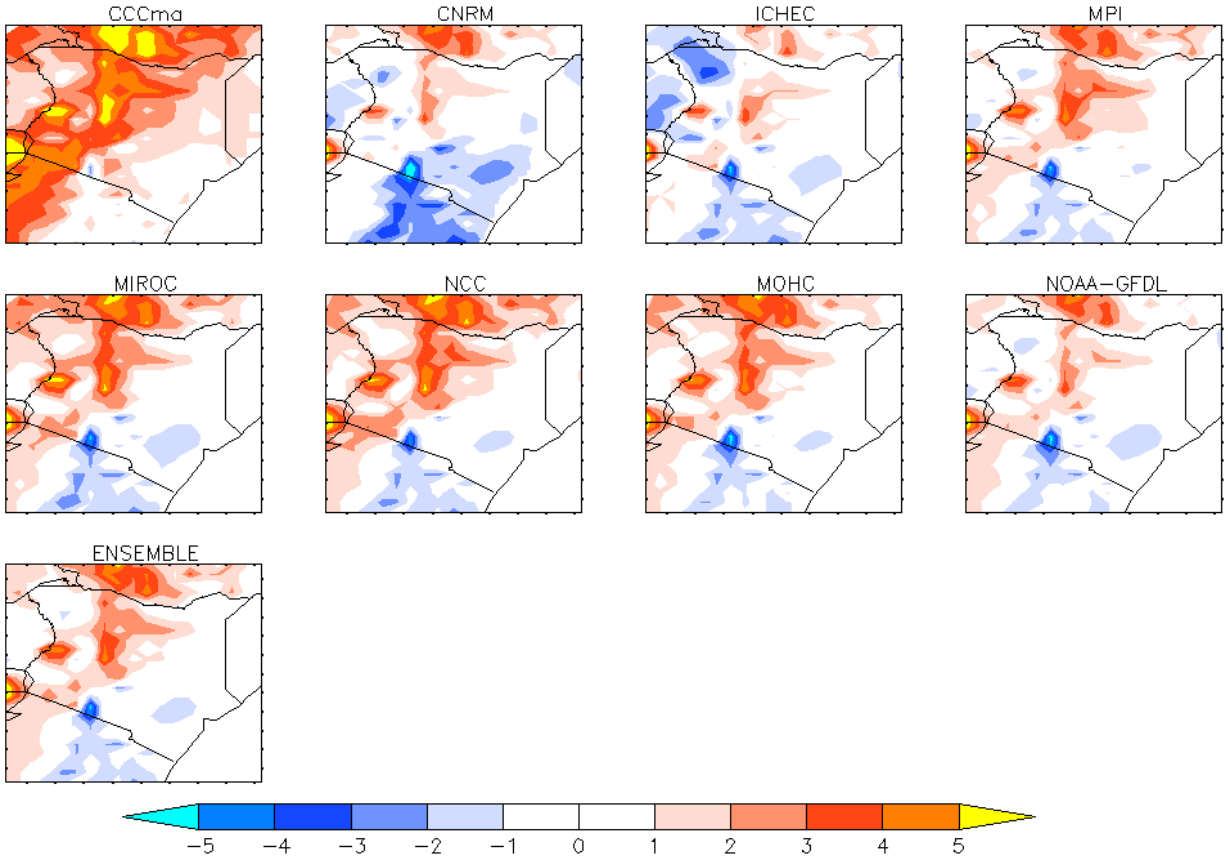

Figure 33: Deviation of average (1970-2000) minimum temperature (in °C) from the observed (CRU) for the CORDEX models and ensemble during JJA season over Kenya. Blue shades indicate underestimation while red shades indicate underestimation.

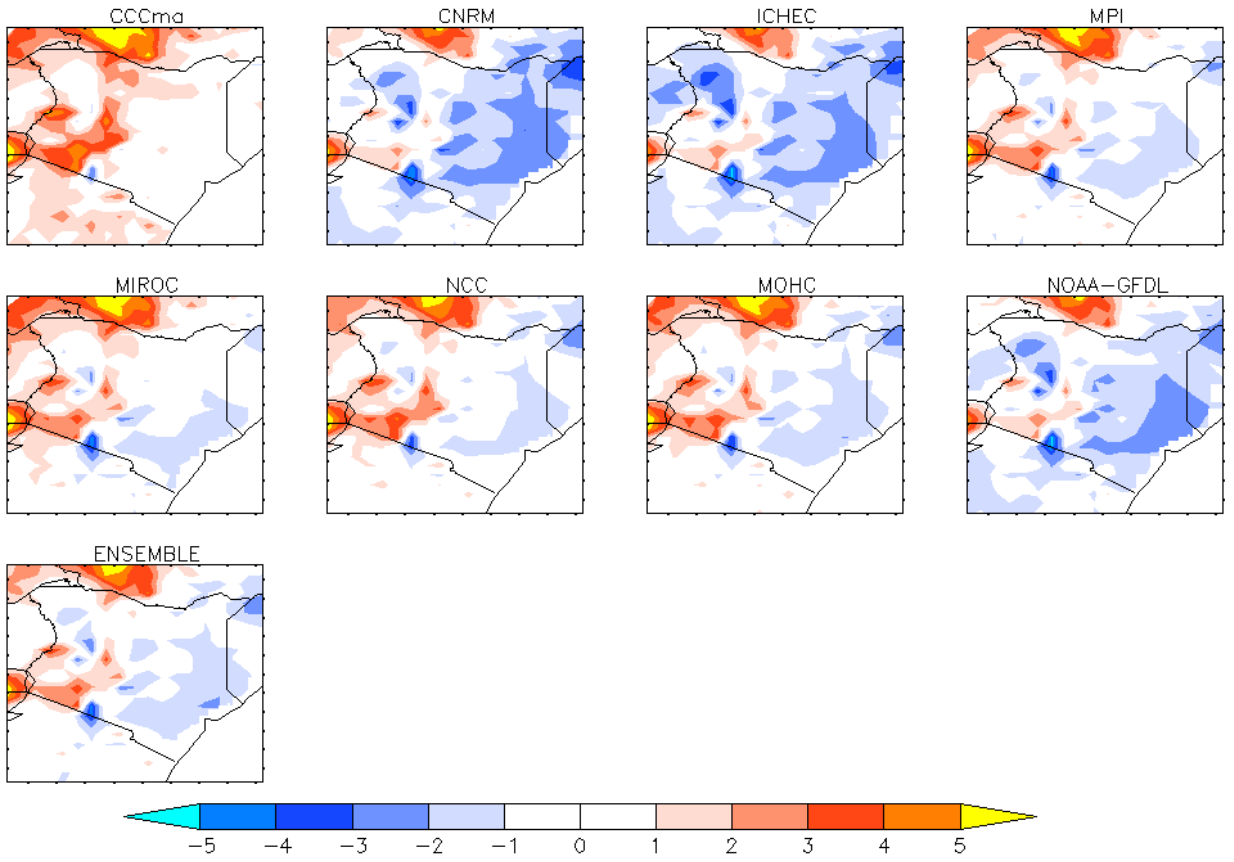

Figure 34: Deviation of average (1970-2000) minimum temperature (in °C) from the observed (CRU) for the CORDEX models and ensemble during OND season over Kenya. Blue shades indicate underestimation while red shades indicate underestimation.

4.4.4 Correlation Analysis

The Pearson's correlation between the observed (CRU) rainfall (temperature) and the models rainfall (temperature) were evaluated and plotted spatially. Figures 35, 36 and 37 represent the spatial plots of correlation for rainfall, maximum temperature and minimum temperature respectively. The critical point for the correlation coefficient (r) was found to be $|r| \geq 0.316$ with twenty eight degrees of freedom at 95% confidence interval using a two tailed student-t-test. Values with $|r| \geq 0.316$ were considered to be significant.

In Figure 35, consistent rainfall correlations values greater than +0.2 over several places in the study region during MAM season were observed. Areas around Lake Victoria basin recorded correlation values of between -2 and +2 confirming that the models are not able to replicate circulation systems in the Lake Victoria basin. The ensemble had several places with significant

correlations as compared to the individual models.

Maximum temperature correlations had the highest values with some places having values of between +0.4 and +0.6 during MAM season as shown in Figure 36. Significant correlation areas were mainly located in the northern parts of Kenya. Negative correlation values of maximum temperature were observed in the south eastern parts of Kenya these were however not considered to be significant.

In Figure 37, high correlation values of minimum temperature of between +0.6 and +0.8 were observed in central and north western parts of Kenya during OND season. All models had similar spatial distributions of minimum temperature. The CCCma, MOHC and CNRM had similar spatial distribution of minimum temperature to that of the ensemble. Areas where the correlation coefficient was not significant included the, western (for some models), eastern and coastal parts of Kenya. These correlation patterns are similar to the patterns of the difference plots where areas with high difference values are the ones that recorded low correlation coefficient values.

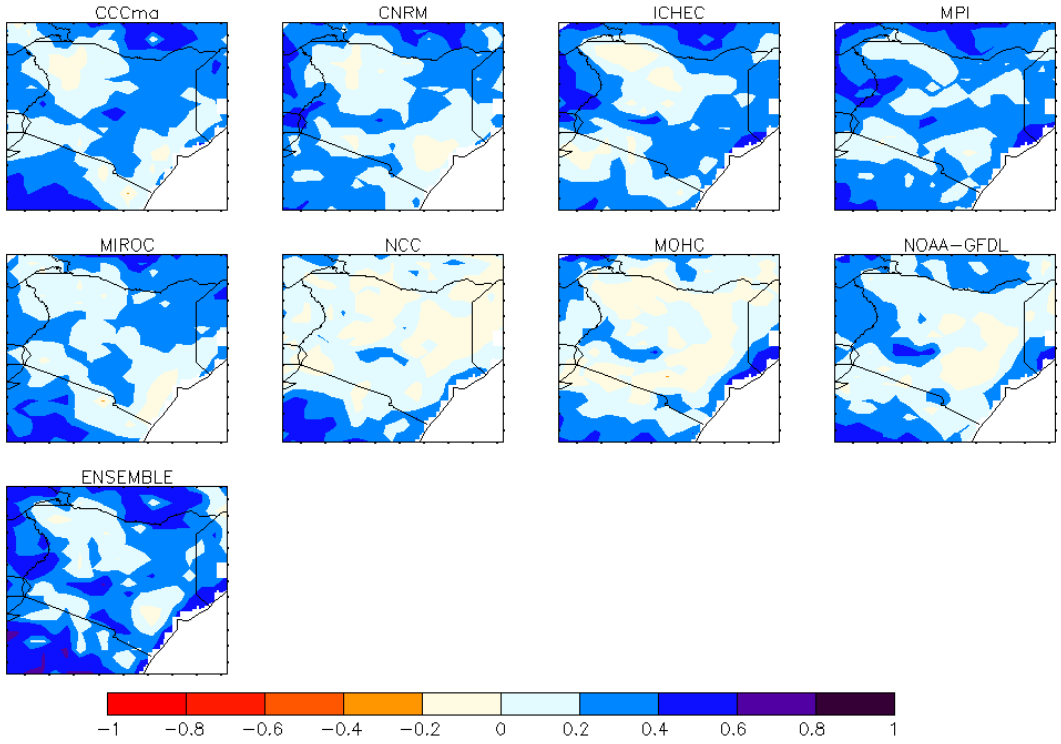

Figure 35: Correlation between the observed (CRU) rainfall and the simulated rainfall from CORDEX models and the ensemble during the MAM season in the period 1971-2000 over Kenya. Negative (positive) correlation values are represented in shades of red (blue).

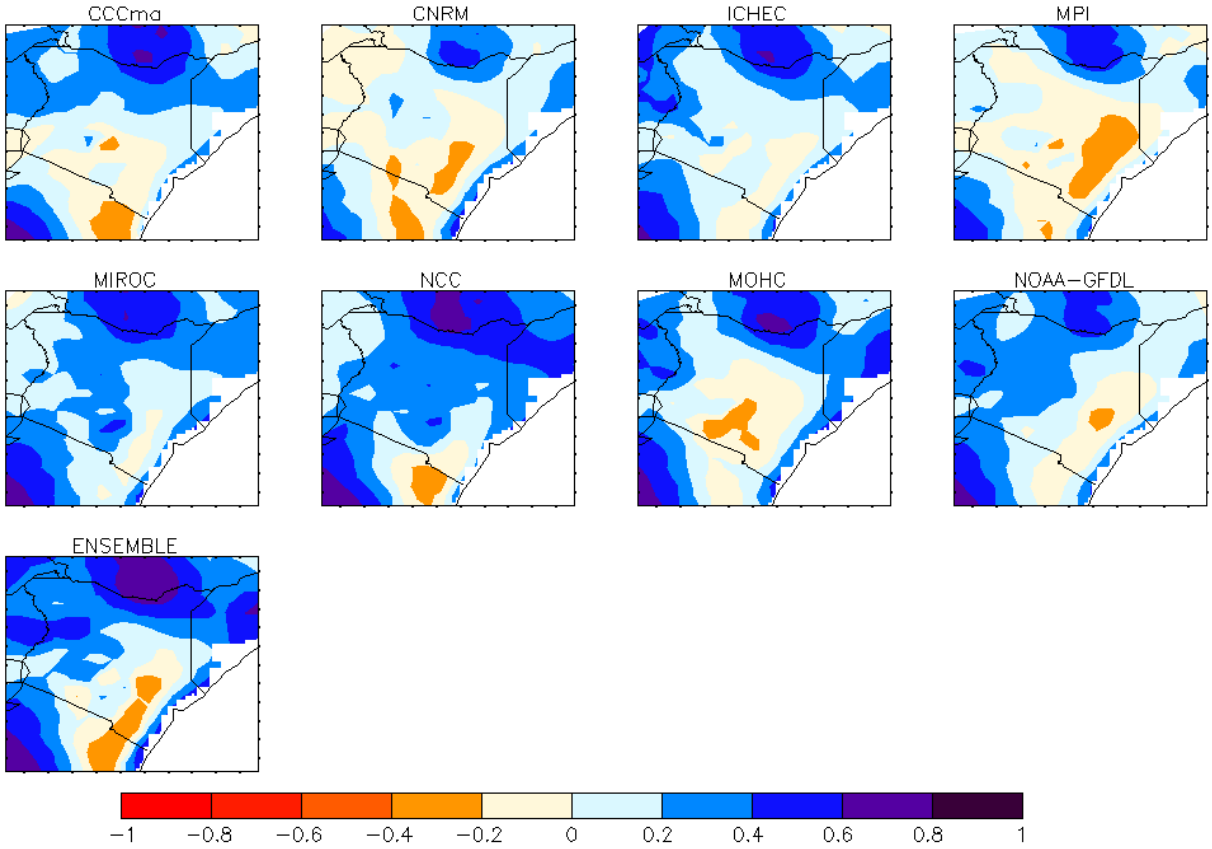

Figure 36: Correlation between the observed (CRU) maximum temperature and the simulated maximum temperature by the CORDEX models and the ensemble during the OND season in the period 1971-2000 over Kenya. Negative (positive) correlation values are represented in shades of red (blue).

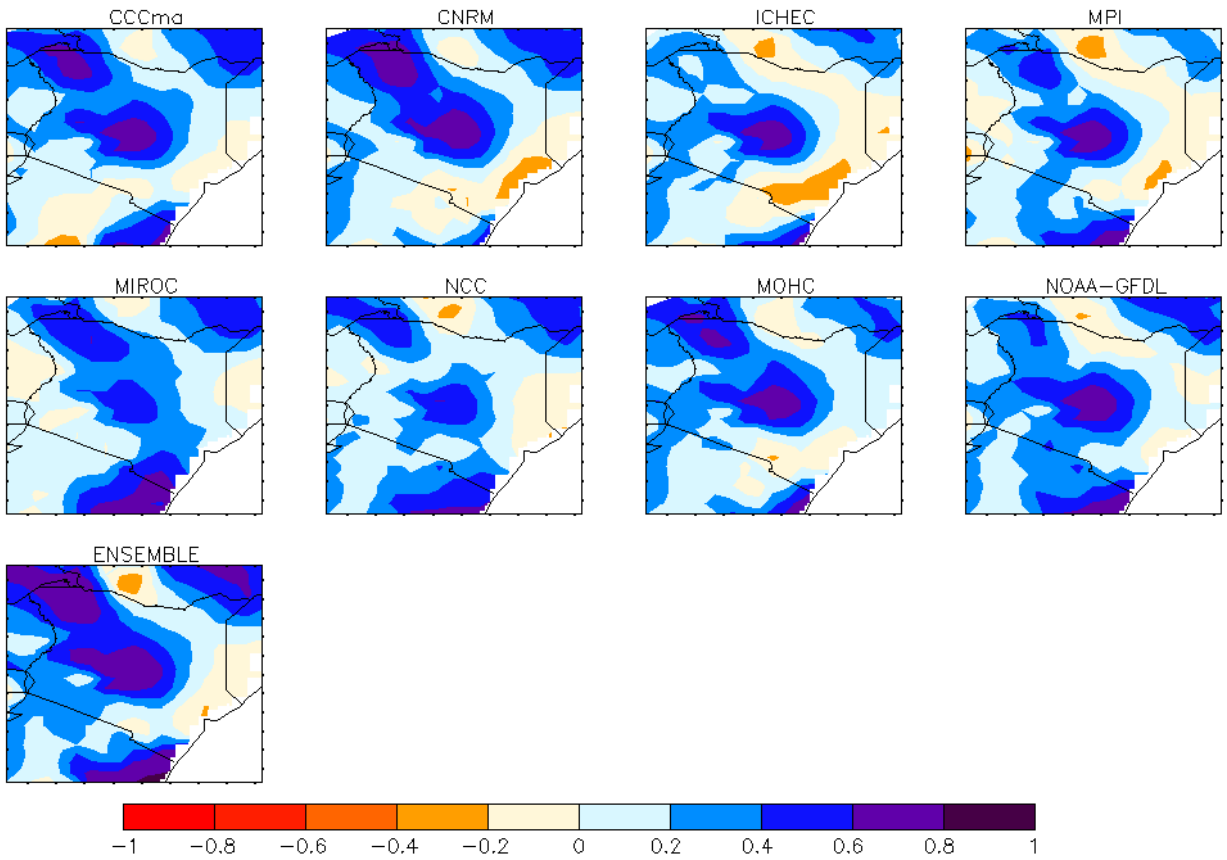

Figure 37: Correlation between the observed (CRU) minimum temperature and the simulated minimum temperature by the CORDEX models and the ensemble during the OND season in the period 1971-2000 over Kenya. Negative (positive) correlation values are represented in shades of red (blue).

4.4.5 Time Series Plots

This section presents the results of time series plots for some selected stations in the study area. Annual cycle of temperature and rainfall were plotted using monthly climatology (1971-2000) for all the stations. Time series of monthly rainfall from 1970 to 2000 are also presented for selected stations.

4.4.5.1 Annual Cycle

The region experiences two rainfall peaks which occur during MAM and OND seasons in most places, except over Western and Coastal areas. This is in relation to the apparent movement of the position of the ITCZ. Figures 38 to 40 represent the results of the plots of annual cycles of rainfall, and maximum and minimum temperature for selected stations which represent highlands, arid and semi-arid, western and coastal areas of Kenya

For the areas which experience two rainfall peaks, for example Wajir and Mombasa, the models simulated the two seasonal rainfall peaks as shown in Figure 38. However, other areas where three rainfall peaks are usually observed, such as Kakamega and Nyeri, the models did not simulate the third season which usually occurs during June-August as seen in Figure 38. In all the areas, the ensemble is a better approximation with respect to capturing the pattern of the observed as compared to the individual models.

The results of the annual cycle of maximum temperature are presented in Figure 39. Annual cycle of maximum temperature over several parts of Kenya, is well simulated by all the models for example, over Mombasa and Wajir. The CORDEX models including the ensemble were not able to simulate the annual cycle of the observed maximum temperature over Nyeri and Kakamega.

Figure 40 shows the performance of the CORDEX models in simulating the seasonal peaks of minimum temperature. The annual cycle of minimum temperature is well simulated over Mombasa as and Wajir. The skill of all models including the ensemble was low for stations in highland areas such as Nyeri and Kakamega compared to other models. These results showed that the CORDEX models were not able to capture the apparent seasonal shift in position of the overhead sun.

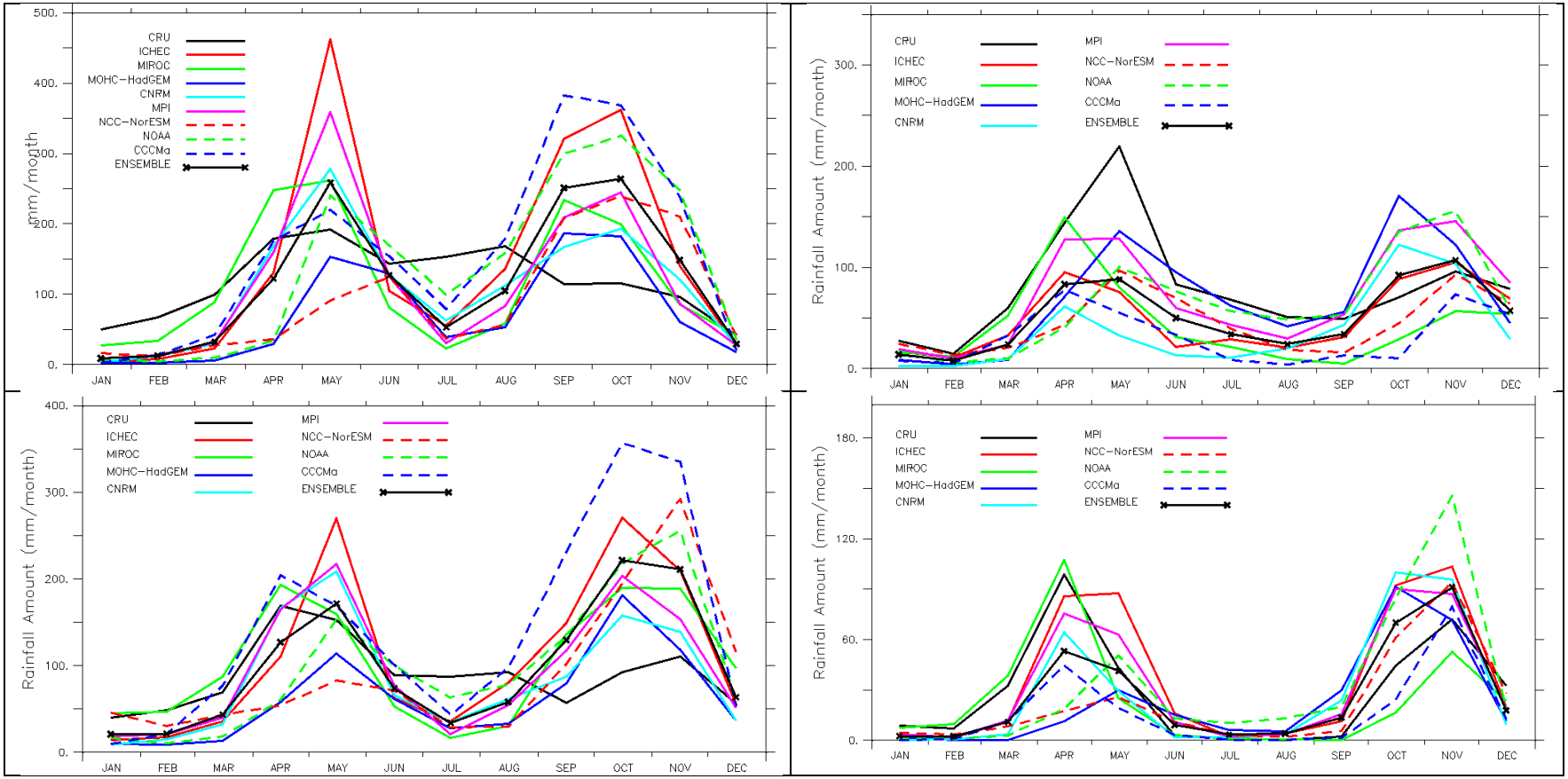

Figure 38: Mean annual cycle of rainfall (in mm) over Kakamega (top-left), Mombasa (top-right), Nyeri (bottom-left) and Wajir (bottom-right) as simulated by the observed (CRU), CORDEX models and the ensemble during the period 1971-2000.

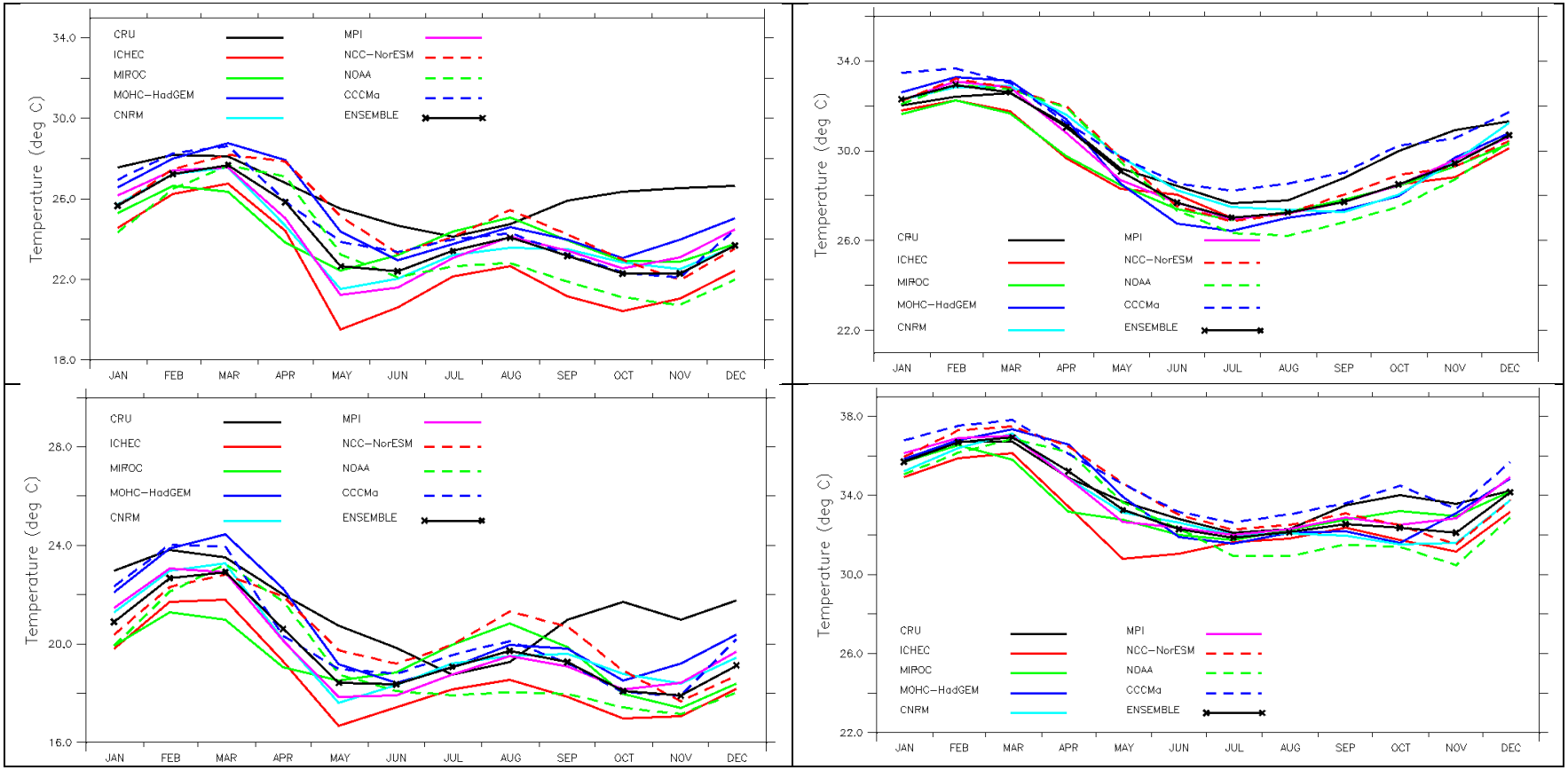

Figure 39: Mean annual cycle of maximum temperature (in °C) over Kakamega (top-left), Mombasa (top-right), Nyeri (bottom-left) and Wajir (bottom-right) as simulated by the observed (CRU), CORDEX models and the ensemble during the period 1971-2000.

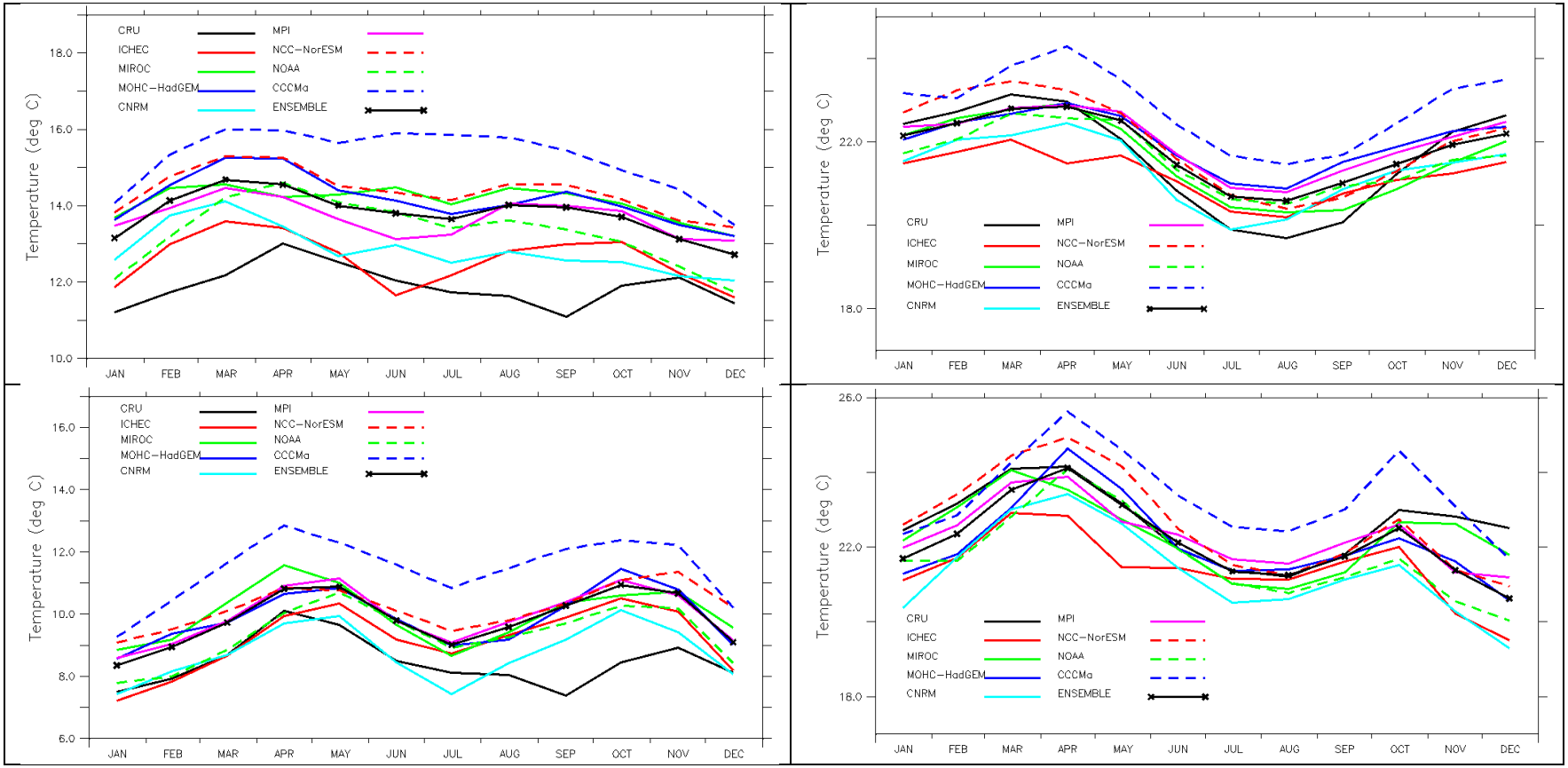

Figure 40: Mean annual cycle of minimum temperature (in °C) over Kakamega (top-left), Mombasa (top-right), Nyeri (bottom-left) and Wajir (bottom-right) as simulated by the observed (CRU), CORDEX models and the ensemble during the period 1971-2000.

4.4.5.2 Inter-annual variability

This section presents the results of the time series showing the inter-annual variability for the observed, the CORDEX models and the ensemble over the study area. The plots of inter-annual variability was done to assess the skill of the models in simulating the observed rainfall due to different systems that affect rainfall in the study area, for example ENSO. Figure 41 represents the plots of the inter-annual variability over selected stations in Kenya.

In Figure 41, the skill of the models in simulating the observed inter-annual variability is low over Kakamega, Mombasa, Nyeri and Wajir stations. The models were not able to capture major rainfall peaks which were the result of variability in the climate system. An example is the 1997/98 El niño year which was only captured by the CNRM model in Kakamega. CNRM model was able to capture several peaks in Wajir station compared to other models. These findings confirm the earlier results assessment of model skill in simulating tele-connection signals which found that the models were not able to reproduce the rainfall due to large scale circulation systems such as ENSO.

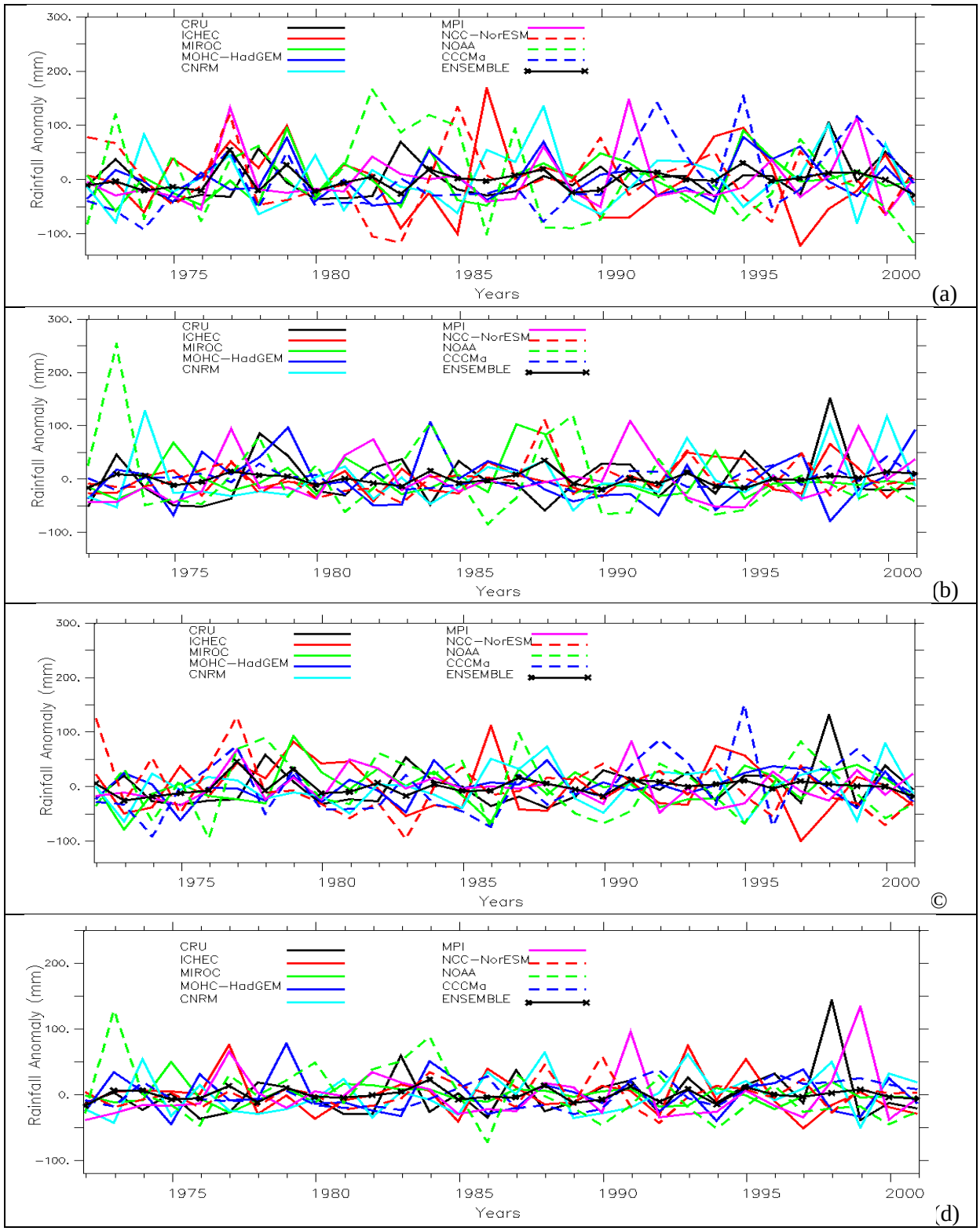

Figure 41: Comparison of inter-annual variability in CORDEX models, ensemble and the observed (CRU) in terms of their anomalies (in mm) during the OND season over Kakamega (a), Mombasa (b), Nyeri (c) and Wajir (d) between 1971 and 2000.

4.5 Analysis of Future Climate Patterns of Temperature and Rainfall Extremes over Kenya

This section provides the results of the analyzed extremes in rainfall and temperature from the CORDEX climate projections.

4.5.1 Frequency of Wet Days

The number of wet days in the three seasons, MAM, JJA and OND, was calculated for the reference period (1961-1990) and future period (2021-2050). The future change was then expressed as a percentage of the baseline period. The following figures, Figures 42, 43 and 44, present the results of this analysis for the three seasons. In Figure 42, a reduction in the frequency of wet days in the future, during MAM, under RCP4.5 scenario is expected in the northern parts of Kenya as simulated by ICHEC, MPI and ENSM2. There is an expected reduction in the frequency of wet days in several parts of Kenya as simulated by the NCC model. Most models show no change in the future frequency of wet days over significant parts of Kenya. In Figure 43, reduced frequency of wet days is expected in areas which normally receive rainfall during JJA season as simulated by all the models except the MPI model. During OND season, an increase in the number of wet days in several parts of the country is expected in the future as simulated by most models except the NCC model which projects a decrease over the entire country as shown in Figure 44.

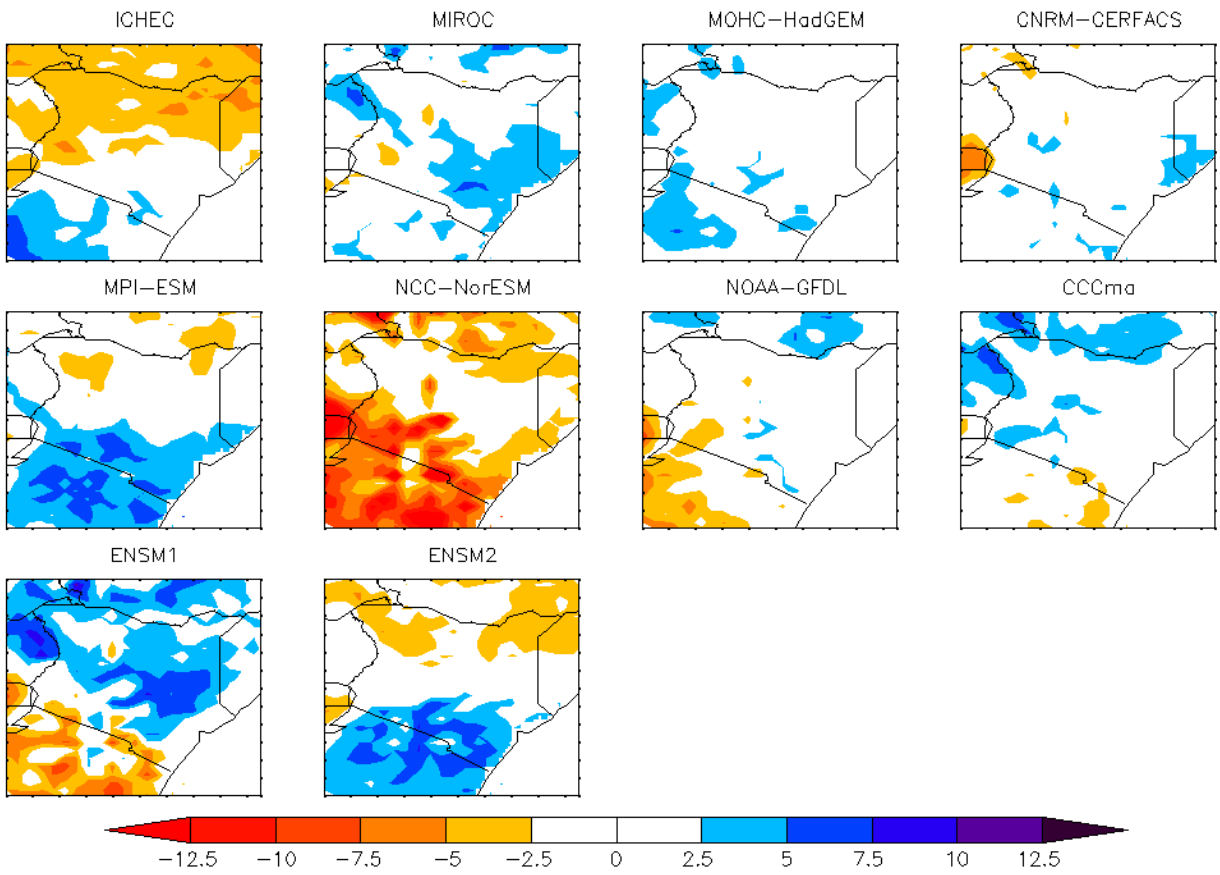

Figure 42: Simulated difference (in days) between future (2021-2050) wet days and baseline (1961-1990) wet days during the MAM season under the RCP4.5 scenario over Kenya. ENSM1 is the average of CCCma, MIROC, NCC and NOAA while ENSM2 is the average of CNRM, ICHEC and MPI.

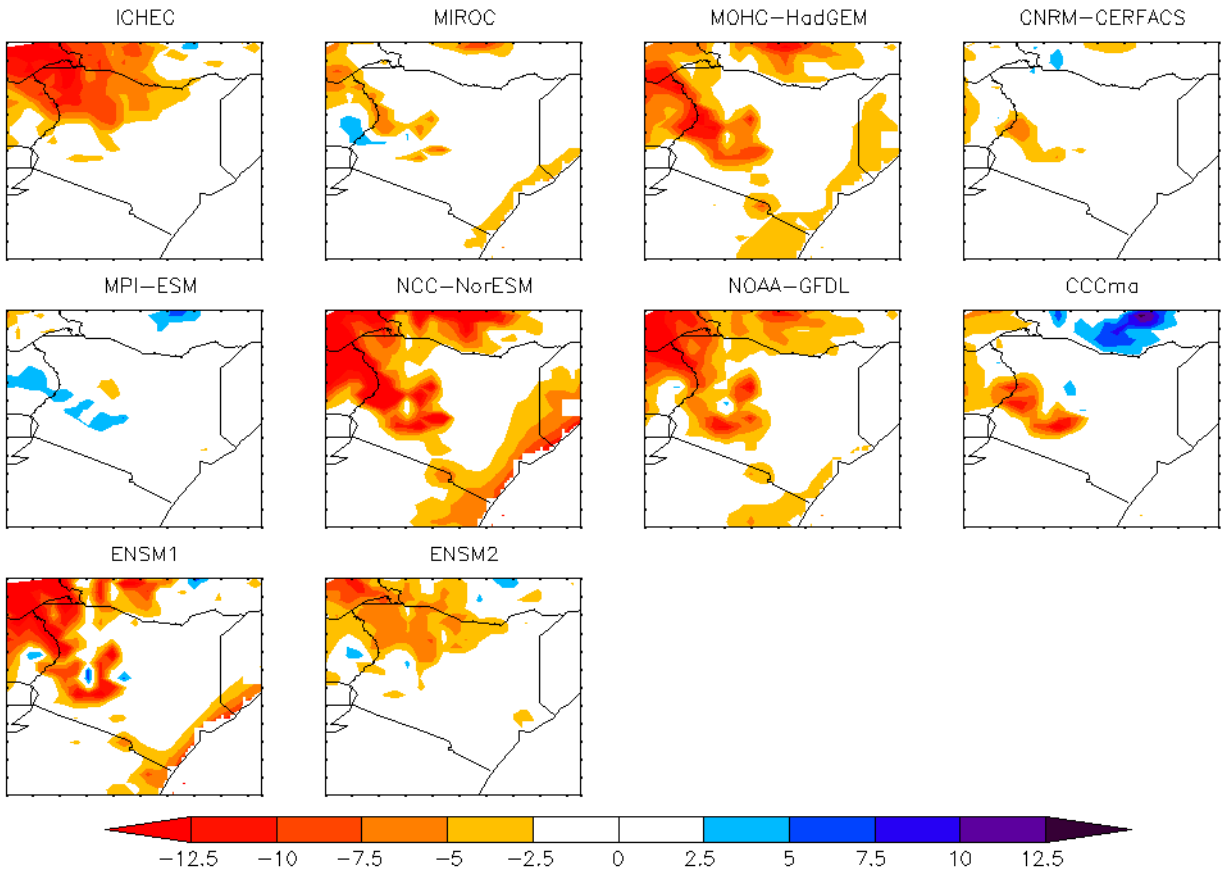

Figure 43: Simulated difference (in days) between future (2021-2050) wet days and baseline (1961-1990) wet days during the JJA season under the RCP4.5 scenario over Kenya. ENSM1 is the average of CCCma, MIROC, NCC and NOAA while ENSM2 is the average of CNRM, ICHEC and MPI.

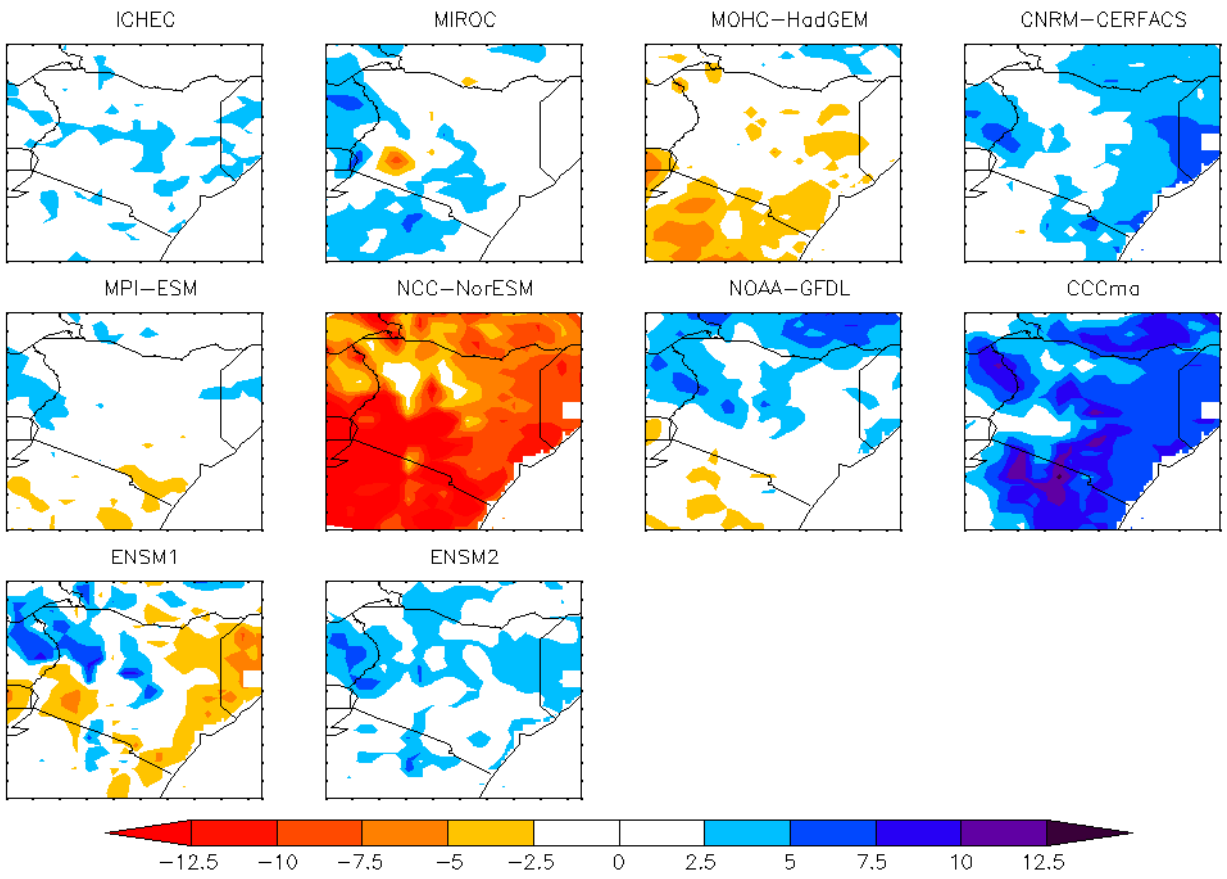

Figure 44: Simulated difference (in days) between future (2021-2050) wet days and baseline (1961-1990) wet days during the OND season under the RCP4.5 scenario over Kenya. ENSM1 is the average of CCCma, MIROC, NCC and NOAA while ENSM2 is the average of CNRM, ICHEC and MPI.

4.5.1 Frequency of Extreme Wet Days (R99P)

Percentile indices are more robust across a large region because they account for the influence of local climate effects (Omondi *et al.*, 2014) They are therefore best suited for comparing regions with different climatic zones. Figures 45, 46 and 47 represent the spatial plots of future frequency of extreme wet days. ENSM1 is the average of models with 365 calendar days including CCCma, MIROC, NCC and NOAA. ENSM2 is the average of the models with standard ($365\frac{1}{4}$ days) calendar days including CNRM, ICHEC and MPI.

In Figure 45, the future frequency of extreme wet days is expected to increase over several parts of the country, as simulated by MIROC, MOHC, NOAA, NCC and ESM1, during MAM season under RCP4.5 scenario with decreases being expected in the north western parts of the country.

ESM2 showed no change in the future frequency of wet days during MAM. In Figure 46, a decrease in future frequency of wet days was observed during JJA season from ICHEC, MOHC, NCC, NOAA and CCCma models. No change in the future frequency of extreme wet days was simulated by the two ensembles over most parts of the country. Marked increase in the frequency of wet days is expected during OND season especially in the eastern parts of the country as simulated by all the models shown in Figure 47. CCCma and ESM1 simulated an increase in the frequency of wet days over most parts of the Kenya.

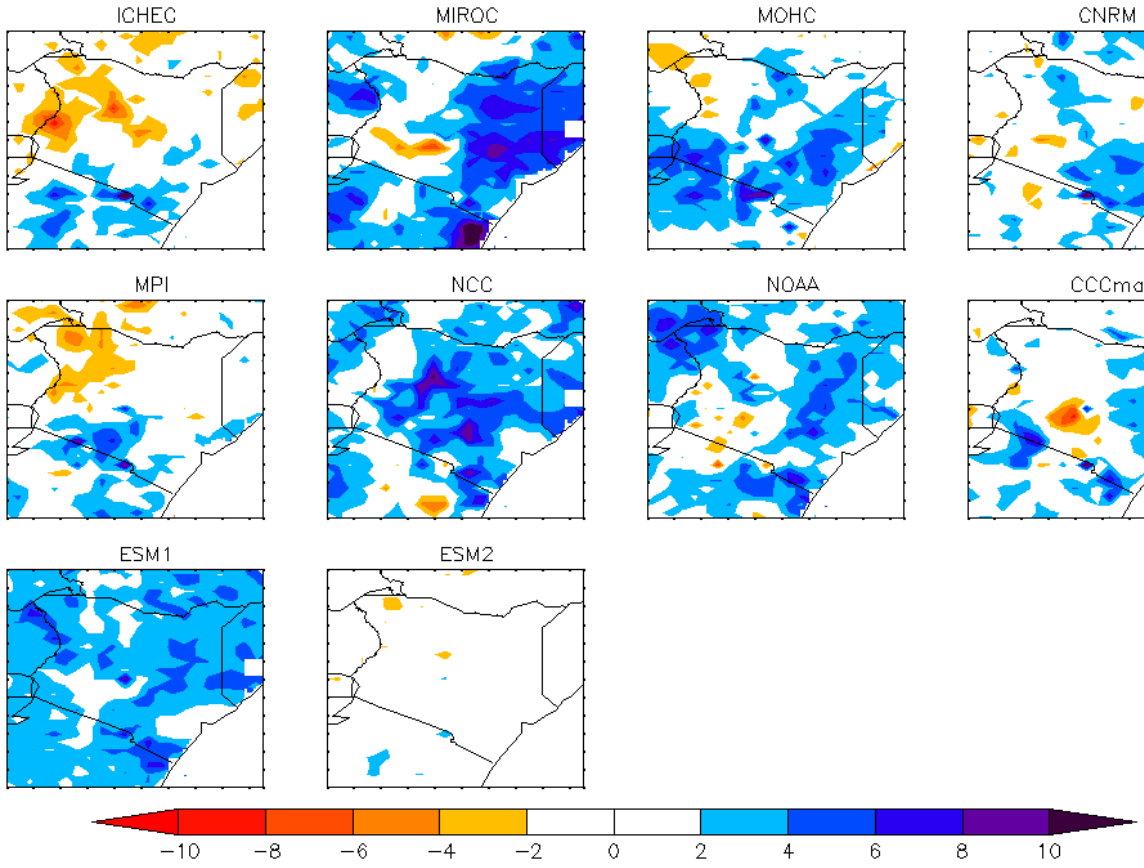

Figure 45: Simulated difference (in days) between future (2021-2050) extreme wet days (R99P) and baseline (1961-1990) extreme wet days during the MAM season under the RCP4.5 scenario over Kenya. ENSM1 is the average of CCCma, MIROC, NCC and NOAA while ENSM2 is the average of CNRM, ICHEC and MPI.

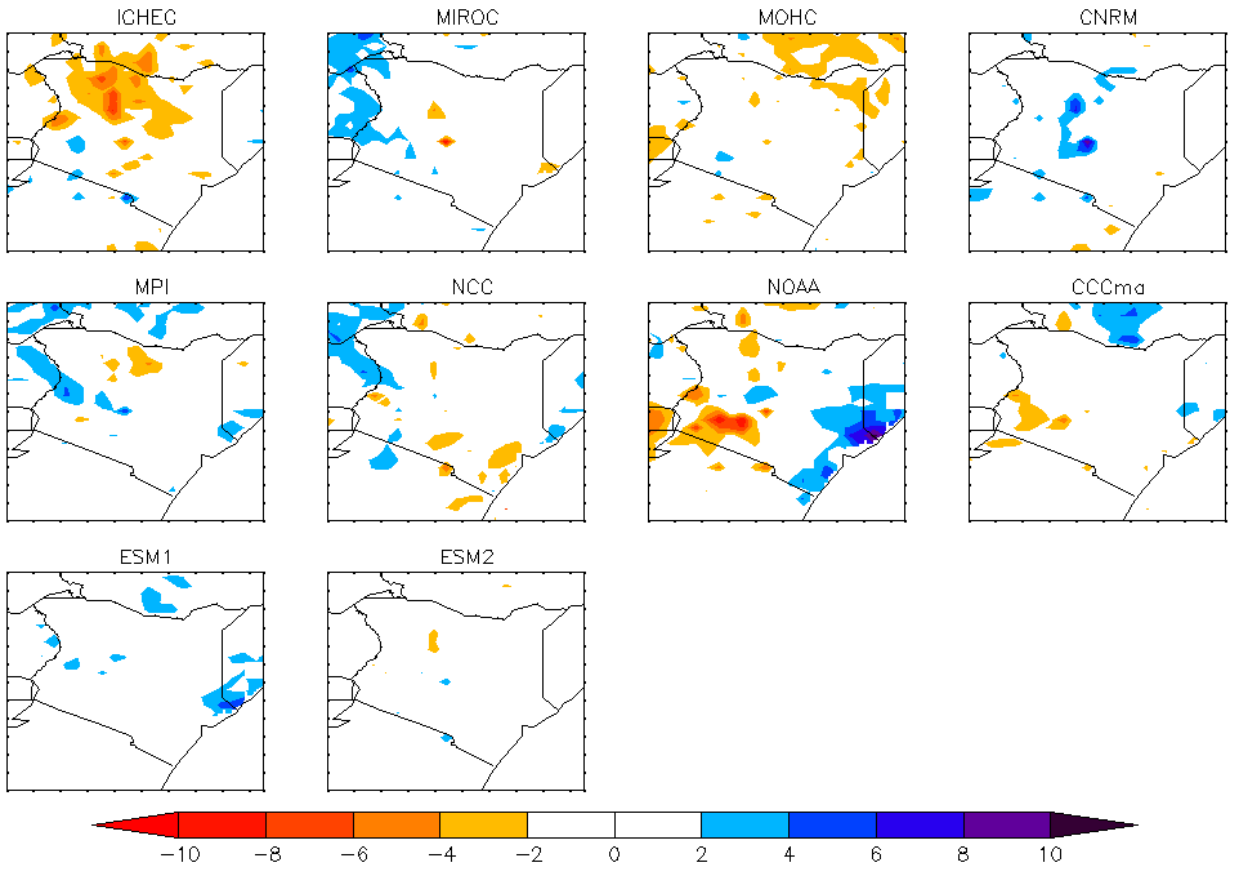

Figure 46: Simulated difference (in days) between future (2021-2050) extreme wet days (R99P) and baseline (1961-1990) extreme wet days during the JJA season under the RCP4.5 scenario over Kenya. ENSM1 is the average of CCCma, MIROC, NCC and NOAA while ENSM2 is the average of CNRM, ICHEC and MPI.

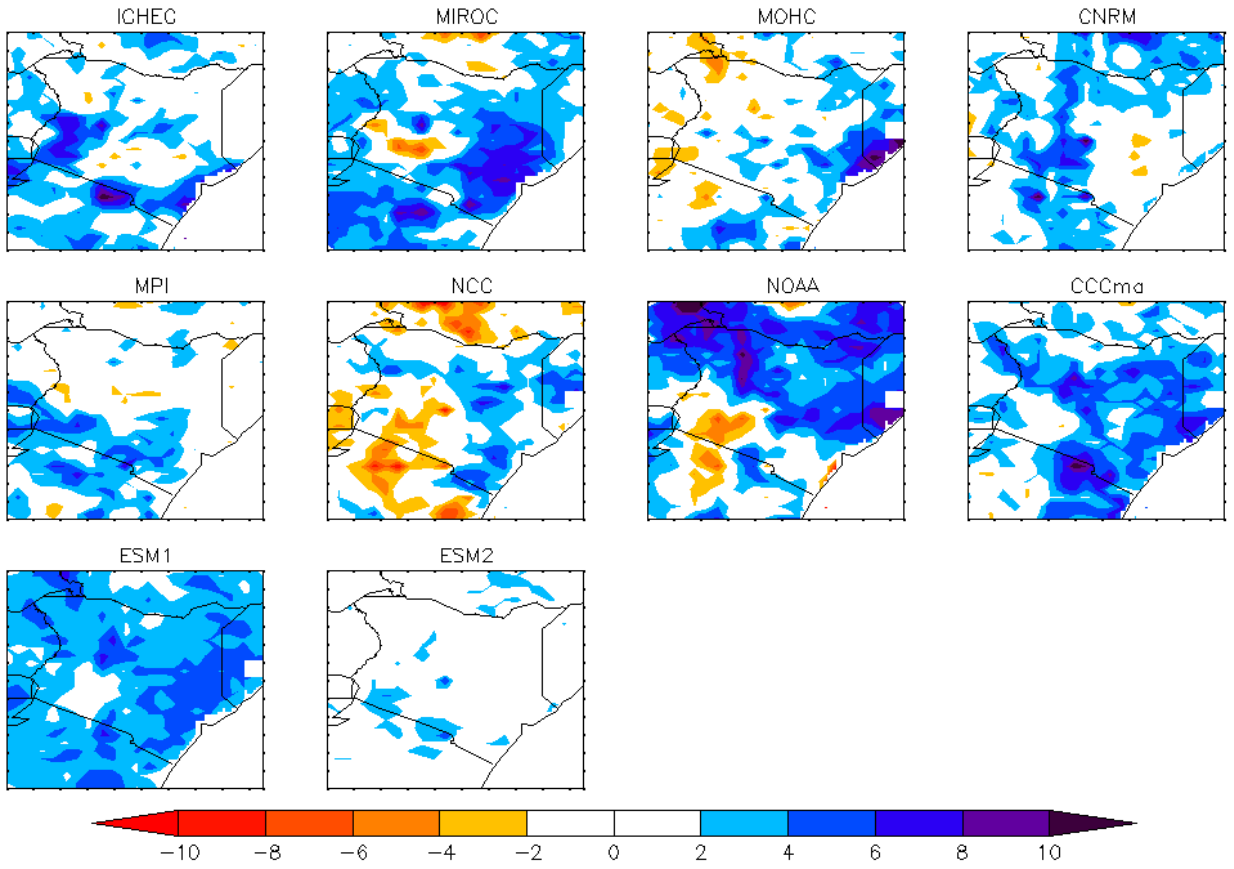

Figure 47: Simulated difference (in days) between future (2021-2050) extreme wet days (R99P) and baseline (1961-1990) extreme wet days during the OND season under the RCP4.5 scenario over Kenya. ENSM1 is the average of CCCma, MIROC, NCC and NOAA while ENSM2 is the average of CNRM, ICHEC and MPI.

4.5.2 Frequency of Days Warmer than 90th Percentile

The frequency of days in the future with minimum and maximum temperature greater than the 90th percentile of the baseline (1961-1990) threshold was also investigated. The subsequent figures, Figure 48, 49 and 50, show the results of the analysis. The frequency of days with minimum temperature greater than the 90th percentile of the baseline threshold had similar patterns over the study region for the six models used during MAM as shown in Figure 48. The models show as much as 60 to 70 percent increase in the future frequency of days with minimum temperature warmer than the 90th percentile under RCP4.5 scenario. The result from Figure 49 shows similar patterns for the six models during OND. There was no marked change in the number of days in the future with maximum temperature greater than the 90th percentile (TX90P) of the baseline threshold during the three seasons as shown in Figure 50 for the OND season.

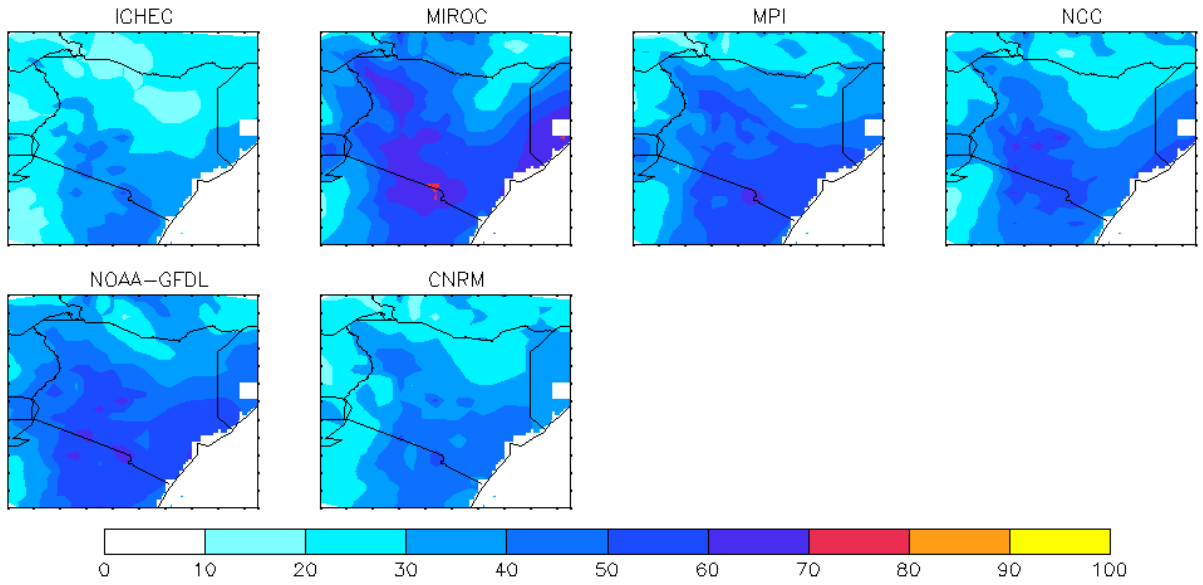

Figure 48: Percentage of days in the future (2021-2050) with minimum temperature warmer than the 90th percentile threshold of the baseline period (1961-1990) during MAM season under RCP4.5 scenario over Kenya.

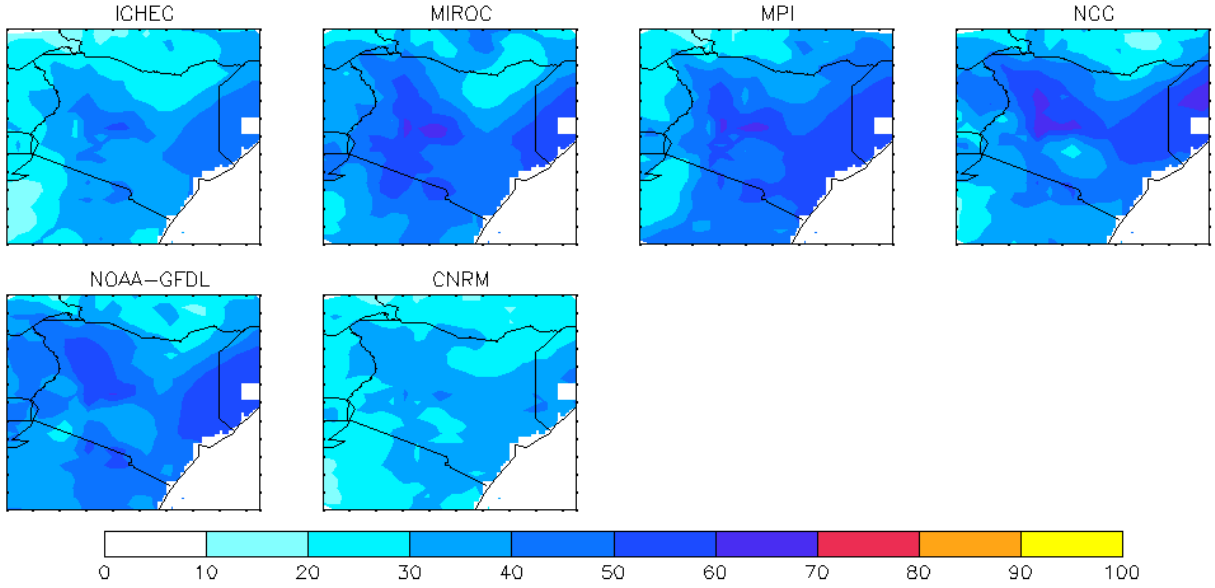

Figure 49: Percentage of days in the future (2021-2050) with minimum temperature warmer than the 90th percentile threshold of the baseline period (1961-1990) during OND season under RCP4.5 scenario over Kenya.

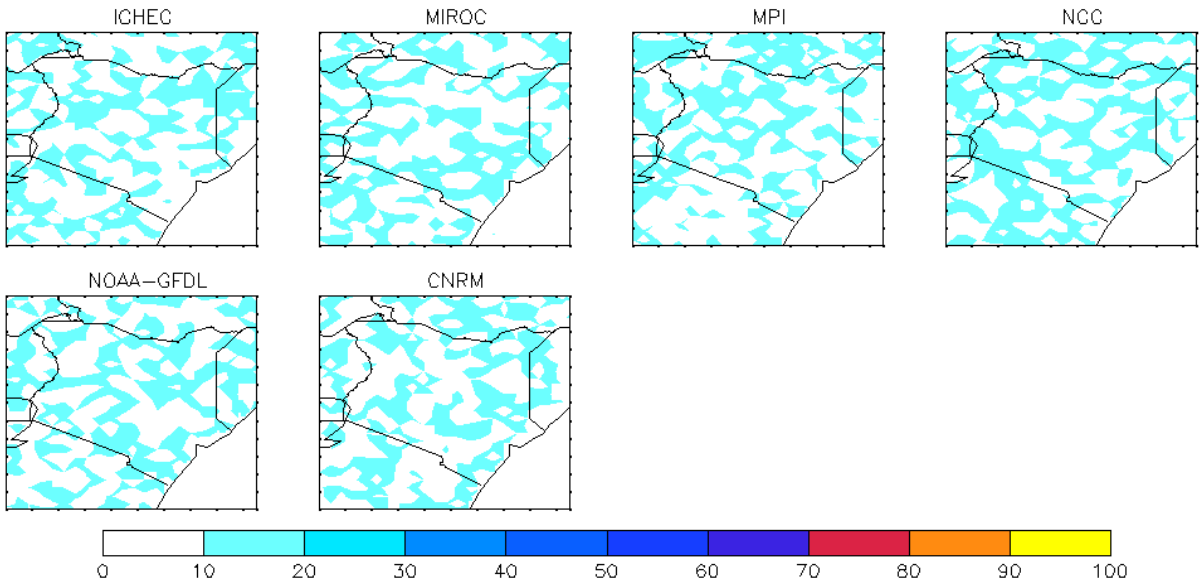

Figure 50: Percentage of days in the future (2021-2050) with maximum temperature warmer than the 90th percentile threshold of the baseline period (1961-1990) during OND season under RCP4.5 scenario over Kenya.

CHAPTER FIVE

5.0 CONCLUSIONS AND RECOMMENDATIONS

5.1 Conclusions

This study analyzed extremes using CORDEX Africa model projections over Kenya by first determining the spatial and temporal distribution in the observed temperature and rainfall extremes using extreme climate indices. The skill of the models in simulating the observed temperature and rainfall over Kenya was then investigated using several methods, including spatial and time series analysis, difference plots and correlation analysis. Finally, projections from CORDEX RCMs were analyzed for future extremes in temperature and rainfall using extreme climate indices.

Rainfall indices were less spatially coherent as compared to temperature indices confirming results from earlier studies (e.g., Omondi *et al.,* 2014). Positive precipitation trends were observed in the northern parts of the study region (especially areas around Marsabit and Wajir).Weak positive trends of temperature extremes were observed in most parts of the study region suggesting slight warming. Negative trends of temperature were mostly observed in the western parts of the study area.

The skill of some of the models in simulating rainfall was poor especially in the northeastern parts of the study region during the MAM season. The skill was better during the JJA and OND seasons. The ensemble had better skill in simulating the observed rainfall and temperature compared to some of the individual models. The skill in simulating both minimum and maximum temperature is better than that of rainfall during all the three seasons for all the models.

The skill of the models in reproducing the effect of tele-connection signals, El Niño and La Niña, was poor. The skill of the models in relation to the average deviation from the observed was relatively better for JJA season than both MAM and OND seasons. The models under-predict rainfall during the MAM and over-predict rainfall during the OND seasons. Model simulated rainfall had low correlation values as compared to model simulated temperature. On the average, the models tend to simulate increased temperatures during MAM and JJA seasons.

The models were able to simulate the annual cycles of rainfall and temperature except in areas which experience three rainfall seasons. This can be attributed to the local scale features and circulation systems, especially around the highland areas, which are not well resolved by the models. Results of the time-series of inter-annual variability further confirmed the poor skill of the models in simulating the rainfall due to tele-connection signals. The results indicate that CORDEX models were not able to replicate the local circulation systems that affect rainfall over the Lake Victoria basin and the mountainous regions.

The study showed that the models are not in agreement about the future number of wet days especially during MAM and OND which are the major rainfall seasons in the study area. The indication from these models is that the number of wet days and the number of extreme wet days (R99P) will increase over several parts of the study area in the future (2021-2050) under RCP4.5 scenario. There is a clear indication that the number of days with minimum temperature warmer than the 90^{th} percentile of the baseline period will increase by at least 20% in the future under the RCP4.5 scenario. The percentage increase in the number of days with maximum temperature greater than 90^{th} percentile of the baseline period did not however show any significant change under the RCP4.5 scenario.

Climate extreme indices indicate that maximum and minimum temperatures have decreased in the western parts of the country. The diurnal temperature range has increased in the coastal parts of Kenya; however, there has been a decrease in the urban centers especially in Nairobi and Kisumu. Mean monthly maximum and minimum temperatures have increased in the arid and semi-arid parts of Kenya. Rainfall indices indicate that dry days have decreased while wet days have increased in some parts of the northern arid and semi-arid regions. Total precipitation has increased in some parts of the arid and semi-arid regions and has decreased in urban centers and western parts of Kenya. Extreme wet days have slightly increased over the central highlands.

Most models suggest an increase in the future number of wet days in the southern arid and semi-arid parts of Kenya during the MAM season. Decrease in wet days is expected in areas that usually receive rainfall during the JJA season. Much of the arid and semi-arid regions are expected to experience increase in wet days in the future during the OND season. Increase in the number of extreme wet days is expected in the western parts of Kenya during the MAM, JJA and

OND seasons. Much of the country is expected to warm by at least 20% of the 90th percentile baseline threshold in all the seasons.

The findings from this study provide the much needed information to stakeholders to put in place adaptation strategies that will help protect the lives and livelihoods of people living in places where significant changes are expected considering the RCP4.5 scenario.

5.2 Recommendations

This section provides the necessary recommendations to various sectors which will protect lives and livelihoods and improve the understanding of extreme climate events in Kenya.

5.2.1 Recommendations to Planners

The areas which are anticipated to have an increase in the number of extreme rainfall days in the future are expected to experience increased flood episodes, outbreaks of water borne diseases and infrastructural damage. Areas where increase in temperature is anticipated, especially highland regions, are expected to experience increased frequency outbreaks of malaria. Policy makers should use information from this study to put in place the necessary contingency measures to cushion people against the anticipated risks that will result from these climate extremes.

5.2.2 Recommendations to Scientists

This study analyzed extremes based on daily observed annual records of rainfall and temperature although rainfall usually occurs in certain seasons. Seasonal analysis of extremes is necessary especially to those who carry out their planning based on seasonal predictions such as small holder farmers, most of whom are concentrated in the developing countries such as Kenya and who still depend on rain fed agriculture. It is therefore recommended that future studies be based on analyzing extremes on seasonal timescales.

The study has shown that individual models have challenges in simulating local scale circulation systems as well as global systems. Further studies of individual models, especially sensitivity studies in the region, are necessary to improve the skill of the models in the region.

Bias correction of the model outputs is also necessary before carrying out any analysis especially for rainfall. Future studies should therefore perform the necessary bias corrections before proceeding with further analysis of projection data from these models. This will provide robust results of future climate extremes to end users.

References

Aguilar, E., A. Aziz Barry, M. Brunet, L. Ekang, A. Fernandes, M. Massoukina, J. Mbah, A. Mhanda, D. J. do Nascimento, T. C. Peterson, O. Thamba Umba, M. Tomou and X. Zhang (2009) Changes in temperature and precipitation extremes in western central Africa, Guinea Conakry, and Zimbabwe, 1955–2006, *Journal of Geophysical Research,* **114***, D02115, doi:*10.1029/2008JD011010.

Aguilar, E., Auer I., Brunet M., Peterson T. C., and Wieringa J., (2003) Guidelines on climate metadata and homogenization. World Meteorological Organization, WMO-TD No. 1186, WCDMP No. 53, Geneva, Switzerland, 55

Alexander, L. V., Klein Tank A. M. G., Tagipour A., Zhang X., Peterson T. C., Haylock M., Kumar K. R., Stephenson D. B., Zhai P., Burn J., Rusticucci M., Collins D., Revadekar J., Aguilar E., Caesar J., Trewin B., Griffiths G., Brunet M., Vazquez-Aguirre J. L., Gleason B., Rahimzadeh F., Vincent L., Taylor M., and New M., (2006) Global observed changes in daily climate extremes of temperature and precipitation, *Journal of Geophysical Research*, **111**, D05109, doi:10.1029/2005JD006290.

Alexandersson, H., (1986) A homogeneity test applied to precipitation data, *Journal of Climate*, **6**.

Asnani, G.C., (1993) *Tropical meteorology*. Indian Institute of Tropical Meteorology: Pune, India, pp1202

Buishand, T. A., (1982) Some methods for testing the homogeneity of rainfall records. *Journal of Hydrology*, **58**:11–27

Bosire, E. N., (2012) Assessment of the Predictability of Rainfall on Seasonal Time Scales over East Africa Using the Climate Forecast System Model. *MSc. Thesis, Department of Meteorology, University of Nairobi, Kenya.*

Chan, J. C. L., (1995) Tropical Cyclone Activity in the Western North Pacific in Relation to the Stratospheric Quasi-Biennial Oscillation. *Monthly Weather Review*, **123**, 2567-2571.

Chaturvedi, R. K., J. Joshi, M. Jayaraman, G. Bala and N. H. Navindranath, (2012) Multi-model climate change projections for India under representative concentration pathways. *Current Science*, **103**, 7.

Choi, G., Fukuda Y., Huong P. T. T., Collins D., Afzaal M., Lias N., Ren G., Trewin B., Pianmana T., Kwon W-T., Zhou Y., Baldi M., Gomboluudev P., Boo K. O., and Cha Y-M., (2009) Changes in means and extreme events of temperature and precipitation in the Asia-Pacific Network region, 1955–2007, *International Journal of Climatology*, **29**: 1906–1925 DOI: 10.1002/joc.1979

Coles, S. G., (2001) *An Introduction to Statistical Modeling of Extreme Values.* Springer Series in Statistics, Springer, 224 pp.

Costa, A. C. and Soares, A. (2009) Trends in extreme precipitation indices derived from a daily rainfall database for the South of Portugal. *International Journal of Climatology*, **29**:1956–1975. doi:10.1002/joc.1834

Endris, H. S., P. Omondi, S. Jain, C. Lennard, B. Hewitson, L. Chang'a, J. L. Awange, A. Dosio, P. Ketiem, G. Nikulin, H-J. Panitz, M. Büchner, F. Stordal and L. Tazalika, (2013) Assessment of the Performance of CORDEX Regional Climate Models in Simulating East African Rainfall. *Journal of Climate*, **26**, 8453–8475

Fink, A., and P. Speth, (1997) Some potential forcing mechanisms of the year-to-year variability of the tropical convection and its intraseasonal (25-70-day) variability. *International Journal of Climatology*, **17**, 1513-1534.

Folland, C. K., Owen, M. Ward N., and Colman, A., (1991) Prediction of Seasonal Rainfall in the Sahel Region using Empirical and Dynamical Methods, *Journal of Forecasting*, **1**, 21 - 56

FAO (1998) Flood victims in East Africa hit by Rift Valley fever epidemic, published online at http://www.fao.org/NEWS/1998/980105-e.htm, accessed 23rd March 2015

Gbobaniyi, E., Sarr, A., Sylla, M. B., Diallo, I., Lennard, C., Dosio, A., Dhiédiou, A., Kamga, A., Klutse, N. A. B., Hewitson, B., Nikulin, G. and Lamptey, B. (2014) Climatology,

annual cycle and interannual variability of precipitation and temperature in CORDEX simulations over West Africa. *International Journal of Climatology*, **34**:2241–2257. doi:10.1002/joc.3834

George N. Kiladis and Henry F. Diaz., (1989) Global Climatic Anomalies Associated with Extremes in the Southern Oscillation. *Journal of Climate*, **2**, 1069–1090.

Godinez-Dominguez, J. Rojo-Va´zquez, V. Galva´n-Pin˜a and B. Aguilar-Palomino., (2000) Changes in the structure of a coastal fish assemblage exploited by a small scale gillnet fishery during an El Niño-La Niña event. *Estuarine, Coastal and Shelf Science*, **51**(6), 773-787.

Griffiths, G. M., Chambers L. E., Della-Marta P. M., Ouprasitwong N., Gosai A., Solofa D., Haylock M. R., Iga N., Tahani L., Lata R., Manton M. J., Laurent V., Thuy D. T., Tibig L., Nicholls N., Maitrepierre L., Trewin B., Baek H.-J., Choi Y., Nakamigawa H., Vediapan K., and Zhai P., (2005) Change in mean temperature as a predictor of extreme temperature change in the Asia–Pacific region, *International Journal of Climatology*, **25**: 1301–1330. DOI: 10.1002/joc.1194

Halpert, M. S., and Ropelewski, C. F., (1992) Surface temperature patterns associated with the Southern Oscillation. *Journal of Climate*, **5**(6), 577-593.

Hankin, S., Callahan, J., Manke, A., O'Brien, K., and Li, J. (2007) *FERRET user's Guide Version 6.02* (p. 609). NOAA/PMEL/TMAP.

Harris, I., Jones, P.D., Osborn, T.J. and Lister, D.H. (2014) Updated high-resolution grids of monthly climatic observations – the CRU TS3.10 Dataset. *International Journal of Climatology*, **34**:623–642. doi:10.1002/joc.3711

Hastenrath, S. (1976) Variations in low-latitude circulation and extreme climatic events in the tropical Americas. *Journal of the Atmospheric Sciences*, **33**(2), 202-215.

Hatsushika, H., and K. Yamazaki., (2001) Interannual variations of temperature and vertical motion at the tropical tropopause associated with ENSO. *Geophysical Research Letters*, **28**, 2891-2894.

Haylock, MR, Hofstra N, Klein Tank AMG, Klok EJ, Jones PD, and New M. (2008) A European daily high-resolution gridded data set of surface temperature and precipitation for 1950–2006. *Journal of Geophysical Research*, **113**: D20119. DOI: 10.1029/2008JD010201.

Haylock, M. R. and Goodess, C. M., (2004) Interannual variability of European extreme winter rainfall and links with mean large-scale circulation. *International Journal of Climatology*, **24**:759–776. doi:10.1002/joc.1033

Hendon, H. H., and B. Liebmann., (1990) The intraseasonal (30-50 day) oscillation of the Australian summer monsoon. *Journal of the Atmospheric Sciences*, **47**, 2909-2923.

Indeje, M., (2000) Prediction and numerical simulation of regional climate of equatorial Eastern Africa. *PhD Thesis, North Carolina State University*, U.S.A. pp327

Indeje, M., H. M. F. Semazzi, and J. L. Ogallo., (2000) ENSO signal in East African rainfall seasons. *International Journal of Climatology*, **20**, 19–46.

Ininda, J. M., (1995) Numerical simulation of the influence of sea surface temperature anomalies on the East African seasonal rainfall. *PhD. Thesis, Department of Meteorology, University of Nairobi, Kenya.*

IPCC 2007: Climate Change (2007) The Physical Science Basis. Contribution of Working Group I to the Fourth Assessment Report of the Intergovernmental Panel on Climate Change [Solomon, S., D. Qin, M. Manning, Z. Chen, M. Marquis, K.B. Averyt, M.Tignor and H.L. Miller (eds.)]. Cambridge University Press, Cambridge, United Kingdom and New York, NY, USA.

IPCC (2013) Climate Change (2013) The Physical Science Basis. Contribution of Working Group I to the Fifth Assessment Report of the Intergovernmental Panel on Climate Change [Stocker, T.F., D. Qin, G.-K. Plattner, M. Tignor, S.K. Allen, J. Boschung, A. Nauels, Y. Xia, V. Bex and P.M. Midgley (eds.)]. Cambridge University Press, Cambridge, United Kingdom and New York, NY, USA, 1535 pp.

Kalognomou, E., C. Lennard, M. Shongwe, I. Pinto, A. Favre, M. Kent, B. Hewitson, A. Dosio, G. Nikulin, H. Panitz, and M. Büchner, (2013) A diagnostic evaluation of precipitation in

CORDEX models over southern Africa. *Journal of Climate*, **26**(23), 9477-9506.

Karl, T.R., N. Nicholls, and A. Ghazi, (1999) CLIVAR/GCOS/WMO workshop on indices and indicators for climate extremes: Workshop summary. *Climatic Change*, **42**, 3-7.

Katz, R.W., (1999) Extreme value theory for precipitation: sensitivity analysis for climate change, *Advances in Water Resources*, **23**,133-139

Keggenhoff, I., Elizbarashvili, M., Amiri-Farahani, A., and King, L. (2014) Trends in daily temperature and precipitation extremes over Georgia, 1971–2010. *Weather and Climate Extremes*, **4**, 75-85.

Kenyon, J., and Heger G. C., (2008) Influence of Modes of Climate Variability on Global Temperature Extremes, *Journal of Climate*, **21,** 3872- 3889, DOI: 10.1175/2008JCLI2125.1

Kessler, W. S., M. J. McPhaden, and K. M. Weickmann, (1995) Forcing of intraseasonal Kelvin waves in the equatorial Pacific. *Journal of Geophysical Research*, **100**, 10613-10631.

Kharin, V.V., F.W. Zwiers, X. Zhang and G.C. Hegerl, (2007) Changes in temperature and precipitation extremes in the IPCC ensemble of global coupled model simulations. *Journal of Climate*, **20**, 1419-1444, DOI: 10.1175/JCLI4066.1

Kharin, V. V., and F. W. Zwiers, (2000) Changes in the extremes in an ensemble of transient climate simulations with a coupled atmosphere–ocean GCM. *Journal of Climate*, **13**, 3760–3788.

Kijazi, A. L., and Reason C. J. C., (2009) Analysis of the 2006 Floods over Northern Tanzania. *International Journal of Climatology*, **29:** 955-970

King'uyu, S. M., L. A. Ogallo., and E. K. Anyamba., (2000) Recent Trends of Minimum and Maximum Surface Temperatures over Eastern Africa, *Journal of Climate*, **13**, 2876-2886.

Klein, Tank A. M. G., Santhosh K., Revadekar J. V., Budhathoki K. P., Amanmurad D., Peterson T. C., Joshi U. R., Jaswal A. K., Yeleuova K., Hussain A., Asanova V. S., Quadir D. A.,

Kolli R. K., Vandasheva S., Afzaal M., Jones P. D., Dorji S., Zou X., Sikder A. B., Faleyeva M., Chandrapala L., New M. G., Tang H., Deshpande N. R., Gomboluudev P., Anvar H., and Spektorman T., (2006) Changes in daily temperature and precipitation extremes in central and south Asia, *Journal of Geophysical Research*, **111**, doi:10.1029/2005JD006316.

Kruger, A. C., (2006) Observed trends in daily precipitation indices in South Africa: 1910–2004, *International Journal of Climatology*, **26**: 2275–2285. DOI: 10.1002/joc.1368

Kohler, M.A. (1949) Double-mass analysis for testing the consistency of records and for making adjustments, *Bulletin of the American Meteorological Society*, **30**, 188-189.

Kostopoulou, E., and Jones P. D., (2005) Assessment of climate extremes in the Eastern Mediterranean, *Meteorology and Atmospheric Physics*, **89**, 69–85, DOI 10.1007/s00703-005-0122-2

Larkin, N. K., and D. E. Harrison, (2002) ENSO warm (El Niño) and cold (La Niña) event life cycles: Ocean surface anomaly patterns, their symmetries, asymmetries, and implications. *Journal of Climate*, **15**, 1118-1140.

Lau, K., P. H. Chan, (1985) Aspects of the 40-50-day oscillation during the northern winter as inferred from outgoing long-wave radiation. *Monthly Weather Review*, **113**, 1889-1909.

Ly, M., Traore S. B., Alhassane A., and Sarr B., (2013) Evolution of some observed climate extremes in the West African Sahel, *Weather and Climate Extremes.*, **1**, 19–25. http://dx.doi.org/10.1016/j.wace.2013.07.005

Madden, R., and P. Julian, (1971) Detection of a 40-50 day oscillation in the zonal wind in the tropical Pacific. *Journal of Atmospheric Science*, **28**, 702-708.

Madden, R., and P. R. Julian, (1972) Description of global scale circulation cells in the Tropics with 40–50 day period. *Journal of Atmospheric Science,* **29**, 1109-1123.

Madden, R. A., and P. R. Julian, (1994) Observations of the 40-50-day tropical oscillation - A review. *Monthly Weather Review*, **122**, 814-837.

Marengo, J. A., Jones, R., Alves, L. M., and Valverde, M. C. (2009) Future change of temperature and precipitation extremes in South America as derived from the PRECIS regional climate modeling system. *International Journal of Climatology*, **29**(15), 2241-2255.

Mason, S. J., and A. M. Joubert., (1997) Simulated changes in extreme rainfall over Southern Africa, *International Journal of Climatology*, **17**, 291–301.

McPhaden, M. J., (2002) El Niño and La Niña: Causes and global consequences. *Encyclopedia of Global Environmental Change,* Anonymous John Wiley and Sons, LTD, 353-370

Nandintsetseg, B., Greene J. S., and Goulden C. E., (2007) Trends in extreme daily precipitation and temperature near Lake H¨ovsgol, Mongolia. *International Journal of Climatology,* **27**: 341–347. DOI:10.1002/joc.1404

Ogallo, L. J., (1988) Relationships between seasonal rainfall in East Africa and the Southern Oscillation. *Journal of Climatology*, **8**, 31–43, doi:10.1002/joc.3370080104.

Okoola, R. E., (1999) Synoptic systems affecting Eastern Africa. *Lecture notes of the first Drought Monitoring Centre (DMC), Nairobi climate prediction capacity building training workshop for the Greater Horn of Africa, Nairobi, Kenya. Drought Monitoring Centre-Nairobi, 51 - 62*

Oettli, P. and Camberlin, P., (2005) Influence of topography on monthly rainfall distribution over East Africa. *Climate Research*, **28**: 199-212

Okeyo, R. E., (1987) The influence of Lake Victoria on the convective activities over the Kenya Highlands. *Journal of the Meteorological Society, Japan,* **65:** 689-695

Omondi, P. A., Awange, J. L., Forootan, E., Ogallo, L. A., Barakiza, R., Girmaw, G. B., Fesseha, I., Kululetera, V., Kilembe, C., Mbati, M. M., Kilavi, M., King'uyu, S. M., Omeny, P. A., Njogu, A., Badr, E. M., Musa, T. A., Muchiri, P., Bamanya, D. and Komutunga, E. (2014) Changes in temperature and precipitation extremes over the Greater Horn of Africa region from 1961 to 2010. *International Journal of Climatology*, **34**:1262–1277. doi:10.1002/joc.3763

Partal, T, and Kahya E. (2006) Trend analysis in Turkish precipitation data. *Hydrological Processes*, **20**: 2011–2026.

Peterson, T.C., Folland, C., Gruza, G., Hogg, W., Mokssit, A., and Plummer, N. (2001) Report on the Activities of the Working Group on Climate Change Detection and Related Rapporteurs 1998-2001. WMO, Rep. WCDMP-47, WMO-TD 1071, Geneve, Switzerland, 143pp.

Peterson, T. C., Easterling, D. R., Karl, T. R., Groisman, P., Nicholls, N., Plummer, N., ... and Parker, D. (1998) Homogeneity adjustments of in situ atmospheric climate data: a review. *International Journal of Climatology*, **18**(13), 1493-1517.

Ramage, C., (1971) Monsoon Meteorology. *International Geophysics Series*, **15**, Academic Press, San Diego, Calif., 296 pp.

Reason, C.J.C. (2001) Sensitivity of the Southern African circulation to dipole sea-surface temperature patterns in the South Indian Ocean. *International Journal of Climatology*, **22**, 377–393.

Roth, M., T.A. Buishand, G. Jongbloed, A.M.G. Klein Tank, J.H. van Zanten., (2014) Projections of precipitation extremes based on a regional, non-stationary peaks-over-threshold approach: A case study for the Netherlands and north-western Germany. *Weather and Climate Extremes*, **4**, 1-10.

Sadler, J. G., Lander, M. A., Hori, A. M., and Oda, L. K., (1987) Tropical marine climatic atlas. **2**, Pacific Ocean. Report UHMET 87-02, Department of Meteorology, University of Hawaii, Honolulu, HI.

Saji, N.H., Goswami B.N., Vinayachandran P.N., Yamagata T., (1999) A dipole mode in the tropical Indian Ocean, *Nature*, **401**, 360-363.

Schulzweida, U., Kornblueh, L., and Quast, R. (2006). CDO user's guide. *Climate Data Operators, Version*, *1*(6).

SEI Project Report, (2009) Economics of Climate Change in Kenya: Final Report Submitted in

Advance of COP15.

Sen, PK. (1968) Estimates of the regression coefficients based on Kendall's tau. *Journal of the American Statistical Association,* **63**: 1379–1389.

Shongwe, M. E., G. J. Van Oldenborgh, and B. J. J. M. Van Den Hurk., (2009) Projected Changes in Mean and Extreme Precipitation in Africa under Global Warming. Part I: Southern Africa, *Journal of Climate,* **22,** 3819- 3837.

Shongwe, M. E., G. J. V. Oldenborgh., B.V. D. Hurk., and M. V. Aalst., (2011) Projected Changes in Mean and Extreme Precipitation in Africa under Global Warming. Part II: East Africa, *Journal of Climate,* **24**: 3718- 3733.

Sperling F and Szekely F 2005 Disaster risk management in a changing climate. VARG, Washington DC.

Trewartha, G. T. (1981). *The earth's problem climates* (Vol. 371). Madison, WI: University of Wisconsin Press.

Troup, A. J. (1965) The southern oscillation. *Quarterly Journal of the Royal Meteorological Society*, **91**(390), 490-506.

Vincent, L. A., P. Booneeady, H. Seeward, E. Aguilar, R. Virasami, B. Montfraix, M. Saindou, A. F. Hassane, L. Y. A. Randriamarolaza, G. Jumaux, F. R. Faniriantsoa, D. Roy, and V. Amelie., (2011) Observed trends in indices of daily and extreme temperature and precipitation for the countries of the western Indian Ocean, 1961–2008, *Journal of Geophysical Research,* **116**, D10108, doi:10.1029/2010JD015303.

Vincent, L. (1990) Time Series Analysis: Testing the Homogeneity of Monthly Temperature Series, Survey Paper No. 90-5, Department of Mathematics and Statistics, York University, Ontario, 50 pp.

Walker, G. T., and E. W. Bliss, (1932) World weather V. *Mem. Royal Meteorological Society*, **4**, 53-84

Wang, H., Chen Y., Xun S., Lai D., Fan Y., and Li Z., (2012) Changes in daily climate extremes in the arid area of northwestern China. *Theoretical and Applied Climatology*, **112**, 15-28. DOI 10.1007/s00704-012-0698-7

Wang, Y., R. L. Leung, J. L. McGregor, D. K. Lee, W. C. Wang,Y. Ding, and F. Kimura, (2004) Regional climate modeling:Progress, challenges, and prospects. *Journal of the Meteorological Society of Japan,* **82**, 1599–1628.

Welzer, H., (2012) Climate Wars: What People Will Be Killed for in the 21st Century, Binding: Hardcover Publisher: Polity Press, Cambridge, England Date published: 2012 ISBN-13: 9780745651453 ISBN: 0745651453

WHO (2015) Flooding and Communicable Diseases fact Sheet, Retrieved on 27th January 2015 from http://www.who.int/hac/techguidance/ems/flood_cds/en/

Williams, C. J. R., D. R. Kniveton and R. Layberry., (2007) Climatic and oceanic associations with daily rainfall extremes over southern Africa, *International Journal of Climatology,* **27**: 93–108. DOI: 10.1002/joc.1376

WMO (2003) Report of the GCOS/GTOS/HWRP Expert Meeting on Hydrological Data for Global Studies, WMO/TD–No. 1156.

World Bank (2012) *Turn down the heat: why a 4°C warmer world must be avoided*. Washington DC: World Bank.

You, Q., Kang, S., Aguilar, E., Pepin, N., Flügel, W. A., Yan, Y., ... & Huang, J. (2011) Changes in daily climate extremes in China and their connection to the large scale atmospheric circulation during 1961–2003. *Climate Dynamics*, **36**(11-12), 2399-2417.

Zhang, X., and Yang, F. (2004) RClimDex (1.0) user manual. *Climate Research Branch Environment Canada*, **22.**